Redox-neutral *S*-nitrosation Mediated by a Dicopper Center

Wenjie Tao[a], Curtis E. Moore[a], and Shiyu Zhang*[a]

[a] Dr. W. Tao, Dr. C. E. Moore, Prof. Dr. S. Zhang
Department of Chemistry & Biochemistry, The Ohio State University, 100 West 18th Avenue, Columbus, Ohio 43210, United States
E-mail: zhang.8941@osu.edu

Abstract: An unprecedented redox-neutral *S*-nitrosation of thiol has been achieved at dicopper(I,I) center. Treatment of dicopper (I,I) complex with excess NO• and thiol generates a dicopper (I,I) di-*S*-nitrosothiol complex $[Cu^{I}Cu^{I}(RSNO)_2]^{2+}$ or dicopper (I,I) mono-*S*-nitrosothiol complex $[Cu^{I}Cu^{I}(RSNO)]^{2+}$, which readily release RSNO in 88-94% yield. The *S*-nitrosation reaction proceeds through a mixed-valence $[Cu^{II}Cu^{III}(\mu\text{-O})(\mu\text{-NO})]^{2+}$ species, which deprotonates RS-H at the basic μ-O site and nitrosates the RS^- at the μ-NO site. The $[Cu^{II}Cu^{III}(\mu\text{-O})(\mu\text{-NO})]^{2+}$ complex is also competent for *O*-nitrosation of MeOH, which is isoelectronic to thiol. In this case, a rare $[Cu^{II}Cu^{II}(\mu\text{-NO})(OMe)]^{2+}$ intermediate has been isolated and fully characterized, suggesting the *S*-nitrosation proceeds through the intermediary of analogous $[Cu^{II}Cu^{II}(\mu\text{-NO})(SR)]^{2+}$ species. The redox- and proton-neutral *S*-nitrosation process reported here represents the first functional model of ceruloplasmin in mediating *S*-nitrosation of external thiols, adding further implications for biological copper sites in the interconversion of NO•/RSNO.

Introduction

Nitric oxide is an important signaling molecule that regulates a range of biological processes through *S*-nitrosation (or *S*-nitrosylation) of cysteine residues on proteins. Both excessive and insufficient protein *S*-nitrosation can lead to misfolding that contributes to neurodegenerative diseases, e.g. Alzheimer's disease (AD),[1–3] Parkinson's disease,[1,2,4,5] and Amyotrophic Lateral Sclerosis.[6] Dysregulation of *S*-nitrosothiols (RSNOs) could be a result of altered nitric oxide (NO•) synthase activity or aberrant (de)nitrosation activity of copper proteins. Cu,Zn superoxide dismutase (CuZnSOD) and ceruloplasmin (CP) are closely related to the depletion[6] and accumulation[7,8] of RSNO, respectively.

A central research topic in this paradigm is to understand the chemical mechanism by which RSNOs are formed at metal centers. Covalent attachment of NO• to thiols (R-SH) requires removal of one electron and one proton (Scheme 1 top). Thus, it is a common belief that *S*-nitrosation requires an external oxidant, e.g. O_2[9,10], $O_2^{\bullet-}$[11], Fe[12–15], and Cu^{II} [7,16,17] For example, addition of NO• to heme proteins, e.g. nitrophorin, hemoglobin, can lead to the formation of $\{FeNO\}^6$ thiolate complex[18–20] and subsequent *S*-nitrosation with simultaneous reduction of Fe^{III} to Fe^{II} (Scheme 1A).[14,21] Lu et. al. reported the reductive *S*-nitrosation of an engineered copper azurin, where the Cu^{II}-bound cysteine in type 1 copper (T1) site was converted to *S*-nitroso-cysteine residue along with a Cu^{I} center.[22] Simultaneously, Warren et. al. demonstrated reversible *S*-nitrosation of synthetic models of T1 site (Scheme 1B) and structurally characterized the first *S*-nitrosothiol copper adduct $[Cu^{I}](\kappa^1\text{-N(O)SR})$.[23] In addition to T1 site, type 2 copper (T2) and binuclear type 3 copper (T3) sites are also critically involved in RSNO formation. Akaike et.al found that RSNO-generation activity at CP was significantly suppressed by various T2 and T3 site inhibitors, such as azide, cyanide, and fluoride.[7] Since CP contains both T1 and T2/T3 sites, it is unclear which copper center is responsible for *S*-nitrosative reactivity of CP. Although T1 site has been shown to directly interact with NO•,[22,23] the RSNO-producing activity was observed predominantly with multicopper proteins that contain both T1 and T2/T3 sites, whereas the efficacy of RSNO formation by T1-only proteins (e.g. azurin) is lower than that of free copper ion ($CuSO_4$).[7] Together, these observations suggest possible roles of binuclear and trinuclear copper centers in the conversion of NO• and RSH to RSNO, which has yet to be explored.

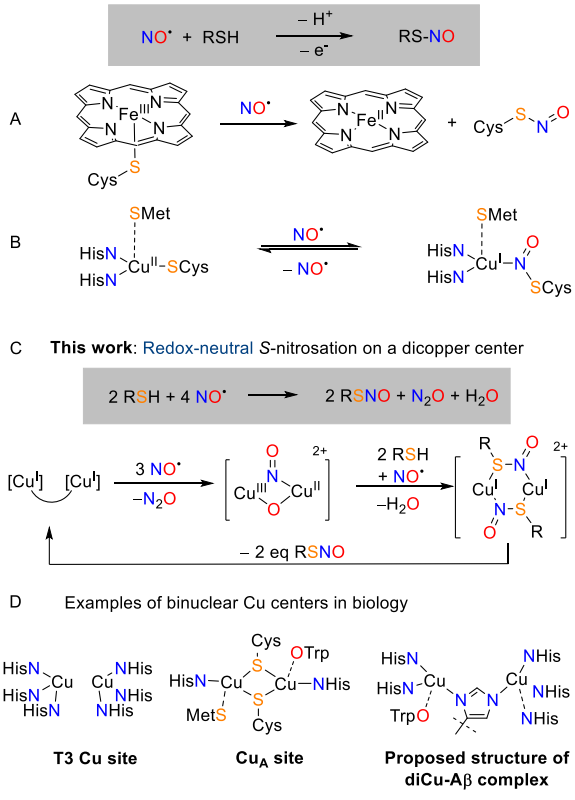

Scheme 1. Reductive *S*-nitrosation on (A) heme iron and (B) Type 1 copper site. (C) Redox-neutral *S*-nitrosation by a dicopper model complex, which is a functional model of CP mediated RSNO formation. (D) Examples of dinuclear Cu centers in biology.

Herein, we report a new *S*-nitrosation pathway facilitated by a dicopper complex, which represents the first functional model that mimics CP's ability to generate external *S*-nitrosothiols (Scheme 1C).[7,8] Activation of NO• at dicopper complex generates a $[Cu_2(\mu\text{-O})(\mu\text{-NO})]^{2+}$ species,[24] which can nitrosate thiol through (i) deprotonation of RS-H at the basic μ-O site, and (ii) reductive coupling of thiolate (RS^-) at the μ-NO site (Scheme 2). Many biological and biomimetic systems show reductive *S*-nitrosation, but now we report a redox-neutral *S*-nitrosation mechanism, where NO• provides both the NO motif in RSNO and oxidizing equivalents by coupling of NO• to N_2O at dicopper center. Our studies provide implications into how binuclear[25] and multinuclear copper centers (Scheme 1D) could potentially participate in the formation of low mass *S*-nitrosothiols,[26–28] e.g. *S*-nitrosoglutathione, *S*-nitroso-*L*-cysteine, which serve as oxygen-stable reservoirs of NO•.[29–31]

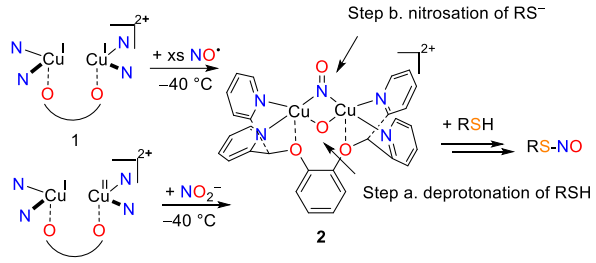

Scheme 2. Proposed S-nitrosation reaction from dicopper(II,III) μ-oxo, μ-nitrosyl complex **2**.

Results and Discussion

Reactivity of $[LCu_2(\mu\text{-O})(\mu\text{-NO})]^{2+}$ with thiols

Previously, we described that activation of NO• at dicopper (I,I) complexes supported by 1,2-bis(di(pyridin-2-yl)methoxy)benzene (Py_4DMB, **L**) affords a dicopper (II,III) μ-oxo, μ-nitrosyl complex ($[LCu_2(\mu\text{-O})(\mu\text{-NO})]^{2+}$ **2**, Scheme 2).[24] Complex **2** can also be accessed from nitrite (NO_2^-) via cleavage of the O-NO bond at a dicopper (I,II) synthon. We demonstrated that the μ-oxo motif is active toward oxygen atom transfer and C-H hydroxylation. The reactivity of μ-NO motif, however, remains unexplored. Since biological and biomimetic copper nitrosyl complexes are known to engage in the interconversion of *S*-nitrosothiol, NO•, and nitrite,[23,32] we posit that the μ-NO site in complex ($[LCu_2(\mu\text{-O})(\mu\text{-NO})]^{2+}$ (**2**) may engage thiol in *S*-nitrosation. The proximal μ-O site can serve as internal base to deprotonate thiols and facilitate S-NO bond formation (Scheme 2). We first investigated the reaction of **2** with a primary thiol, 2-phenylethanethiol (PE-SH) as a model substrate for cysteine. Addition of PE-SH to complex **2** in the presence of excess NO• in acetone at –80 °C cleanly produces a dark green species **3-PE** with strong absorbance at 575 nm (ε = 2400 $M^{-1}cm^{-1}$) and a shoulder at 675 nm (ε = 1450 $M^{-1}cm^{-1}$) (Figure 1, black trace), similar to the characteristic UV-vis features of fully characterized $^{iPr2}TpCu^I(\kappa^1\text{-N-}Ph_3CSNO)$[23]. Complex **3-PE** is highly thermal-sensitive, and it decays quickly at temperatures above −60 °C. Complete generation of **3-PE** requires two equivalents of PE-SH (Figure S28-29), suggesting **3-PE** contains two thiol motifs. Considering the UV-Vis titration evidence, we anticipate that **3-PE** might be a dicopper(I,I) di-*S*-nitrosothiol adduct; therefore, it is denoted as $[LCu^ICu^I(PE\text{-}SNO)_2]^{2+}$.

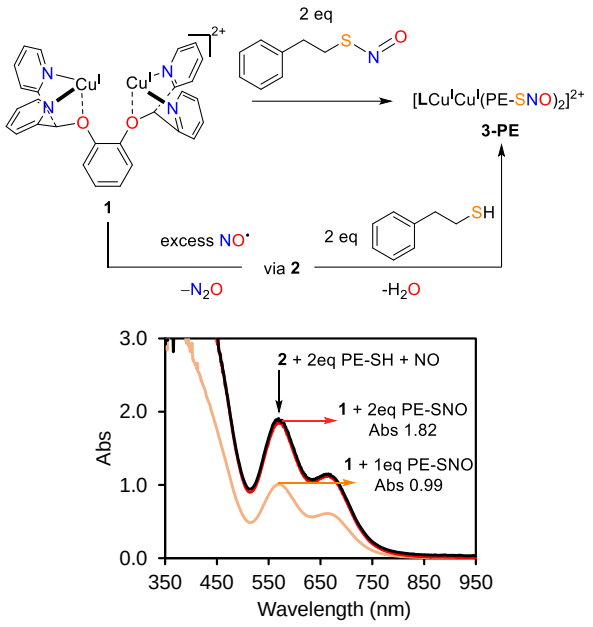

Figure 1. Reaction scheme (top) and corresponding UV-Vis spectra (bottom) of the reaction of **1** with excess NO• and two equivalents of PE-SH at –80 °C (black). The UV-vis spectrum of reaction of **1** with 1 eq PE-SNO (orange) and 2 eq PE-SNO (red) at –80 °C.

To further explore this hypothesis, we attempted to independently synthesize dicopper(I,I) di-*S*-nitrosothiol complex **3-PE** by treating dicopper(I,I) complex **1** with two equivalents of corresponding RSNO. *S*-nitroso-2-phenylethanethiol (PE-SNO, Figure 1) can be isolated by treating 2-phenylethanethiol (PE-SH) with $NaNO_2$ or KNO_2 under acidic conditions (see supporting information).[33] Addition of two equivalents of PE-SNO to the dicopper (I,I) precursor **1** at −80 °C affords the same green species **3-PE** with UV-vis features at 575 (ε = 2400$M^{-1}cm^{-1}$) and 675 nm (ε = 1450 $M^{-1}cm^{-1}$, Figure 1, red trace). Complete formation of **3-PE** requires two equivalents of PE-SNO with respect to dicopper complex **1** (Figure 1, 1 eq: orange, 2 eq: red), strongly supporting that **3-PE** contains two PE-SNO moieties. The UV-Vis spectra generated from NO• and thiol or the direct addition of RSNO are almost identical in terms of peak positions and intensities (Figure 1, black and red traces), suggesting that $[LCu^ICu^I(PE\text{-}SNO)_2]^{2+}$ can be prepared in high yields via both routes.

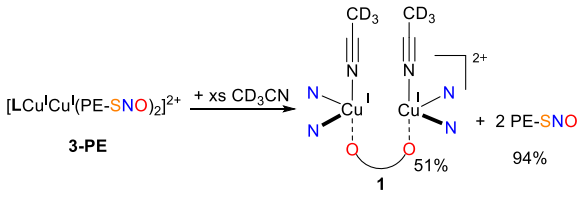

Scheme 3. Displace the bound *S*-nitroso-2-phenylethanethiol from Cu^I by excess amount of CD_3CN.

To further confirm the identity of **3-PE** as a dicopper di-*S*-nitrosothiol adduct, we attempted to displace the *S*-nitrosothiol with a ligand that can tightly bind the dicopper(I,I) center. Addition of excess acetonitrile-d_3 to a solution of **3-PE** generated from the reaction of **2** and two equivalents of PE-SH in acetone-d_6 at −80

°C causes a color change from dark green to light yellow with an absorbance at 550 nm (Figure S39-40), which is characteristic for PE-SNO. ^{1}H NMR analysis of the reaction mixture suggests that two equivalents of PE-SNO are produced in 94% yield. Formation of the dicopper (I,I) acetonitrile complex **1** was also observed in 51% yield (Scheme 3). This reaction is significant because the combined consequence of Scheme 2 and Scheme 3 represents a new way to covalently attach NO• to thiol in redox-neutral and proton-neutral fashion, contrasting to traditional mono-Cu[23,34] or mono-Fe[14,35]-mediated reductive nitrosation pathways.

Encouraged by the reactivity of **2** with primary thiol PE-SH, we further examined the reaction of **2** with a cysteine analog, N-acetyl-*L*-cysteine methyl ester (Cys-SH). The putative dicopper(I,I) *S*-nitrosothiol complex **3-Cys** has a UV-Vis absorbance at 570 nm (ε = 2500 M^{-1}cm^{-1}) and 670 nm (ε = 2200 M^{-1}cm^{-1}, Figure 2, blue trace). **3-Cys** can be prepared via the treatment of **1** with excess NO• followed by two equivalents of Cys-SH (Figure 2). The formation of Cys-SNO from this reaction is determined by addition of excess acetonitrile-d_3 to displace the copper-bound Cys-SNO. Quantitative ^{1}H NMR analysis of the reaction mixture suggests that two equivalents of Cys-SNO are produced in 88% yield. Formation of the dicopper (I,I) acetonitrile complex was also observed in 34% yield. Alternatively, **3-Cys** can be synthesized from the treatment of **1** with Cys-SNO (Figure 2 red trace). Interestingly, the plot of UV-Vis absorbance vs. equivalent of Cys-SNO used exhibits a maximum at a 1:1 ratio of **1**: Cys-SNO (Figure S43-44), suggesting that **3-Cys** is a dicopper mono-*S*-nitrosothiol complex [**L**Cu^{I}Cu^{I}(Cys-SNO)]$^{2+}$. Only one equivalent of Cys-SNO can bind to dicopper(I,I) **1** perhaps because the intramolecular amide (NHAc) and ester (CO_2Me) functional groups on Cys compete with RSNO coordination.

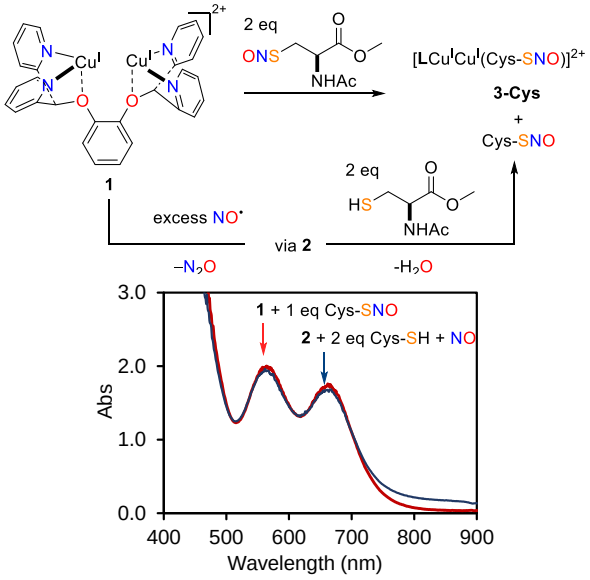

Figure 2. Reaction scheme (top) and corresponding in-situ UV-Vis spectra of the synthesis of **3-Cys**. **3-Cys** can be generated from either treatment of **1** with NO• and Cys-SH (blue trace, −80 °C) or addition of 2 equivalents of Cys-SNO to complex **1** (red trace, −80 °C).

Characterization of [LCu$^{I}_2$(PE-SNO)$_2$]$^{2+}$ adduct 3-PE.

Our effort in structurally characterizing **3-PE** was hampered by its thermal sensitivity. We found that **3-PE** decomposes to mono-copper(II) complex [**L**Cu^{II}]PF$_6$ even at –60 °C over a few days, which is presumably due to the loss of NO• along with the expulsion of copper(II) thiolate clusters (Scheme 4).[36]

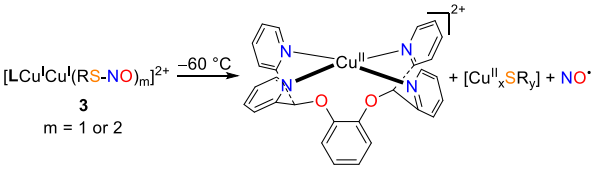

Scheme 4. The decomposition pathway of dicopper(I,I) S-nitrosothiol intermediate above −60 ℃.

To determine the binding mode of PE-SNO at **3-PE**, the reaction of two equivalents of PE-S^{15}NO with **1** was monitored with ^{15}N NMR. At room temperature, the ^{15}N NMR spectrum of PE-S^{15}NO displays a broad resonance at 771 ppm vs. NH_3. Upon cooling to −80 °C, the *syn* and *anti* configurations of PE-SNO can be resolved as two sharp peaks at 830 and 758 ppm (vs. NH_3). Addition of 2.4 equivalents of PE-S^{15}NO to **1** at –80 °C leads to two new resonances at 535 and 521 ppm (vs. NH_3) (Figure 3A), suggesting that PE-SNO might coordinate to the dicopper center in two different binding modes. The ^{15}N chemical shifts of **3-PE** are very similar to previously reported ^{Mes}TpCu(I)(κ^1-N(O)SCPh$_3$) (560 ppm vs. NH_3),[23] which strongly suggests that both the ^{15}N atoms coordinate directly to the Cu(I) center.

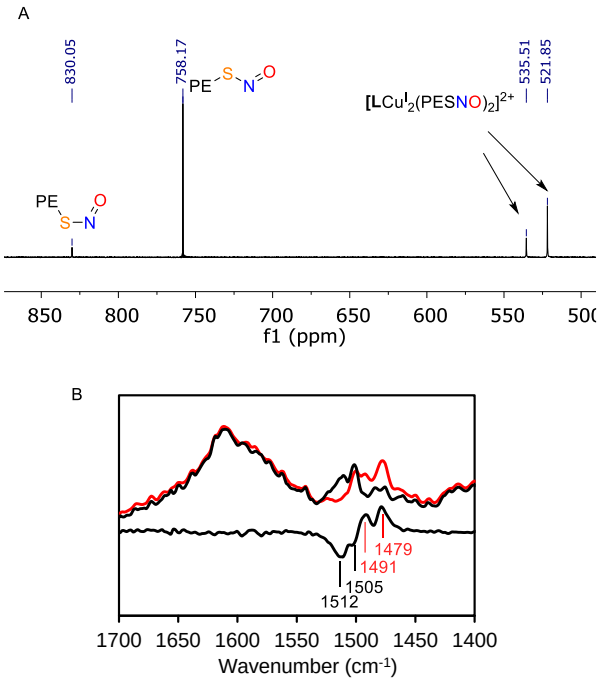

Figure 3. (A) ^{15}N NMR (acetone-d_6, −80 °C) spectrum of the reaction of **1** with 2.4 eq of PE-S^{15}NO. (B) In-situ IR spectra for the formation of **3-PE-^{14}N** and **3-PE-^{15}N** (−78 °C, 20 mM [Cu$_2$], THF-d_8) generated from the reaction of **1** with two equivalents of PE-S^{14}NO (dark blue) or PE-S^{15}NO (red). The difference spectrum of ^{14}N and ^{15}N sample is shown in black.

The reaction of **1** and PE-SNO is further investigated by solution IR spectroscopy. Two new ^{15}N-label-sensitive bands at 1512(-21) and 1505(-26) cm^{-1} grow in when **1** is treated with two equivalents of PE-SNO in THF-d_8 at –78 °C (Figure 3B). These vibration frequencies are much higher than the N=O stretch observed for the fully-characterized ^{Mes}TpCu(I)(κ^1-N(O)SCPh$_3$) complex (1424 cm^{-1}).[23] The presence of two different N=O stretches can be explained by the symmetric and unsymmetric

coupling of two PE-SNO units. It is well-known that coordination of RSNO to metal center or Lewis acid via S, O, N atoms can alter the strength of N=O and S-N bond.[23,37–40] While k^1-N coordination of *S*-nitrosothiols weakens the N=O bond and strengthens the N-S bond, k^1-S coordination has the opposite effects (Scheme 5A). Therefore, the higher N=O stretches of dicopper(I,I)-bound PE-SNO (1512 and 1505 cm^{-1}) in comparison to free PE-SNO (1495 cm^{-1}, Figure S64-65) strongly suggests that the S atoms of PE-SNO also coordinate/interact with the Cu(I) center.

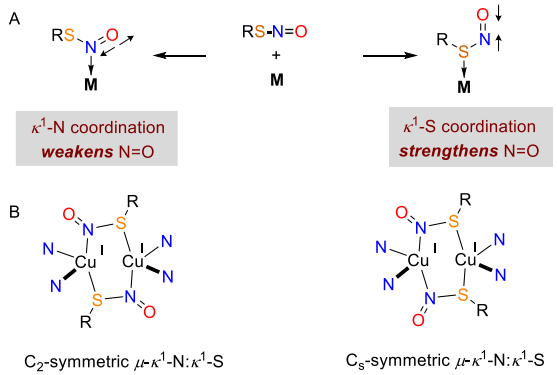

Scheme 5. The N=O stretches in different binding bodes of *S*-nitrosothiol bound to transition metal or Lewis acid and the most likely binding mode of **3-PE**.

Taken together, IR and ^{15}N NMR spectroscopic studies indicate that the binding mode of PE-SNO at the dicopper center is best assigned as μ-κ^1-N: κ^1-S in THF and acetone. The two PE-SNO motifs could be arranged C_2-symmetry or C_s-symmetry (Scheme 5B), which gives rise to the two distinct ^{15}N NMR peaks. It is important to note that there are many possible binding modes of PE-SNO at the dicopper center (C_2-symmetry or C_s-symmetry, *syn* or *anti*, O, S, N-bound), and the interactions of RSNO and Cu are expected to be sensitive to the solvent environment, as the coordination of solvent molecules may lead to different binding modes through S, O, and N atoms. Indeed, we found that the UV-vis spectrum of **3-PE** changes significantly in different solvents with very different coordination ability (Figure S60, THF, acetone, ether, DCM). While we believe it is possible to assign the binding mode in each solvent by performing detailed IR and ^{15}N NMR measurements, such a study is beyond the scope of current work.

O-nitrosation of MeOH with dicopper(II,III) μ-O μ-NO.

A unique feature of *S*-nitrosation via dicopper(II,III) μ-O μ-NO complex **2** is that the highly oxidizing μ-O site can serve as an internal base and oxidant. This is in sharp contrast to previous mono-Fe and mono-Cu-based reductive *S*-nitrosation mechanisms, where thiols must be converted to thiolates and an external oxidant (Fe^{III} or Cu^{II}) is employed prior to S-NO bond formation.[34] To understand the synergy between μ-O and μ-NO moieties in achieving the *S*-nitrosation, we sought to investigate the reaction of dicopper(II,III) μ-O μ-NO complex **2** with alcohols (ROH), which are isoelectronic to thiol (Figure 4A) since no intermediate was observed en route to S-NO bond formation when **2** was treated with thiols. Metal nitrosyl complex capable of *S*-nitrosation can often perform analogous *O*-nitrosation of alcohol via similar mechanisms.[34,35,41]

Reaction of **2** with excess methanol leads to the formation of a new species **4** that absorbs at 475 nm (ε = 2200 $M^{-1}cm^{-1}$), and 540 nm (ε = 2000 $M^{-1}cm^{-1}$), which is stable up to –30 °C (Figure S51). Compound **4** is EPR silent (Figure S68-69), suggesting two antiferromagnetically coupled Cu^{II} centers. In-situ low-temperature IR studies show that **4** exhibits a ^{15}N-sensitive stretch at 1567 (-28) cm^{-1}, which is consistent with an NO^- moiety[24,42] (Figure 4B). Single crystals of **4** were obtained by vapor diffusion of diethyl ether into a solution of **4** in methanol and toluene at −40 °C. X-ray diffraction analysis reveals a dicopper (II,II) μ-NO μ-OMe complex (Figure 4C). Besides the bridging nitrosyl and methoxy, Cu1 is coordinated by a triflate (OTf) anion and Cu2 is coordinated by a methanol solvent molecule, which is hydrogen-bonded with an outer sphere triflate (Figure S61). While the structure is of high quality, the NO and OMe ligand are in positional disorder, making the N-O distance less reliable. Complex **4** is the second example of dicopper μ-NO complex at $Cu^{II}Cu^{II}$ oxidation state. Karlin et. al. reported the only other example of dicopper (II,II) μ-NO complex, which was prepared by treatment of dicopper (I,I) precursor with nitrosonium (NO^+) salt.[42]

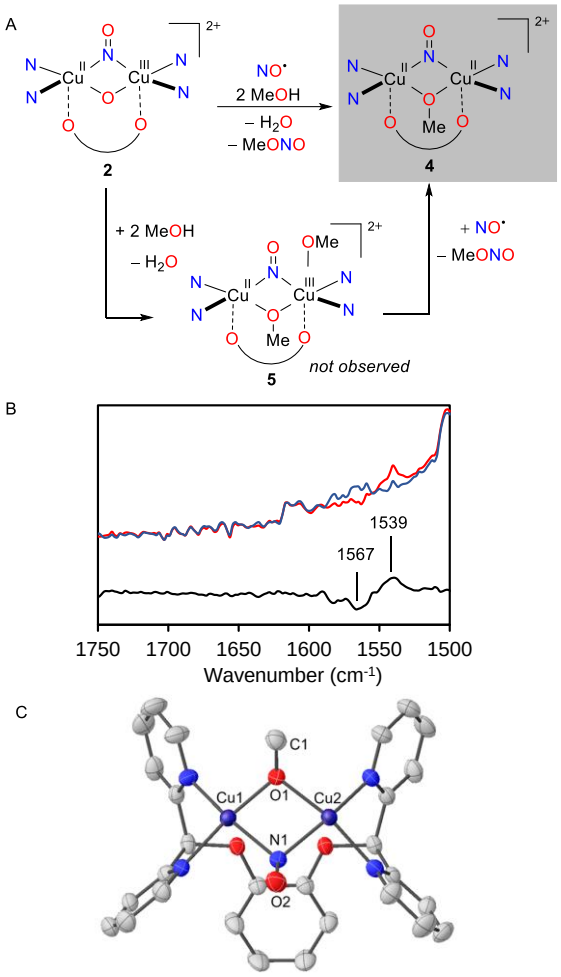

Figure 4. (A) Reaction scheme of **2** with MeOH. (B) Solution IR spectrum (15 mM, a mixture of DCM (0.50 mL), THF (0.40 mL) and methanol (0.20 mL) at –40 °C) of **4**-^{14}N (blue) and **4**-^{15}N (red). The difference spectrum of ^{14}N and ^{15}N sample is shown in black. (C) Solid-state structure of [**L**$Cu^{II}Cu^{II}$(μ-NO)(μ-OMe)] complex **4**. Thermal ellipsoids are set at 50% probability. The triflate anions, solvent molecules, hydrogen atoms, and minor components of disordered atoms are omitted for clarity. Selected bond distance (Å): Cu1–N1 = 1.976(16), Cu2–N1 = 2.00(3), Cu1–O1 = 1.871(15), Cu2–O1 = 1.950(13), N1–O2 = 1.32(5), N1B-O2B = 1.27(4), Cu2-O1S = 2.227(3).

The $Cu^{II}Cu^{II}$ oxidation state in **4** suggests a stepwise *O*-nitrosation mechanism (Figure 4A). First, complex **2** undergoes protonation with methanol to generate a putative dicopper(II,III) μ-NO μ-alkoxide species **5**. Then, reductive *O*-nitrosation of the terminal methoxyl group in **5** causes a one-electron reduction of

the dicopper(II,III) core and affords the observed product **4** with dicopper(II,II) oxidation states and MeO-NO. The characteristic "five-finger" UV-Vis feature of MeO-NO is observed at 325-380 nm, when the reaction of **1** and NO is performed in MeOH at 0.2 mM concentration (Figure S54). This stepwise *O*-nitrosation mechanism to produce key dicopper (II,II) μ-NO μ-OMe intermediate **4** can be potentially applied in the analogous *S*-nitrosation reaction (Scheme 6). Since **2** can deprotonate MeOH, it is reasonable to hypothesize that it can also deprotonate more acidic thiols to afford a putative dicopper(II,III) μ-NO μ-thiolate intermediate **6**. The terminal thiolate on **6** can undergo *S*-nitrosation to furnish the first RS-NO bond[22,23] and generate **7**. Further RS-NO bond formation proceeds at the bridging thiolate to afford the second equivalent of RS-NO and eventually the complex **3-PE**.

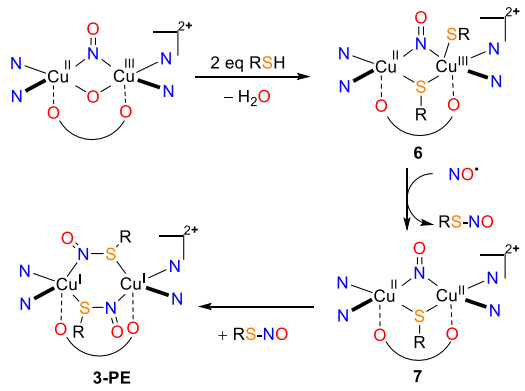

Scheme 6. The possible mechanistic pathway to generate **3-PE** from dicopper(II,III) µ-oxo, µ-nitrosyl **2**.

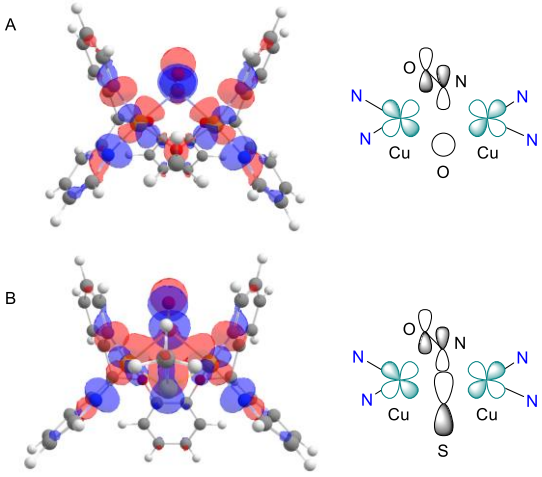

Figure 5. HOMO-1 of a truncated model of **4** and **7** rendered at a contour value of 0.03.

Notably, while dicopper (II,II) μ-NO, μ-OMe complex **4** is stable enough for isolation, the isoelectronic dicopper (II,II) μ-NO, μ-SR complex **7** is not observed in the reaction even at −80 °C. To further understand this key difference between dicopper-promoted *S*-nitrosation and *O*-nitrosation, the electronic structures of **4** and **7** are investigated by density functional theory (DFT) at B3LYP/TZVP/D3 level. To simplify our analysis, the axial ligands (OTf and HOMe) are omitted in the calculation. The optimized geometry of a model of **4** agrees well with the X-ray single-crystal structure (Figure S61). A model of **7** with bridging SMe ligand is optimized as a comparison at the same level of theory. The most significant difference between the electronic structure of **4** and **7** is the HOMO-1, which is primarily composed of the copper d orbitals and NO π^* orbital (Figure 5). While the HOMO-1 of **4** only has minimal density on the bridging OMe ligand (Figure 5A), the HOMO-1 of **7** displays significant contribution from the SMe p orbital, which forms a σ interaction with the nitrosyl π^* orbital (Figure 5B). The better orbital overlap between S and NO in comparison to O and NO might explain the high tendency of **7** to reductively eliminate RSNO.

On the nitrosative reactivity of Ceruloplasmin

Ceruloplasmin (CP), a copper protein that exists in high concentration in plasma (1-5 µM),[43,44] has been shown to catalyze the conversion of glutathione (GSH) to *S*-nitrosoglutathione in vivo.[7] CP contains several T1 electron transfer sites and a T2/T3 copper site.[45,46] Previously, it was proposed that CP nitrosates thiol by oxidizing NO• to nitrosonium (NO^+).[7,47] However, this mechanism contradicts the high aqueous oxidation potential of NO• (+1.2 V vs. NHE)[48] and mild redox potential of Cp (0.4-0.5 V vs. NHE).[49]

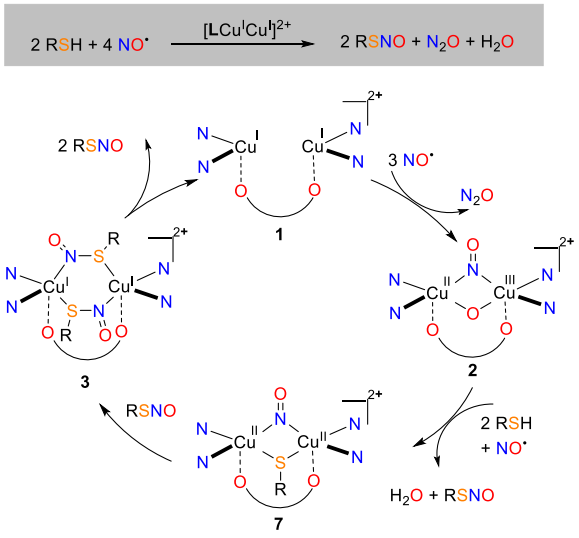

Figure 6. Proposed reaction cycles for redox- and proton-neutral coupling of RSH and NO• to RSNO at a dicopper center.

The mechanistic steps established in this work has important implication in the *S*-nitrosation ability of CP (Figure 6). Considering complex **1** as a functional mimic of binuclear copper centers, a dicopper(II,III) μ-O, μ-NO species **2** can be accessed by activation of NO•.[24] Complex **2** undergoes stepwise *S*-nitrosation to afford dicopper(I,I) di- or mono-*S*-nitrosothiol complex **3**. Release of *S*-nitrosothiol from **3** regenerates the dicopper(I,I) species **1** and completes the reaction cycle. This new mechanism is fully consistent with the redox potential of NO• and its reactivity at copper centers. *S*-nitrosation at T2/T3 site would require the participation of two of three Cu, although the engagement of the third Cu is also possible. Excess NO• could potentially coordinate to the T1 site and prevent electron transfer. However, this process would not impede the coupling of NO• and thiol since the overall *S*-nitrosation reaction is redox-neutral.

Conclusion

In contrast to the prevailing reductive *S*-nitrosation mechanism, we demonstrate that dicopper complex can promote redox- and proton-neutral *S*-nitrosation of thiols. A primary thiol, 2-phenylethanethiol is used as a model substrate to prove the proposed *S*-nitrosation process. We also show the *S*-nitrosation of bioinspired N-acetyl-*L*-cysteine methyl ester to the corresponding RSNO. Spectroscopic characterization suggests that the dicopper(I,I) complex **1** can bind up to two equivalents of RSNO via μ-κ^1-N: κ^1-S binding modes in THF and acetone. Reductive coupling of NO$^\bullet$ at biological and bioinspired FeFe or FeCu centers, e.g. NO reductase, are well known.[50] Seminal work by Tolman and Karlin has shown that synthetic copper complexes can promote a similar NO$^\bullet$ coupling reaction and generate N_2O. We now demonstrate such a dicopper-promoted NO$^\bullet$ process could be a potential strategy to facilitate the storage of NO$^\bullet$ as *S*-nitrosothiol. The new redox-neutral *S*-nitrosation mechanism presented here potentially connects excess NO$^\bullet$ with an elevated level of S-nitrosothiols, adding further implications for the possible involvement of binuclear sites, such as T3, Cu_A and dicopper amyloid b complexes, in the homeostasis of NO and *S*-nitrosothiols. Since dicopper(II,III) μ-O μ-NO complex **2** can be accessed by activation of nitrite (NO_2^-), the reaction cycle depicted in Figure 6 is also relevant to NO_2^-, another ubiquitous, air-stable source of NO$^\bullet$. Conversion of NO_2^- to low-mass *S*-nitrosothiols, e.g. *S*-nitrosoglutathione and *S*-nitrosocysteine, represents an alternative pathway to propagate nitrosative signals far from the dicopper sites.[32]

Acknowledgements

This material is based on work supported by the U.S. National Science Foundation under award No. CHE-1904560. Jamey Bower is acknowledged for EPR measurement and single-crystal X-ray diffraction measurement. Tanya Whitmer is acknowledged for low-temperature NMR measurement. The authors thank The Ohio State University Department of Chemistry and Biochemistry for additional financial support.

Keywords: *S*-nitrosation • Copper • Nitric oxide • *O*-nitrosation • Bimetallic

Reference

[1] M. T. Forrester, M. Benhar, J. S. Stamler, *ACS Chem. Biol.* **2006**, *1*, 355–358.

[2] T. Uehara, T. Nakamura, D. Yao, Z.-Q. Shi, Z. Gu, Y. Ma, E. Masliah, Y. Nomura, S. A. Lipton, *Nature* **2006**, *441*, 513-517.

[3] D. H. Cho, T. Nakamura, J. Fang, P. Cieplak, A. Godzik, Z. Gu, S. A. Lipton, *Science* **2009**, *324*, 102–106.

[4] K. K. K. Chung, B. Thomas, X. Li, O. Pletnikova, J. C. Troncoso, L. Marsh, V. L. Dawson, T. M. Dawson, *Science* **2004**, *304*, 1328–1331.

[5] D. Yao, Z. Gu, T. Nakamura, Z.-Q. Shi, Y. Ma, B. Gaston, L. A. Palmer, E. M. Rockenstein, Z. Zhang, E. Masliah, et al., *Proc. Natl. Acad. Sci. USA* **2004**, *101*, 10810–10814.

[6] C. M. Schonhoff, M. Matsuoka, H. Tummala, M. A. Johnson, A. G. Estevéz, R. Wu, A. Kamaid, K. C. Ricart, Y. Hashimoto, B. Gaston, et al., *Proc. Natl. Acad. Sci. USA* **2006**, *103*, 2404–2409.

[7] K. Inouet, T. Akaike, Y. Miyamoto, T. Okamoto, T. Sawa, M. Otagiri, S. Suzuki, T. Yoshimura, H. Maeda, *J. Biol. Chem.* **1999**, *274*, 27069–27075.

[8] P. Moriel, I. R. O. Pereira, M. C. Bertolami, D. S. P. Abdalla, *Free Radic. Biol. Med.* **2001**, *30*, 318–326.

[9] V. G. Kharitonov, A. R. Sundquist, V. S. Sharma, *J. Biol. Chem.* **1995**, *270*, 28158–28164.

[10] M. N. Möller, Q. Li, J. R. Lancaster, A. Denicola, *IUBMB Life* **2007**, *59*, 243–248.

[11] M. G. Espey, D. D. Thomas, K. M. Miranda, D. A. Wink, *Proc. Natl. Acad. Sci. USA* **2002**, *99*, 11127–11132.

[12] M. Boese, P. I. Mordvintcev, A. F. Vanin, R. Busse, A. Mulsch, *J. Biol. Chem.* **1995**, *270*, 29244–29249.

[13] A. F. Vanin, I. V. Malenkova, V. A. Serezhenkov, *Nitric Oxide* **1997**, *1*, 191–203.

[14] A. Weichsel, E. M. Maes, J. F. Andersen, J. G. Valenzuela, T. K. Shokhireva, F. A. Walker, W. R. Montfort, *Proc. Natl. Acad. Sci. USA* **2005**, *102*, 594–599.

[15] C. A. Bosworth, J. C. Toledo, J. W. Zmijewski, Q. Li, J. R. Lancaster, *Proc. Natl. Acad. Sci. USA* **2009**, *106*, 4671–4676.

[16] L. Tao, A. M. English, *Biochemistry* **2003**, *42*, 3326–3334.

[17] A. J. Jordan, R. K. Walde, K. M. Schultz, J. Bacsa, J. P. Sadighi, *Inorg. Chem.* **2019**, *58*, 9592–9596.

[18] V. K. K. Praneeth, F. Paulat, T. C. Berto, S. D. B. George, C. Näther, C. D. Sulok, N. Lehnert, *J. Am. Chem. Soc.* **2008**, *130*, 15288–15303.

[19] N. Xu, D. R. Powell, L. Cheng, G. B. Richter-Addo, *Chem. Commun.* **2006**, 2030.

[20] A. P. Hunt, N. Lehnert, *Inorg. Chem.* **2019**, *58*, 11317–11332.

[21] B. P. Luchsinger, E. N. Rich, A. J. Gow, E. M. Williams, J. S. Stamler, D. J. Singel, *Proc. Natl. Acad. Sci. USA* **2003**, *100*, 461–466.

[22] S. Tian, J. Liu, R. E. Cowley, P. Hosseinzadeh, N. M. Marshall, Y. Yu, H. Robinson, M. J. Nilges, N. J. Blackburn, E. I. Solomon, et al., *Nat. Chem.* **2016**, *8*, 670–677.

[23] S. Zhang, M. M. Melzer, S. N. Sen, N. Çelebi-Ölçüm, T. H. Warren, *Nat. Chem.* **2016**, *8*, 663–669.

[24] W. Tao, J. K. Bower, C. E. Moore, S. Zhang, *J. Am. Chem. Soc.* **2019**, *141*, 10159–10164.

[25] M. Gennari, C. Duboc, *Acc. Chem. Res.* **2020**, *53*, 2753–2761.

[26] A. Franke, G. Stochel, N. Suzuki, T. Higuchi, K. Okuzono, R. van Eldik, *J. Am. Chem. Soc.* **2005**, *127*, 5360–5375.

[27] S. Basu, A. Keszler, N. A. Azarova, N. Nwanze, A. Perlegas, S. Shiva, K. A. Broniowska, N. Hogg, D. B. Kim-Shapiro, *Free Radic. Biol. Med.* **2010**, *48*, 255–263.

[28] K. A. Broniowska, A. Keszler, S. Basu, D. B. Kim-Shapiro, N. Hogg, *Biochem. J.* **2012**, *442*, 191–197.

[29] S. F. Kim, D. A. Huri, S. H. Snyder, *Science* **2005**, *310*, 1966–1970.

[30] D. T. Hess, A. Matsumoto, S. O. Kim, H. E. Marshall, J. S. Stamler, *Nat. Rev. Mol. Cell Biol.* **2005**, *6*, 150–166.

[31] T. Rassaf, P. Kleinbongard, M. Preik, A. Dejam, P. Gharini, T. Lauer, J. Erckenbrecht, A. Duschin, R. Schulz, G. Heusch, et al., *Circ. Res.* **2002**, *91*, 470–477.

[32] S. Kundu, W. Y. Kim, J. A. Bertke, T. H. Warren, *J. Am. Chem. Soc.* **2017**, *139*, 1045–1048.

[33] C. Zhang, T. D. Biggs, N. O. Devarie-Baez, S. Shuang, C. Dong, M. Xian, *Chem. Commun.* **2017**, *53*, 11266–11277.

[34] J. K. Bower, A. Y. Sokolov, S. Zhang, *Angew. Chem. Int. Ed.* **2019**, *58*, 10225–10229; *Angew. Chem.* **2019**, *131*, 10331-10335.

[35] P. C. Ford, B. O. Fernandez, M. D. Lim, *Chem. Rev.* **2005**, *105*, 2439–2455.

[36] I. G. Dance, *J. Chem. Soc., Chem. Commun.* **1976**, 68–69.

[37] V. Hosseininasab, A. C. McQuilken, A. (Gus) Bakhoda, J. A. Bertke, Q. K. Timerghazin, T. H. Warren, *Angew. Chem. Int. Ed.* **2020**, *59*, 10854–10858; *Angew. Chem.* **2020**, *132*, 10946-10950.

[38] N. Hendinejad, Q. K. Timerghazin, *Phys. Chem. Chem. Phys.* **2020**, *22*, 6595–6605.

[39] Q. K. Timerghazin, G. H. Peslherbe, A. M. English, *Org. Lett.* **2007**, *9*, 3049–3052.

[40] L. L. Perissinotti, D. A. Estrin, G. Leitus, F. Doctorovich, *J. Am. Chem. Soc.* **2006**, *128*, 2512–2513.

[41] M. M. Melzer, S. Jarchow-Choy, E. Kogut, T. H. Warren, *Inorg. Chem.* **2008**, *47*, 10187–10189.

[42] P. P. Paul, Z. Tyeklar, A. Farooq, K. D. Karlin, S. Liu, J. Zubieta, *J. Am. Chem. Soc.* **1990**, *112*, 2430–2432.

[43] P. Bielli, L. Calabrese, *Cell. Mol. Life Sci. C.* **2002**, *59*, 1413–1427.

[44] N. E. Hellman, J. D. Gitlin, *Annu. Rev. Nutr.* **2002**, *22*, 439–458.

[45] E. I. Solomon, U. M. Sundaram, T. E. Machonkin, *Chem. Rev.* **2002**, *96*, 2563–2606.

[46] N. Mano, H.-H. Kim, A. Heller, *J. Phys. Chem. B* **2002**, *106*, 8842–8848.

[47] A. Dejam, C. J. Hunter, M. M. Pelletier, L. L. Hsu, R. F. Machado, S. Shiva, G. G. Power, M. Kelm, M. T. Gladwin, A. N. Schechter, *Blood* **2005**, *106*, 734–739.

[48] D. M. Stanbury, in *Adv. Inorg. Chem.* (Ed.: A.G.B.T.-A. in I.C. Sykes), Academic Press, **1989**, pp. 69–138.

[49] T. E. Machonkin, E. I. Solomon, *J. Am. Chem. Soc.* **2000**, *122*, 12547–12560.

[50] C. Ferousi, S. H. Majer, I. M. Dimucci, K. M. Lancaster, *Chem. Rev.* **2020**, *120*, 5252–5307.

Electronic Supporting Information for:

Redox-neutral *S*-nitrosation Mediated by a Dicopper Center

Wenjie Tao, Curtis E. Moore, and Shiyu Zhang*

Department of Chemistry and Biochemistry, The Ohio State University, Columbus, Ohio 43210

Contents

1.Materials and Methods

General: All reactions were carried out under a nitrogen atmosphere in an MBraun glovebox or using Schlenk techniques. All glassware was dried at 120 °C prior to use.

Instrumentation: Nuclear magnetic resonance (NMR) spectra were recorded on AVIII HD 600 MHz (^{1}H: 600 MHz, ^{13}C: 151 MHz) or Bruker 850 MHz Ascend (^{1}H: 850 MHz, ^{13}C: 214 MHz) at ambient temperature unless otherwise noted. Chemical shift values for protons are referenced to the residual proton resonance of chloroform-d_1 (δ: 7.26 ppm), acetone-d_6 (δ: 2.05 ppm), THF-d_8 (δ: 3.58 ppm) or CD_3CN (δ: 1.94 ppm). Chemical shift values for carbons are referenced to the carbon resonance of chloroform-*d* (δ: 77.16 ppm), acetone-d_6 (δ: 206.26 ppm), THF-d_8 (δ: 67.21 ppm) or CD_3CN (δ: 118.26 ppm). X-ray crystallographic analyses were performed under a cold nitrogen stream (Oxford Cryosystems Cryostream) at 150(2) or 100(2) K on a Bruker D8 Venture instrument with Mo Ka radiation source (λ = 0.7107 Å) and a Photon II detector. Elemental analyses were performed by Midwest Micro Lab (Indianapolis, IN, http://midwestlab.com/). High-resolution mass spectra were recorded on a Bruker MicrOTOF (ESI). EPR measurements were performed in 4 mm low-pressure quartz tubes on a Bruker EMXPlus X-band EPR spectrometer equipped with a Coldedge cryostat with small-volume power saturation. Solution in-situ IR was recorded on a Mettler Toledo RiR15 spectrometer.

Materials: NO (>99.99%) was purchased from Praxair and purified by passing through a column of Ascarite (8-20 mesh, Sigma-Aldrich) and collected in a Schlenk flask type glassware at 1 atm. A specific volume of NO(g) was collected and injected into the reaction flask for the reactions using NO(g). Dichloromethane, acetonitrile, diethyl ether, pentane, tetrahydrofuran was dried and degassed under nitrogen using a Pure Process Technologies (PPT, Nashua, NH) solvent purification system, and stored over 4 Å molecular sieves. Anhydrous acetone was purchased from Acros and was used as received. Anhydrous toluene was dried and degassed under nitrogen using Pure Solv Innovative Technology solvent purification system and stored over 4 Å molecular sieves. $CDCl_3$, CD_3CN, THF-d_8, and acetone-d_6 (Cambridge Isotope Laboratories, Inc.) were dried over 4 Å molecular sieves and deoxygenated by three freeze-pump-thaw cycles prior to use. 2-Phenylethanethiol (Sigma-Aldrich), 1-adamantanethiol (Sigma-Aldrich), 4-methoxythiophenol (Sigma-Aldrich), 4-bromothiophenol (Alfa Aesar), trifluoroacetic acid (Sigma-Aldrich), sodium nitrite-^{15}N (Cambridge Isotope Laboratories, Inc.), di(2-pyridyl)ketone (Combi-Blocks), $NaBH_4$ (Merck KGaA), carbon tetrachloride (Sigma-Aldrich), catechol (Acros), tetrakis(acetonitrile) copper(I) tetrafluoroborate (Sigma-Aldrich), tetrakis(acetonitrile) copper(I) triflate (Sigma-Aldrich), tetrakis(acetonitrile) copper(I) hexafluorophosphate (Sigma-Aldrich), LHMDS (Acros) were purchased and used without further purification. $NaB[3,5\text{-}(CF_3)_2C_6H_4]_4$ ($NaBAr^F{}_4$),[1] 2,2'-(chloromethylene)dipyridine,[2] $Cu(MeCN)_4BAr^F{}_4$,[3] N-acetyl *L*-cysteine methyl ester[4] were synthesized following the literature procedures.

Synthesis of $PhCH_2CH_2SNO$

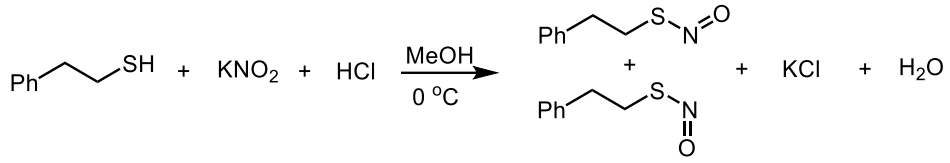

The synthesis of $PhCH_2CH_2SNO$ is enlightened by the reported literature precedents[5–7] and modified as follows. In the glove box, 2-phenylethanethiol (166 mg, 161 μL, 1.20 mmol, 1.0 eq.) and potassium nitrite (205 mg, 2.40 mmol, 2.0 eq.) were dissolved in *ca.* 10 mL of methanol and then transferred into a 15 mL pressure flask. The flask was taken out of glove box, connected to Schlenk line, and cooled in an ice/water bath. Under positive nitrogen flow, HCl (2.40 mmol, 0.60 mL of 4.0 M in dioxane, 2.0 eq.) was injected into the above solution and the mixture was stirred at this temperature for *ca.* 1.0 h. The flask was transferred back into the glove box and the suspension was concentrated under vacuum. Pentane (*ca.* 10 mL) was added to extract the product. The pentane solution was filtered through a plug of Celite and the plug was washed with additional pentane *ca.* 3.0 mL. The combined filtrate was dried under vacuum for 2.0 h, affording a red oil product (155 mg, 77%), which can be stored in the freezer of the glove box at −35 ℃ for months. Based on literature precedents, *S*-nitrosothiols are usually light sensitive. While handing $PhCH_2CH_2SNO$, we tried to avoid light. The ^{13}C NMR spectroscopic results (Figures S2 and S3) of product $PhCH_2CH_2SNO$ at room temperature are consistent with those reported in literature precedents in that there are *syn* and *anti* isomers via rotation around S-N bond[5].

^1H NMR (600 MHz, $CDCl_3$) δ 7.34-7.20 (m, 5H), 3.02-2.99 (m, 2H), 2.97-2.94 (m, 2H). The other isomer has signals at δ 3.77 (b, 2H), 2.84 (b, 2H). We observe two sets of ^1H NMR signals corresponding to the *syn* and *anti* isomers. The aromatic signals are overlapped at region δ 7.34-7.20. Based on the ^1H NMR integrals, the ratio of the two isomers is *ca* 1:1.

^{13}C NMR (151 MHz, $CDCl_3$) δ 140.19, 128.79 (2C), 128.70 (2C), 126.56, 40.37, 35.89. The other isomer has signals at δ 139.35, 128.76 (2C), 128.63 (2C), 126.95, 35.33, 34.96. We observe two sets of ^{13}C NMR signals corresponding to the *syn* and *anti* isomers (Figure S2).

We were unable to characterize the titled compound by HRMS-ESI due to its instability.

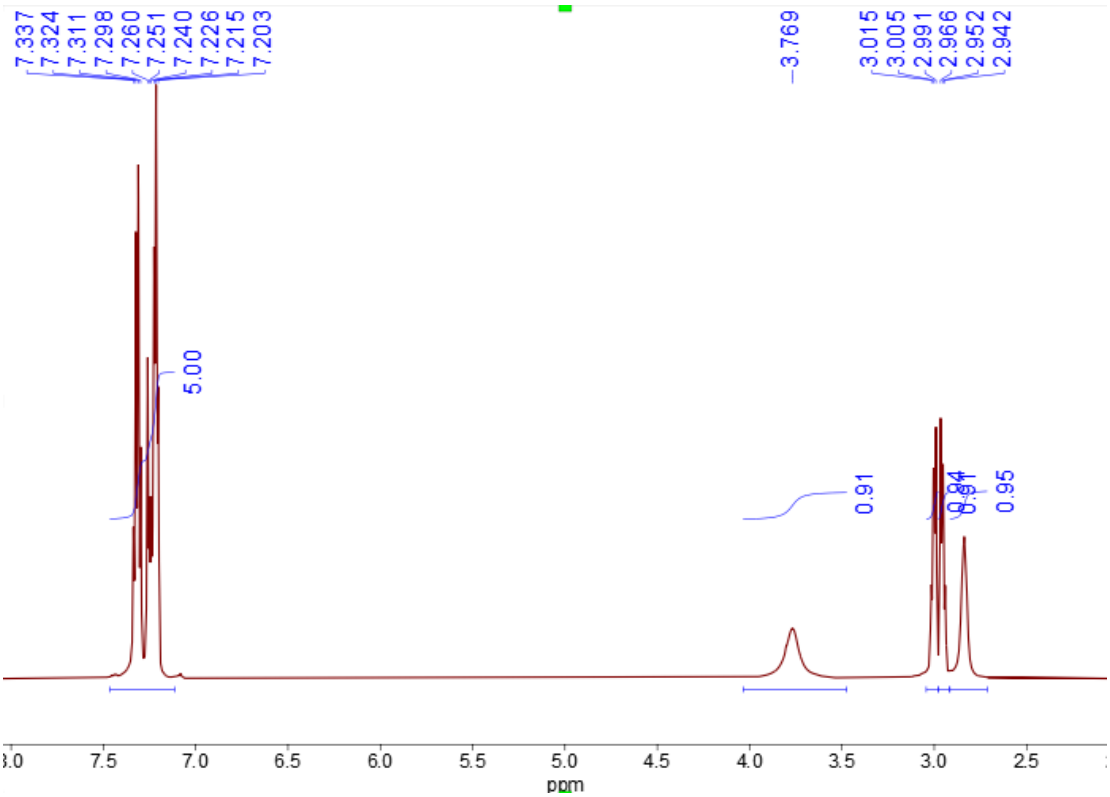

Figure S1: ^{1}H NMR (600 MHz, $CDCl_3$) spectrum of compound $PhCH_2CH_2SNO$.

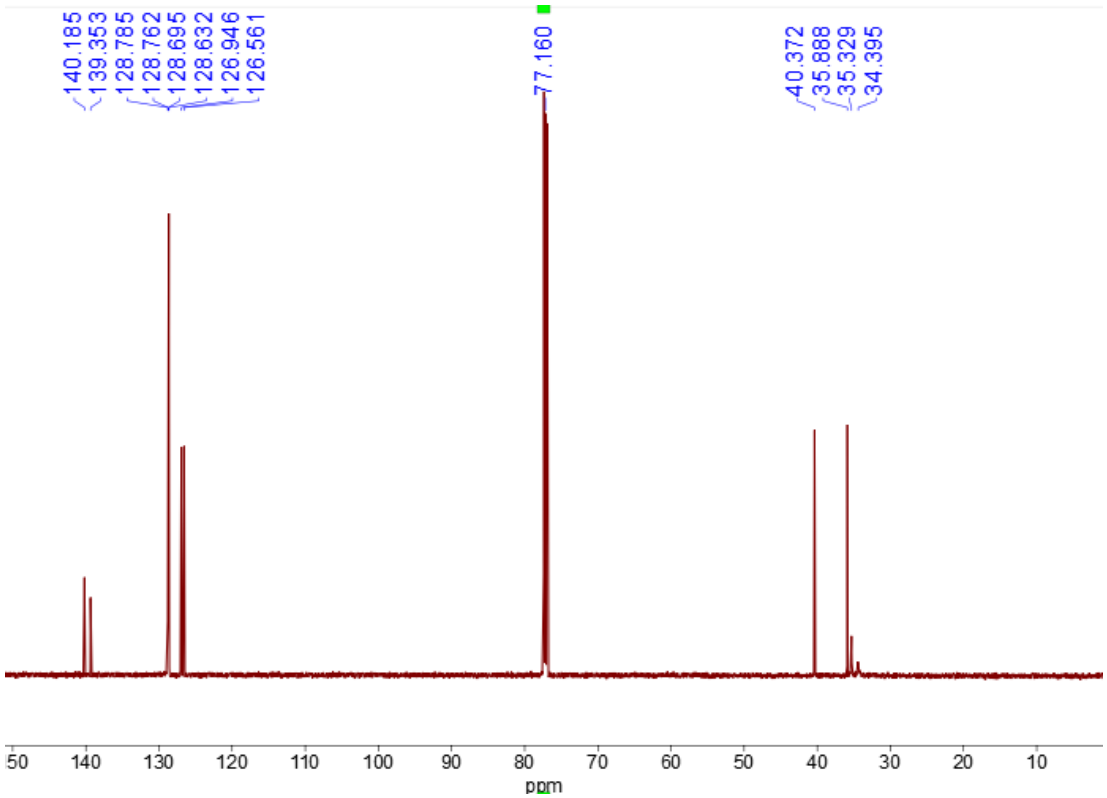

Figure S2: ^{13}C NMR (151 MHz, $CDCl_3$) spectrum of compound $PhCH_2CH_2SNO$.

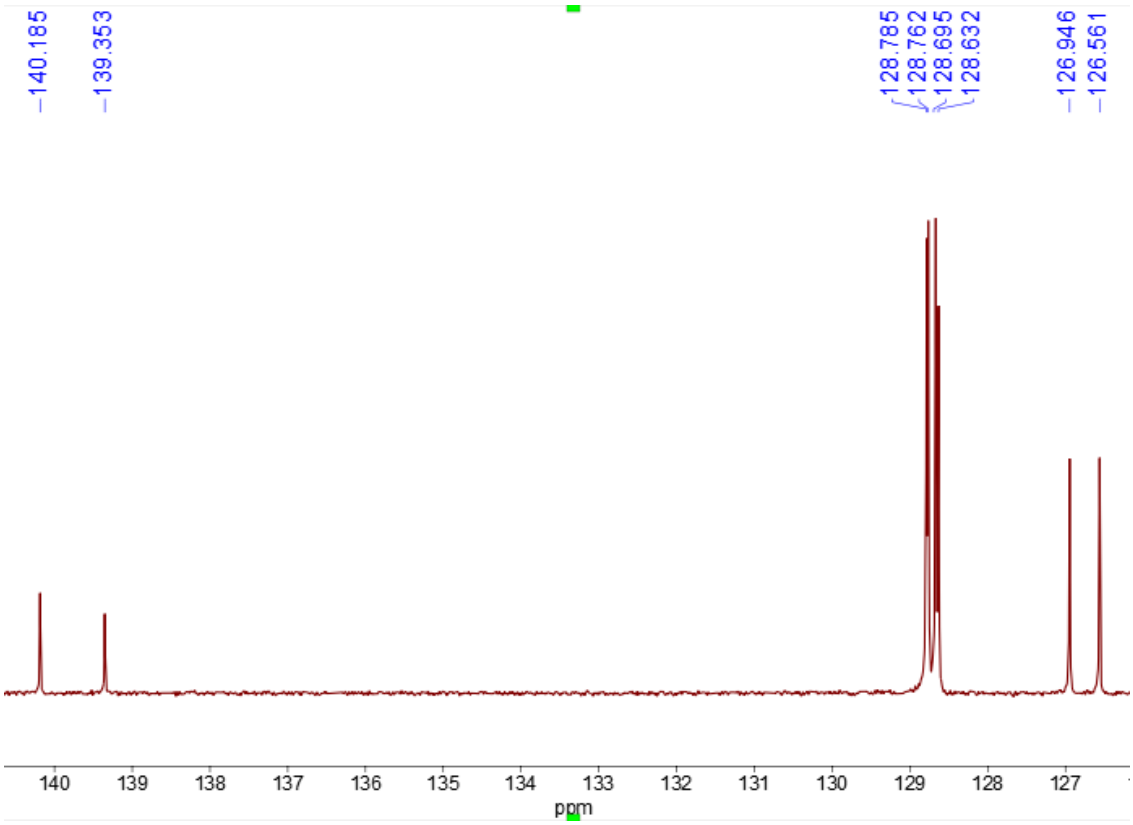

Figure S3: ^{13}C NMR (151 MHz, $CDCl_3$) spectrum (126-141ppm) of compound $PhCH_2CH_2SNO$.

Synthesis of $PhCH_2CH_2S^{15}NO$

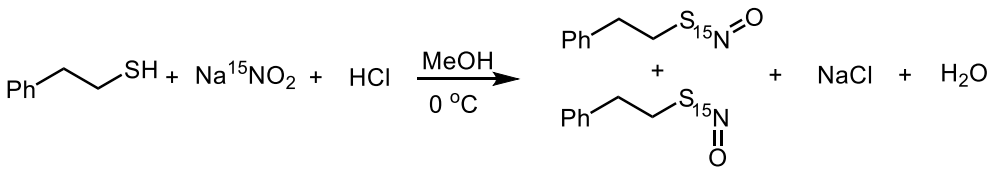

In the glove box, phenyl ethanethiol (247 mg, 1.79 mmol, 1.0 eq.) and sodium nitrite-^{15}N (150 mg, 2.14 mmol, 1.2 eq.) were dissolved in *ca.* 10 mL of methanol and then transferred into a 15 mL pressure flask. The flask was taken out of glove box, connected to Schlenk line, and cooled in an ice/water bath. Under positive nitrogen flow, HCl (2.14 mmol, 0.54 mL of 4.0 M in dioxane, 1.2 eq.) was injected into the above solution and the mixture was stirred at this temperature for *ca.* 1.0 h. The flask was transferred back into the glove box and the suspension was concentrated under vacuum. Pentane *ca.* 10 mL was added to extract the product. The pentane solution was filtered through a plug of Celite and the plug was washed with additional pentane *ca.* 3.0 mL. The combined filtrate was dried under vacuum for 2.0 h, affording a red oil product (254 mg, 84%).

^1H NMR (600 MHz, $CDCl_3$) δ 7.19.-7.32 (m, 5H), 3.75 (b, 2H), 2.82 (b, 2H); The other isomer has signals at: δ 2.98-3.01 (m, 2H), 2.93-2.96 (m, 2H). Based on the ^1H NMR, the ratio of the two isomers is 0.80:1.13 = 1:1.41.

^{13}C NMR (151 MHz, $CDCl_3$) δ 140.14, 128.72 (2C), 128.62(2C), 126.52, 40.33, 35.84. The other isomer's signals are: δ 139.30, 128.74 (2C), 128.59 (2C), 126.90, 35.28, 34.36.

^{15}N NMR (61 MHz, $CDCl_3$) δ 771.1 *vs.* NH_3.

We were unable to characterize the titled compound by HRMS-ESI due to its instability.

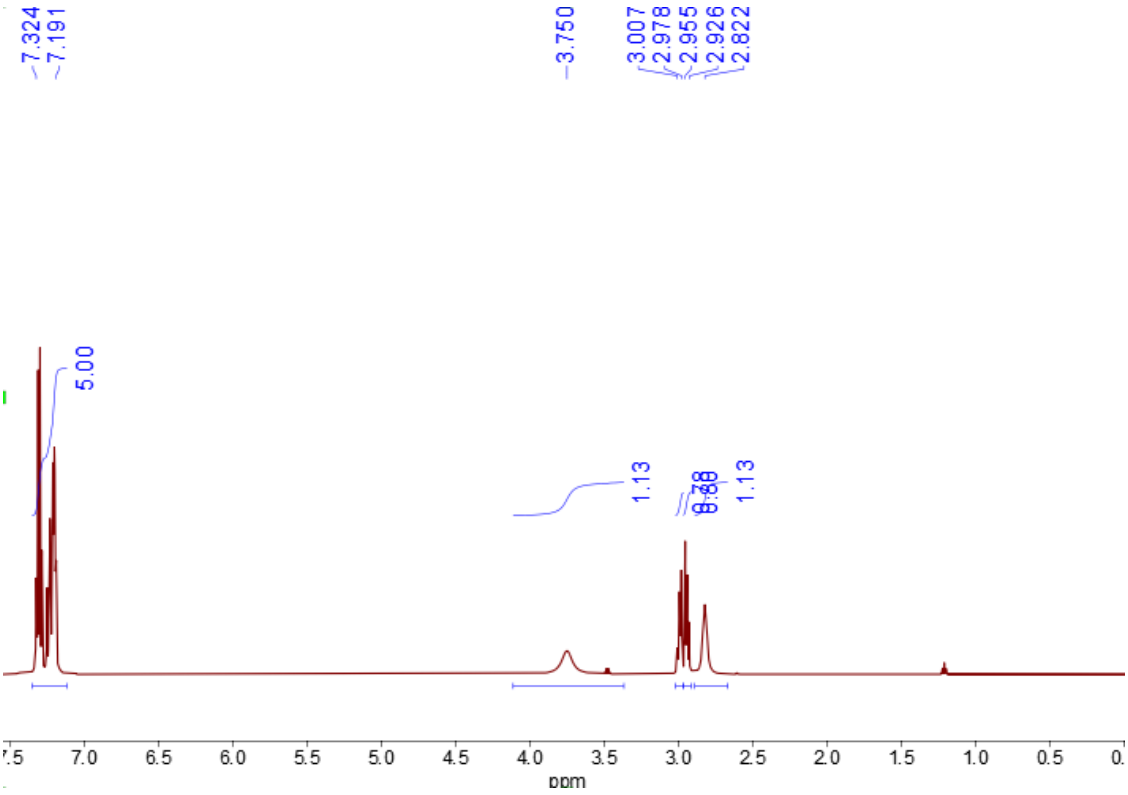

Figure S4: ^{1}H NMR (600 MHz, $CDCl_3$) spectrum of compound $PhCH_2CH_2S^{15}NO$.

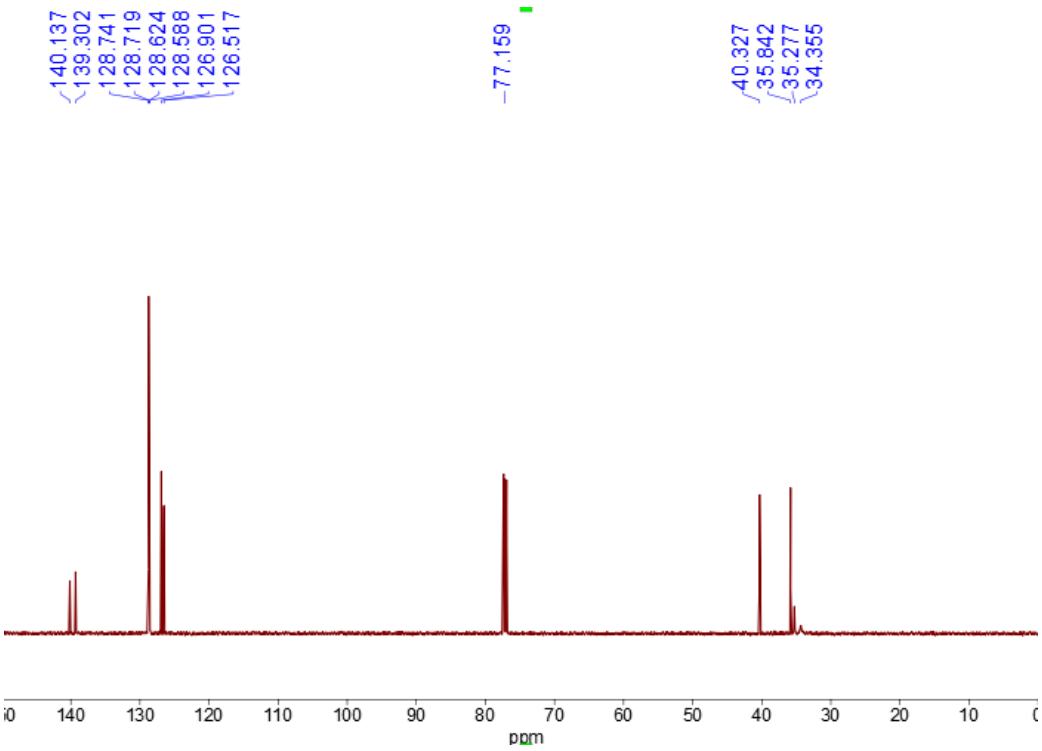

Figure S5: ^{13}C NMR (151 MHz, $CDCl_3$) spectrum of compound $PhCH_2CH_2S^{15}NO$.

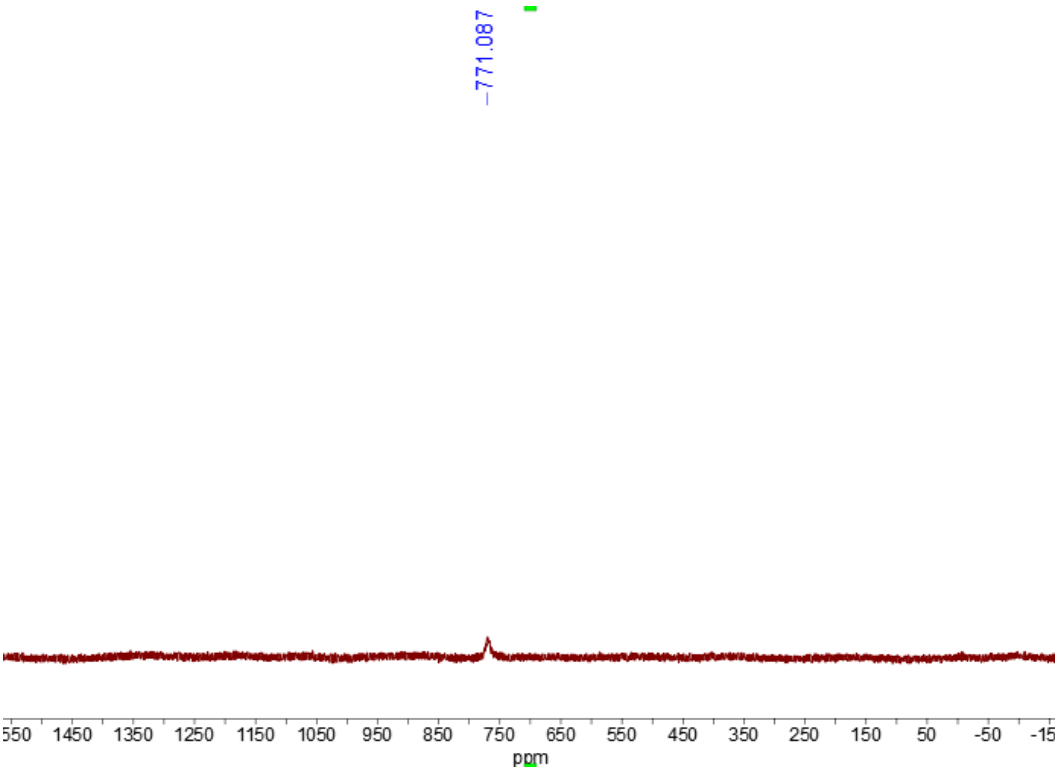

Figure S6: ^{15}N NMR (61 MHz, $CDCl_3$) spectrum of compound $PhCH_2CH_2S^{15}NO$. The ^{15}N chemical shift is referenced to NH_3 (0 ppm).

Synthesis of N-acetyl-*L*-cysteine methyl ester *S*-nitrosothiol

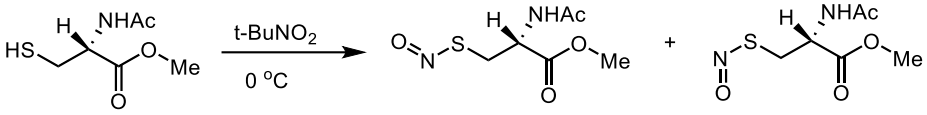

In the glove box, N-acetyl-*L*-cysteine methyl ester (400 mg, 2.26 mmol, 1.0 eq) was dissolved in *ca.* 4.0 mL of tetrahydrofuran and transferred into a 15 mL pressure flask. The pressure flask was taken out of the glove box, connected to Schlenk line, and cooled in −5℃ cold bath. Under positive nitrogen flow, *tert*-butyl nitrite (90%, 0.60 mL, 4.51 mmol, 2.0 eq) was injected into the above flask and the mixture was stirred at this temperature overnight. The color of the solution changed from colorless to dark red. The pressure flask was still maintained in the ice/water bath and connected to a vacuum to remove the volatiles. (Note: the product is unstable at RT, especially under vacuum.) The cold pressure flask was quickly transferred back to the glove box. Diethyl ether *ca.* 3.0 mL was used to extract the product and quickly filtered through a plug of celite. The plug was washed with additional diethyl ether *ca.* 2.0 mL. Pentane (*ca.* 10 mL) was layered on the top of the combined filtrate, and the vial was stored in the freezer of glove box at −35℃ overnight. The supernatant was decanted and the red crystals were quickly dried under vacuum for *ca.* 10 seconds. The vial was put back to the freezer and cooled again before a second drying for 10 seconds under vacuum, affording a red solid product (150 mg, 0.727 mmol, 32%). Elemental analysis was not performed because of its thermal instability.

^{1}H NMR (600 MHz, acetone-d_6) δ 7.49 (s, 1H), 4.78-4.63 (m, 1H), 4.22-4.04 (m, 2H), 3.69 (s, 3H), 1.88 (s, 3H).

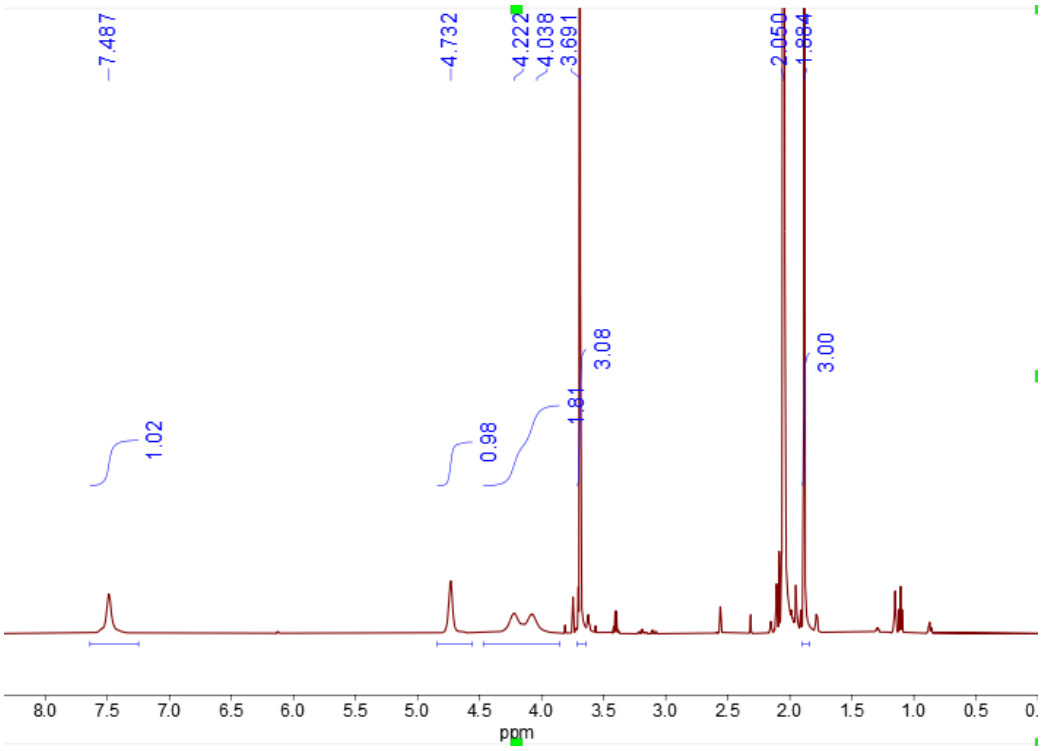

Figure S7: ^{1}H NMR (600 MHz, acetone-d_6) spectrum of N-acetyl-L-cysteine methyl ester *S*-nitrosothiol.

^{1}H NMR in $CDCl_3$ was measured in $CDCl_3$ as well, where we observe more clear evidence of the presence of two isomers.

^{1}H NMR (600 MHz, $CDCl_3$) δ 6.09 (s, 1H), 4.97-5.00 (m, 1H), 4.10-4.26 (m, 2H), 3.73 (s, 3H), 1.97 (s, 3H). The other isomer's signals are: δ 6.50 (d, *J* = 7.2 Hz, 1H), 4.89-4.86 (m, 1H), 3.77 (s, 3H), 2.06 (s, 3H). The methylene signals of two isomers are overlapped.

^{13}C NMR (151 MHz, $CDCl_3$) δ 170.41, 169.90, 53.09, 51.78, 40.90, 34.99, 23.09.

The other isomer's signals are: δ 171.01, 170.13, 52.92, 51.86, 23.24. Two carbon signals of the two isomers are overlapped.

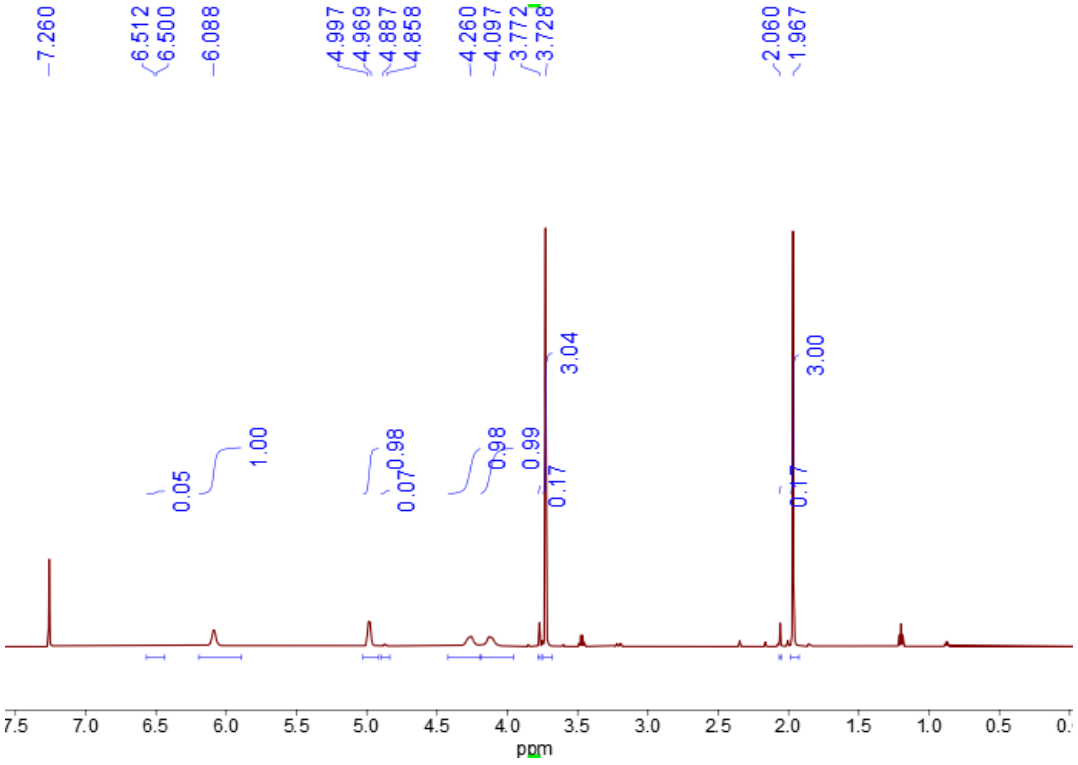

Figure S8: ^{1}H NMR (600 MHz, $CDCl_3$) spectrum of N-acetyl-*L*-cysteine methyl ester *S*-nitrosothiol.

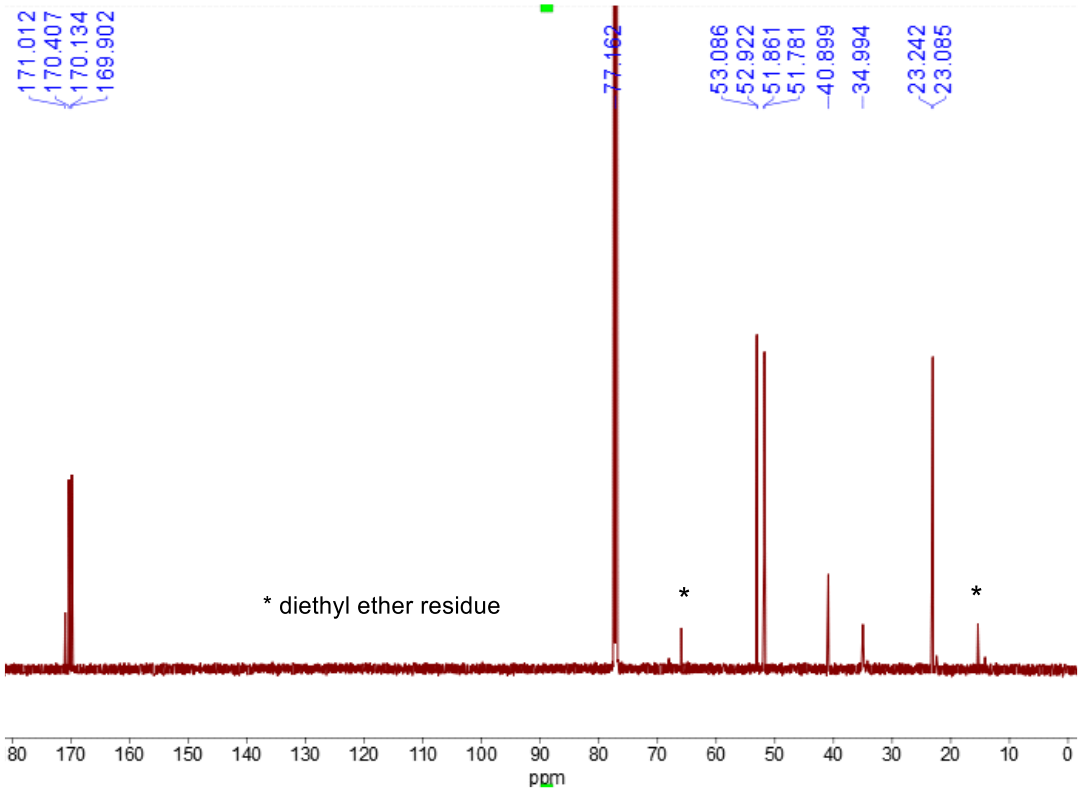

Figure S9: ^{1}H NMR (151 MHz, $CDCl_3$) spectrum of N-acetyl-*L*-cysteine methyl ester *S*-nitrosothiol.

Synthesis of ^{15}NO

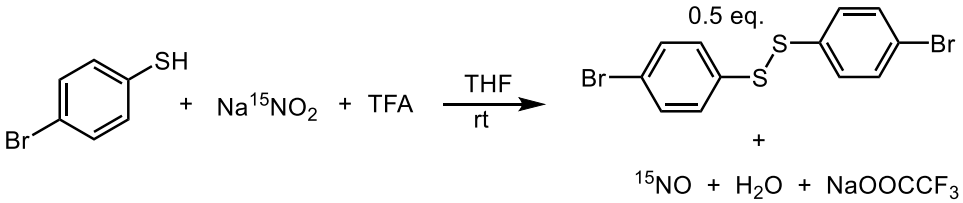

In the glove box, to a 20 mL scintillation vial with septum seal, 4-bromothiophenol (74.2 mg, 0.393 mmol, 1.1 eq.), sodium nitrite-^{15}N (25.0 mg, 0.357 mmol, 1.0 eq.), and degassed dry tetrahydrofuran (2.0 mL) were added. The vial was cooled in the glove box freezer (−35°C) for *ca.* 5 min, and trifluoroacetic acid (26 µL, 0.339 mmol, 0.95 eq.) was injected into the above suspension. The scintillation vial was quickly sealed and a 10 mL syringe with a 20 cm long needle was used to collect the generated ^{15}NO immediately. After stirring the mixture at RT for *ca.* 20 min, *ca.* 7.0 mL of gas was collected, which contained both nitrogen gas and ^{15}NO.

Theoretically, ^{15}NO (0.339 mmol, 8.1 mL) was formed under these conditions and the headspace contained *ca.* 18 mL of nitrogen originally. So in the 7.0 mL of gas collected in the syringe *ca.* 7.0 × 8.1/(8.1+18) = 2.2 mL of ^{15}NO (0.092 mmol) was included, if we consider ^{15}NO dissolved in the solvent is negligible.

Synthesis of 1-PF_6

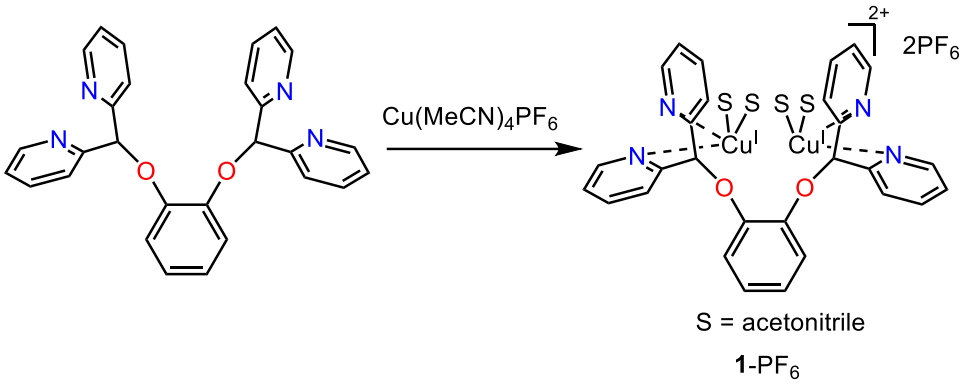

1-PF_6

In the glove box, ligand **L** (150 mg, 0.336 mmol, 1.0 equiv.) and tetrakis(acetonitrile) copper(I) hexafluorophosphate (261 mg, 0.679 mmol, 2.02 equiv.) were dissolved in acetonitrile (*ca.* 4.0 mL), and the resulting mixture was stirred at room temperature overnight. After the reaction, all volatiles were removed under vacuum and the crude product was washed with a mixture of THF (*ca.* 6.0 mL) and diethyl ether (*ca.* 3.0 mL) twice. The remaining solid was extracted with acetonitrile (*ca.* 1.5 mL) and filtered through a plug of Celite, and the plug was washed with additional acetonitrile (*ca.* 1.0 mL). Diethyl ether (*ca.* 12 mL) was slowly layered on the top of the acetonitrile, and the mixture was stored in a −40 °C freezer overnight to afford a yellow oily residue. The supernatant was decanted and the yellow oil was dried under vacuum for *ca.* 1.5 h, affording a yellow solid **1**-PF_6 (358 mg, 99%).

^{1}H NMR (600 MHz, CD_3CN) δ 8.63 (d, *J* = 3.0 Hz, 4H), 7.89 (t, *J* = 7.8 Hz, 4H), 7.82 (d, *J* = 7.8 Hz, 4H), 7.42 (t, *J* = 6.6 Hz, 4H), 7.00-6.98 (m, 2H), 6.89-6.87 (m, 2H), 6.63 (s, 2H), 1.97 (s, 12H).

^{13}C NMR (214 MHz, CD_3CN) δ 157.48, 150.61, 147.94, 139.62, 125.38, 124.07, 122.96, 82.34.

^{19}F NMR (565 MHz, CD_3CN) δ -73.0 (d, *J* = 707 Hz).

^{31}P NMR (243 MHz, CD_3CN) δ -144.6 (sep, *J* = 707 Hz).

Elemental analysis, Calcd for $C_{36}H_{34}Cu_2F_{12}N_8O_2P_2$: C, 42.07; H, 3.33; N, 10.90. Found: C, 42.66; H, 3.48; N, 10.59.

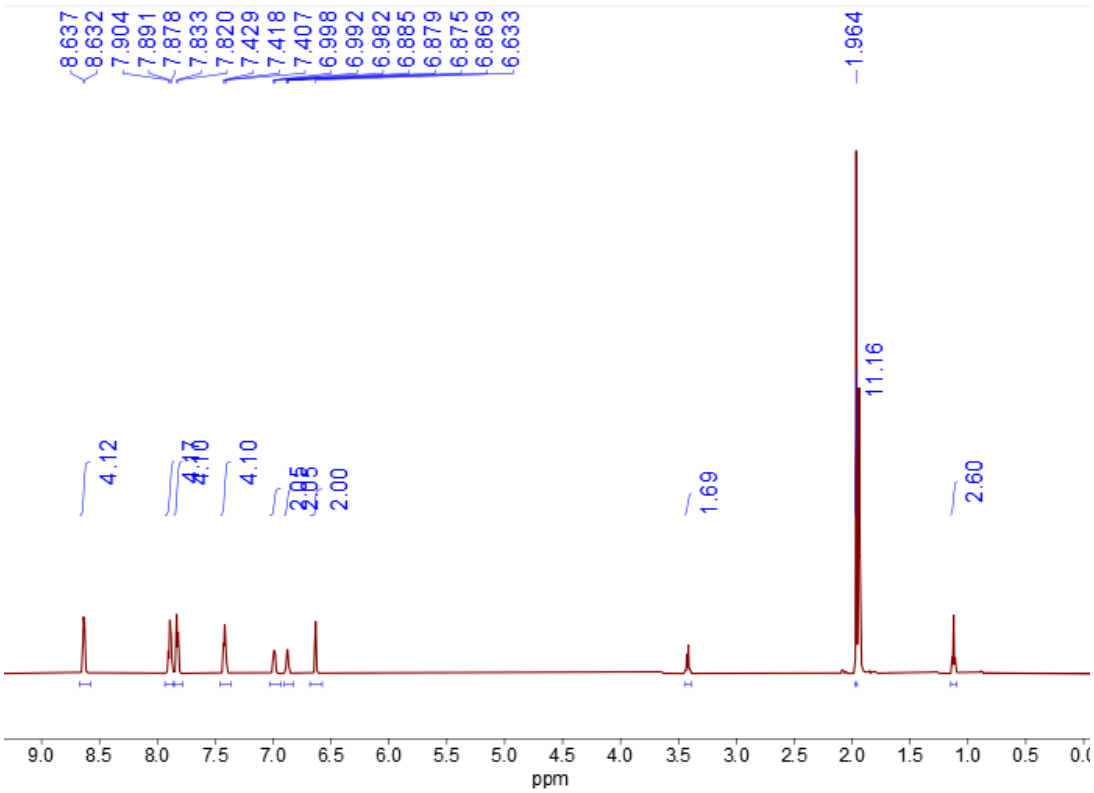

Figure S10: ^{1}H NMR (600 MHz, CD_3CN) spectrum of compound **1**-PF_6.

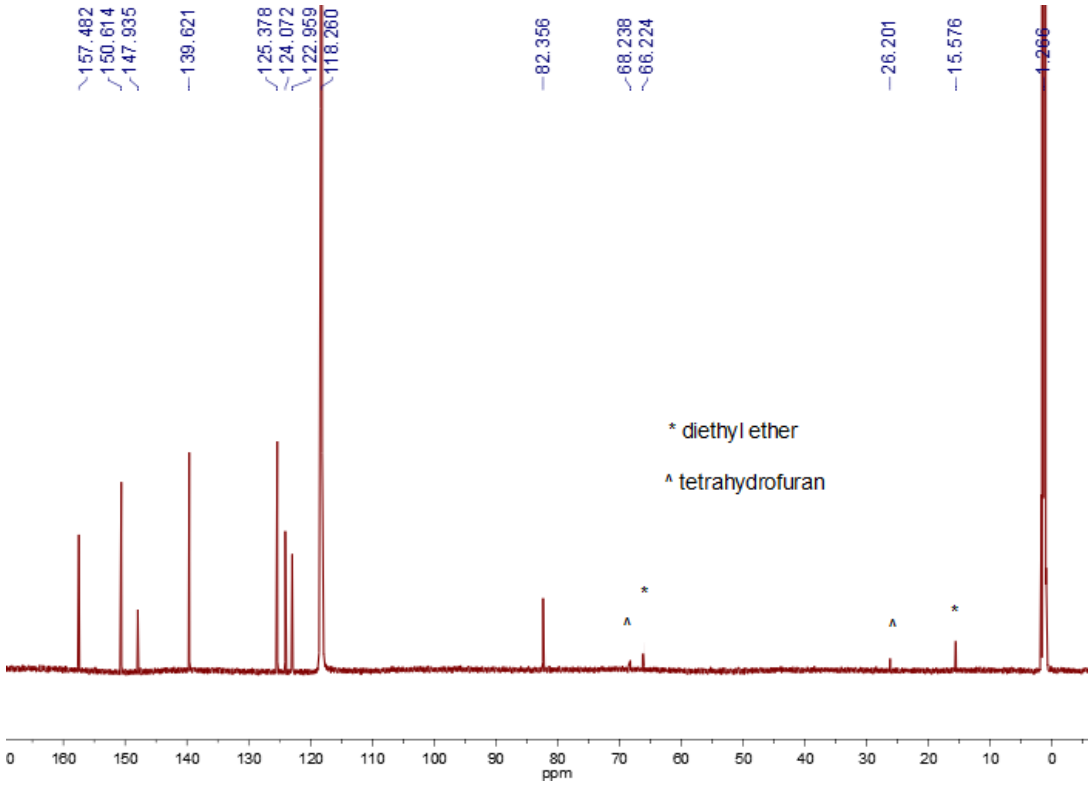

Figure S11: ^{13}C NMR (214 MHz, CD_3CN) spectrum of compound **1**-PF_6.

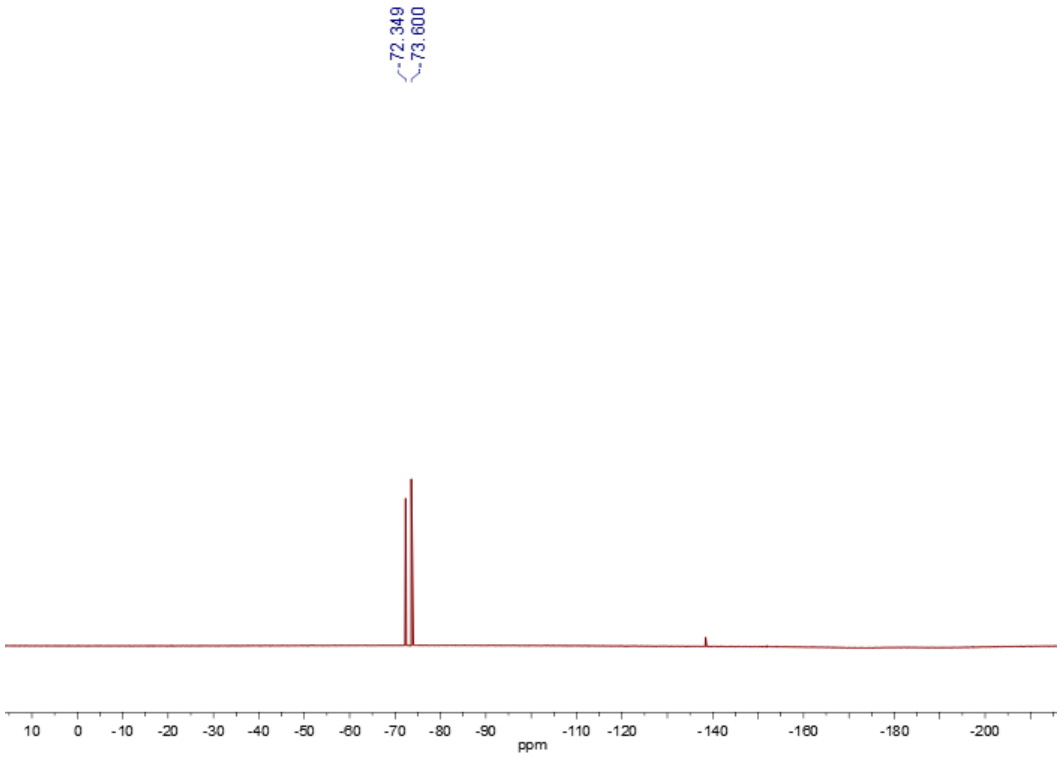

Figure S12: ^{19}F NMR (565 MHz, CD_3CN) spectrum of compound **1**-PF_6.

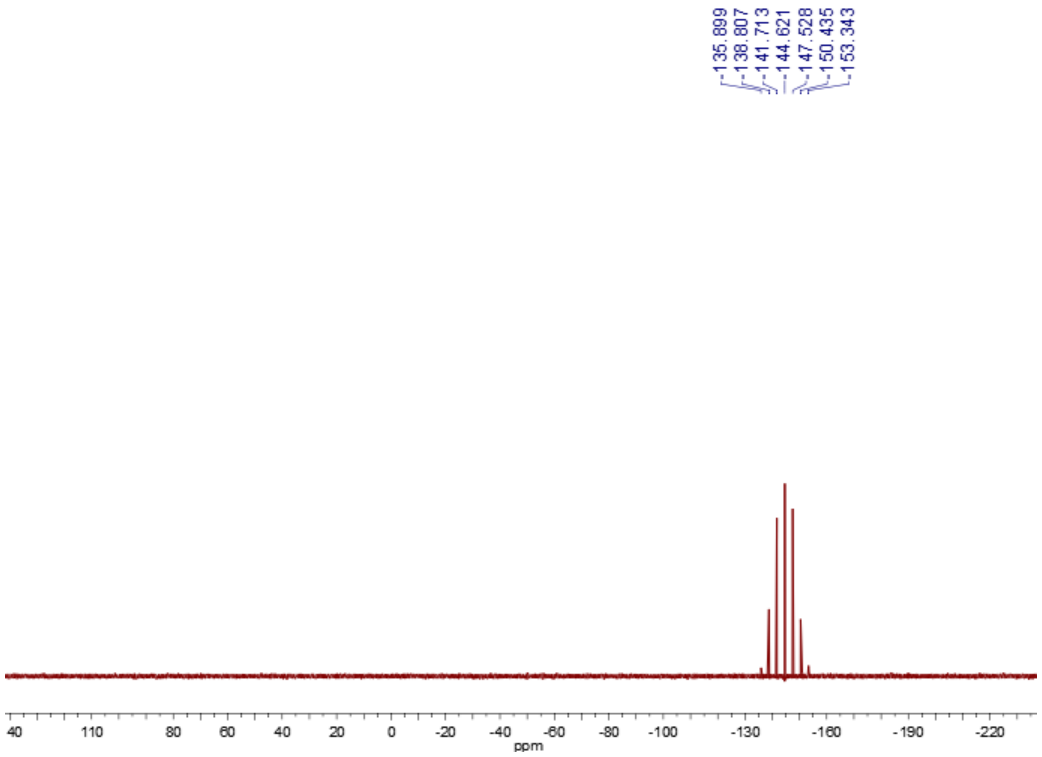

Figure S13: ^{31}P NMR (243 MHz, CD_3CN) spectrum of complex **1**-PF_6.

Synthesis of $LiSCH_2CH_2Ph$

In the glove box, 2-phenylethanethiol (150 mg, 1.09 mmol, 1.0 eq) was dissolved in THF (*ca*. 5.0 mL). To this solution was added a LiHMDS (191 mg, 1.14 mmol, 1.05 eq) solution in THF (*ca*. 4.0 mL). The mixture was stirred at room temperature for 1.0 h. After the reaction, all volatiles were removed under vacuum and the crude white solid was washed with pentane (*ca*. 10 mL) three times to remove the excess amount of LiHMDS. The remaining white precipitate was dried under vacuum for 1.0 h, affording $LiSCH_2CH_2Ph$ as a white solid (150 mg, 96%).

^{1}H NMR (600 MHz, THF-*d8*) δ 7.25-7.12 (m, 4H), 7.03-7.01 (m, 1H), 2.79-2.77 (m, 2H), 2.67-2.64 (m, 2H).

^{13}C NMR (151 MHz, THF-*d8*) δ 144.91 (1C), 128.90 (2C), 128.33 (2C), 125.53 (1C), 46.24 (1C), 28.68 (1C).

Elemental analysis, Calcd for C_8H_9LiS: C, 66.65; H, 6.29. Found: C, 64.32; H, 6.11.

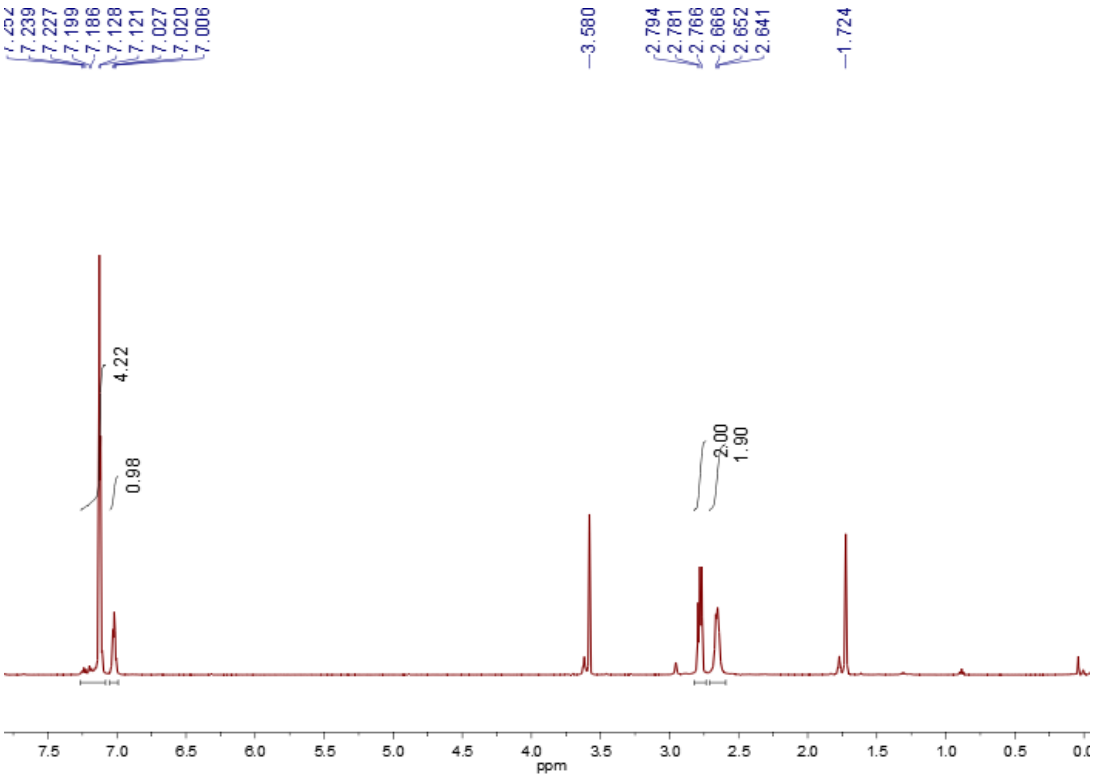

Figure S14: ^{1}H NMR (600 MHz, THF-d_8) spectrum of compound $PhCH_2CH_2SLi$.

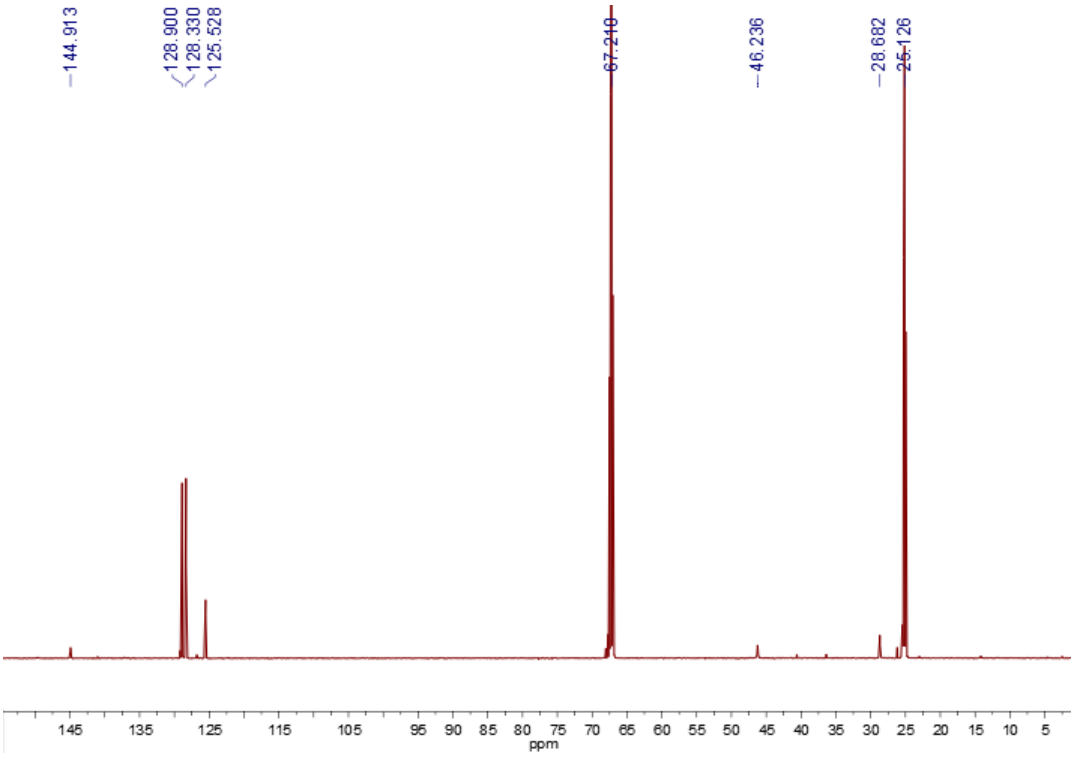

Figure S15: ^{13}C NMR (151 MHz, THF-d_8) spectrum of compound $PhCH_2CH_2SLi$.

Synthesis and characterization of 4-OTf

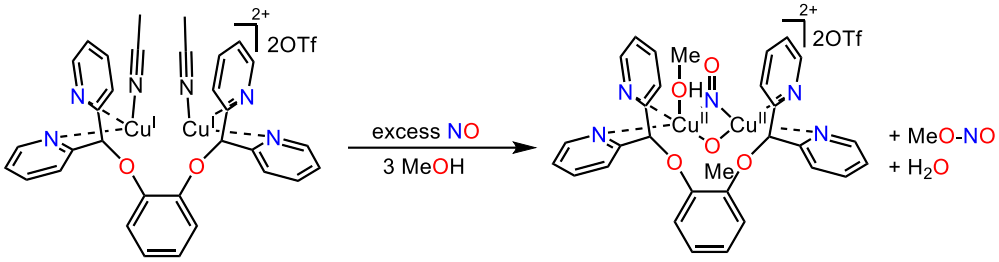

In the glovebox, **1**-OTf (40.0 mg, 41.9 μmol) was dissolved in methanol (5.0 mL) and transferred into a 15 mL pressure flask. The pressure flask was sealed, transferred out of the glovebox, and cooled in a −35 °C cold bath. Under positive nitrogen flow, NO• (10.0 mL, 0.417 mmol, 10 equiv.) was injected into the solution. The flask was sealed and the resulting reaction mixture was stirred in the cold bath at −35 °C overnight. The color of the solution gradually changed from yellow to green and finally to red. The pressure flask was then cooled in a dry ice/acetone bath for *ca.* 5 min and then quickly transferred back to the glovebox. The solution was pipetted into a vial precooled in a −35 °C freezer. Cold diethyl ether (*ca.* 8.0 mL, −35 °C) and cold toluene (*ca.* 2.0 mL, −35 °C) was carefully layered on top of the methanol solution. The dark red crystals formed after several days were collected and dried under vacuum to give **4**-OTf (27.0 mg, 67% yield) as a dark red solid. Elemental analysis of this compound was not performed due to its temperature sensitivity. Single crystal X-ray diffraction analysis was performed by picking single crystals of **4**-OTf to a precooled glass slide with cold oil.

2. UV-Vis and NMR spectroscopy Studies Details

Reaction of 1-BAr$^F_4$ with 2.0 eq. PhCH$_2$CH$_2$SNO in acetone

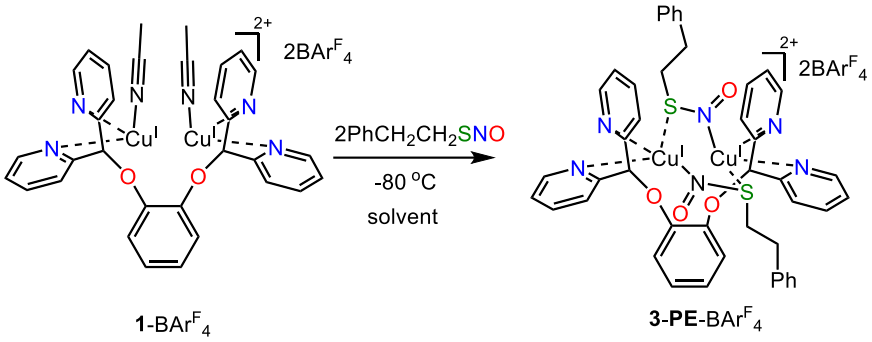

In the glovebox, an acetone solution of **1**-BAr$^F_4$ (5.4 mg, 2.3 μmol, 2.80 mL) was placed in a quartz cuvette equipped with a rubber septum. The cuvette was sealed and transferred to the UV-Vis spectrometer precooled at −80 °C. After the temperature stabilized, PhCH$_2$CH$_2$SNO (0.10 mL, 22.5 mM in acetone, 2.3 μmol, 1.0 equiv.) was injected to the solution, and the reaction progress was monitored by taking a UV-vis spectrum every 60 seconds. A new green species (λ_{max} = 575 nm, ε = 2400 M^{-1}cm^{-1} and λ_{max} = 675 nm, ε = 1450 M^{-1}cm^{-1}) is generated (Figure S16). A second equivalent of PhCH$_2$CH$_2$SNO (0.10 mL, 22.5 mM in acetone, 2.3 μmol, 1.0 equiv.) was injected to the above solution, and the reaction progress was monitored for another 36 min. The stabilized UV-Vis spectra after the addition of one or two equivalents of PhCH$_2$CH$_2$SNO are shown in Figure S17. The new green species started to decay quickly when the cuvette was warmed up to −50 °C in acetone.

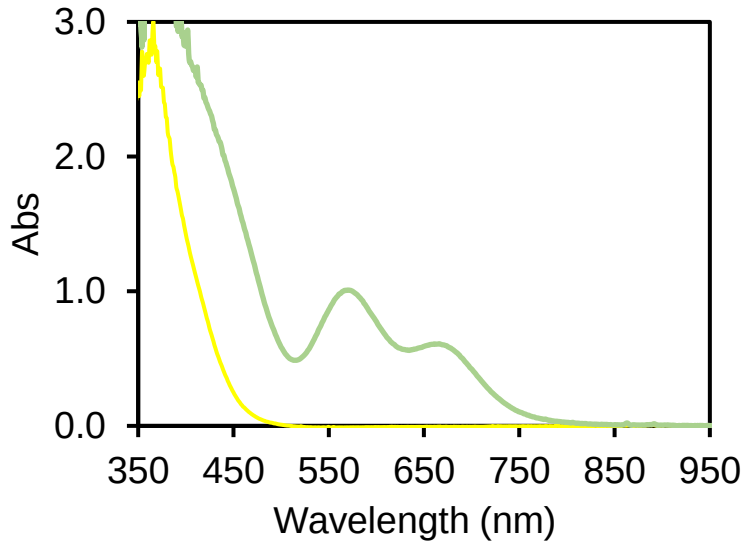

Figure S16. UV-Vis spectra of the reaction mixture of **1**-BAr$^F_4$ (yellow trace) and 1.0 eq. PhCH$_2$CH$_2$SNO (acetone, −80 °C) (light green trace)

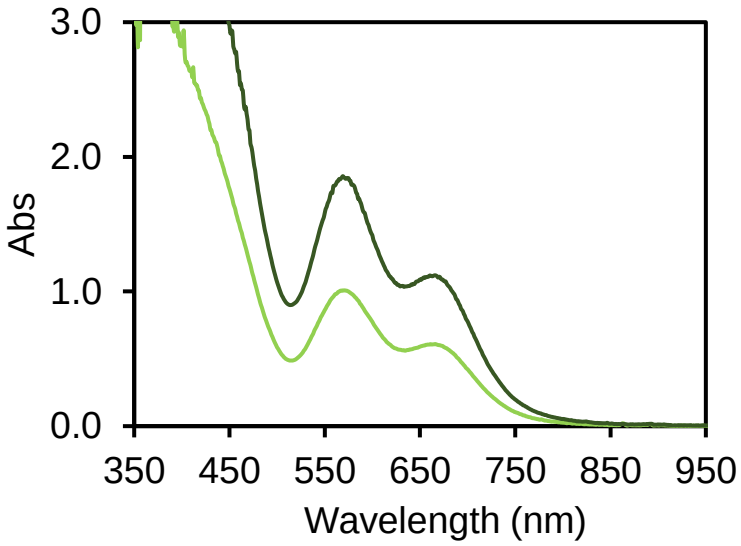

Figure S17. Comparison of UV-Vis spectra between the reaction mixture of **1**-BAr^F_4 and 1.0 eq. of $PhCH_2CH_2SNO$ (light green trace) and 2.0 eq. of $PhCH_2CH_2SNO$ (acetone, −80 °C, dark green trace).

Reaction of 1-BAr^F_4 with 2.0 eq. $PhCH_2CH_2SNO$ in THF

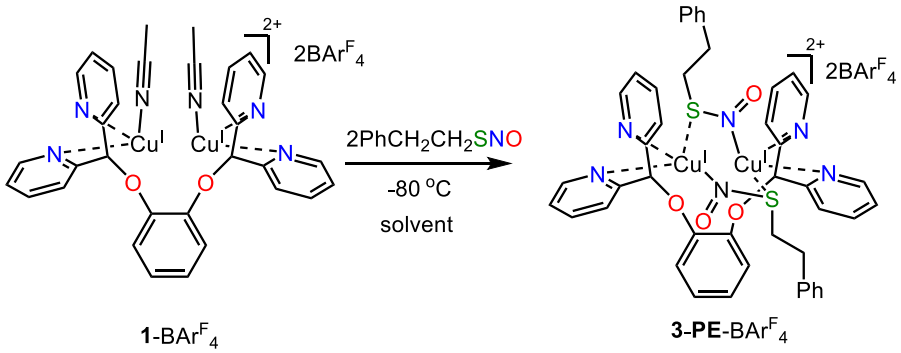

In the glovebox, a tetrahydrofuran solution of **1**-BAr^F_4 (5.4 mg, 2.3 μmol, 2.70 mL) was placed in a quartz cuvette equipped with a rubber septum. The cuvette was sealed and transferred to the UV-Vis spectrometer precooled at −80 °C. After the temperature stabilized, $PhCH_2CH_2SNO$ (0.10 mL, 22.5 mM in THF, 2.3 μmol, 1.0 equiv.) was injected to the solution, and the reaction progress was monitored by taking a UV-vis spectrum every 60 seconds. A new green species (λ_{max} = 595 nm, ε = 2500 $M^{-1}cm^{-1}$ and λ_{max} = 685 nm, ε = 1200 $M^{-1}cm^{-1}$) is generated (Figure S18). When a second equivalent of $PhCH_2CH_2SNO$ (0.10 mL, 22.5 mM in THF, 2.3 μmol, 1.0 equiv.) was injected to the above solution, the reaction progress was monitored for another 8.0 min (Figure S19). When a third equivalent of $PhCH_2CH_2SNO$ (0.10 mL, 22.5 mM in THF, 2.3 μmol, 1.0 equiv.) was injected into the cuvette, the UV-Vis spectra only changed slightly due to dilution. The comparison of UV-Vis spectra when 1.0 eq, 2.0 eq and 3.0 eq. of $PhCH_2CH_2SNO$ are added is shown in Figure S20 and suggests that two equivalents of $PhCH_2CH_2SNO$ can bind to the dicopper(I) complex. The new green species started to decay quickly when the cuvette was further warmed up to −40 °C in THF.

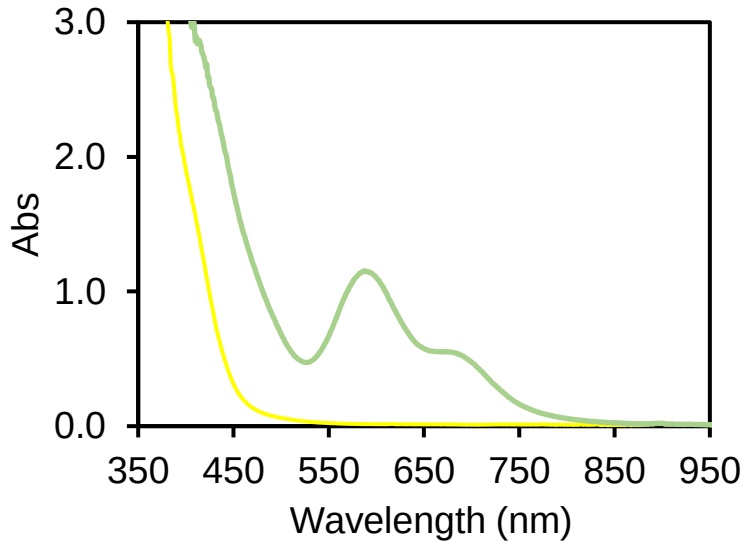

Figure S18. UV-Vis spectra of the reaction mixture of **1**-BAr^{F}_{4} (yellow trace) and 1.0 eq. $PhCH_2CH_2SNO$ (light green trace, THF, −80 °C)

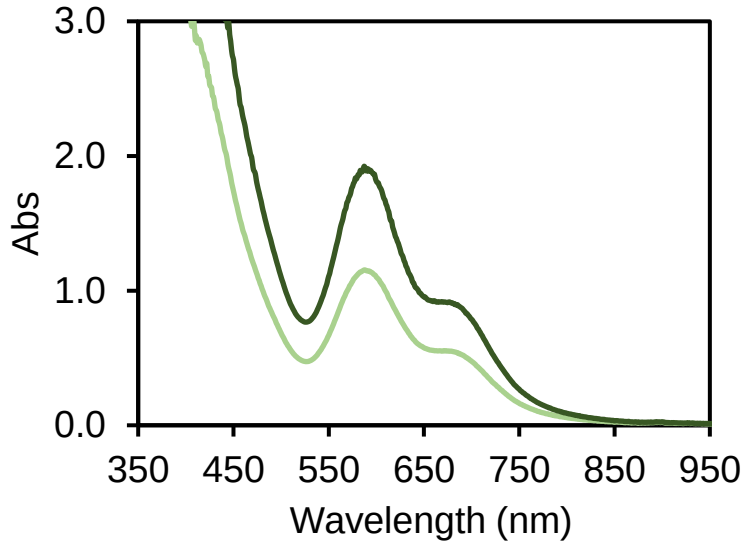

Figure S19. UV-Vis spectra of the reaction mixture of **1**-BAr^{F}_{4} and 1.0 eq. $PhCH_2CH_2SNO$ (THF, −80 °C, light green trace) followed by a second equivalent of $PhCH_2CH_2SNO$ (dark green trace).

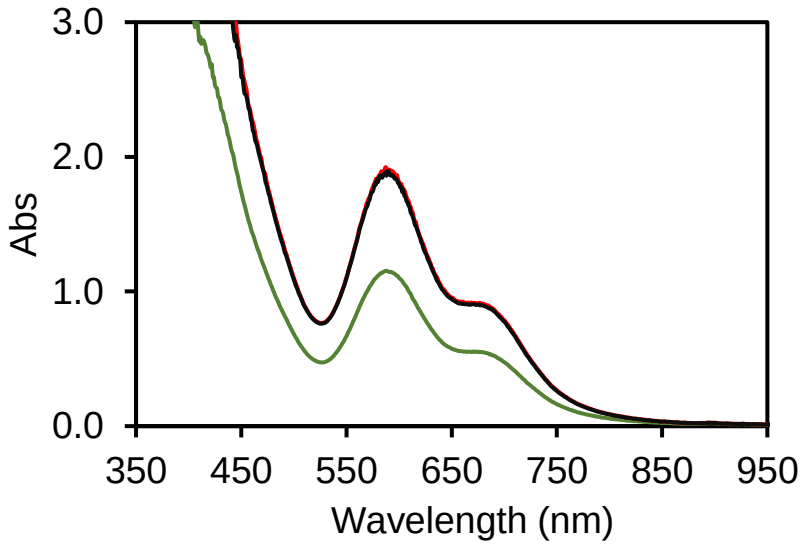

Figure S20. Comparison of UV-Vis spectra between the reaction mixture of **1**-BAr^F_4 and 1.0 eq. of $PhCH_2CH_2SNO$ (green trace), 2.0 eq. of $PhCH_2CH_2SNO$ (red trace) and 3.0 eq. of $PhCH_2CH_2SNO$ (THF, −80 °C) (black trace).

Reaction of 1-PF_6 with 2.0 eq. $PhCH_2CH_2SNO$ in acetone

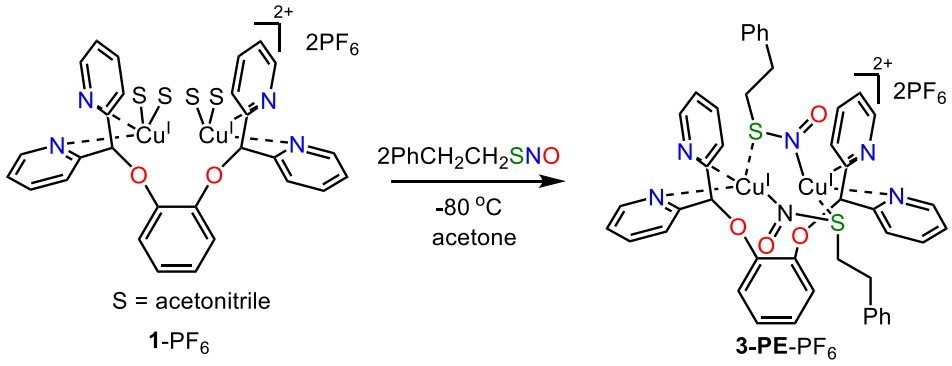

In the glovebox, an acetone solution of **1**-PF_6 (2.3 mg, 2.3 μmol, 2.80 mL) was placed in a quartz cuvette equipped with a rubber septum. The cuvette was sealed and transferred to the UV-Vis spectrometer precooled at −80 °C. After the temperature stabilized, $PhCH_2CH_2SNO$ (0.10 mL, 22.5 mM in acetone, 2.3 μmol, 1.0 equiv.) was injected to the solution, and the reaction progress was monitored by taking a UV-vis spectrum every 60 seconds. A new green species (λ_{max} = 575 nm, ε = 2400 $M^{-1}cm^{-1}$ and λ_{max} = 675 nm, ε = 1450 $M^{-1}cm^{-1}$) is generated (Figure S21). When a second equivalent of $PhCH_2CH_2SNO$ (0.10 mL, 22.5 mM in acetone, 2.3 μmol, 1.0 equiv.) was injected to the above solution, the reaction progress was monitored for another 10 min (Figure S22). The comparison of UV-Vis spectra between **1-BAr^F_4** with 2.0 eq. of $PhCH_2CH_2SNO$ and **1-PF_6** with 2.0 eq. of $PhCH_2CH_2SNO$ is shown in Figure S23, which supports that counter anions (BAr^F_4 and PF_6) have no impact on the binding of *S*-nitrosothiols at the dicopper(I) complex. The new green species with PF_6 counter anion started to decay quickly when the cuvette was further warmed up to -50 °C in acetone.

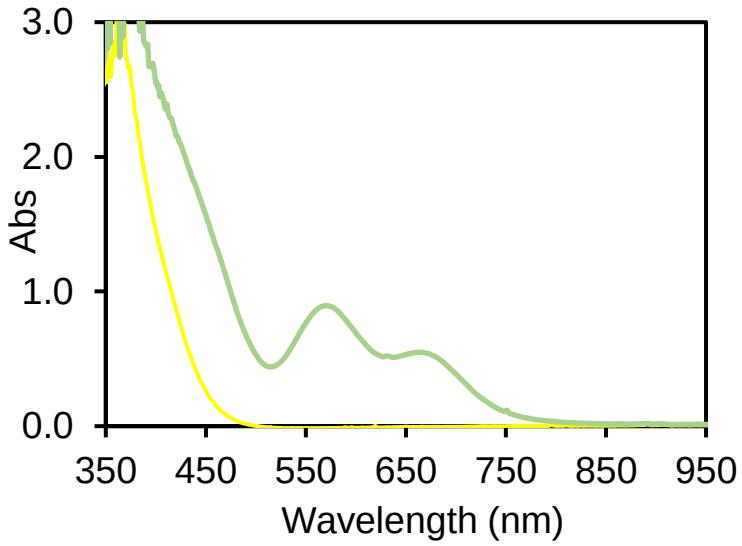

Figure S21. UV-Vis spectra of the reaction mixture of **1**-PF_6 (yellow trace) and 1.0 eq. $PhCH_2CH_2SNO$ (light green trace, acetone, −80 °C)

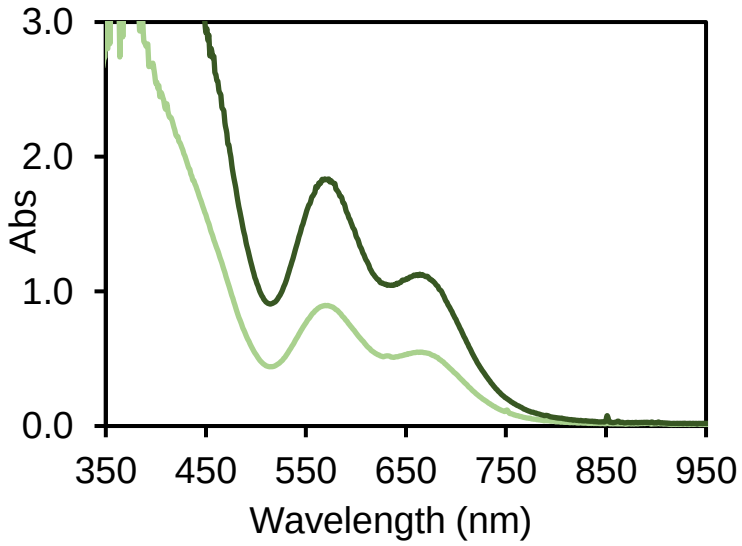

Figure S22. UV-Vis spectra of the reaction mixture of **1**-PF_6 and 1.0 eq. $PhCH_2CH_2SNO$ (light green trace, acetone, −80 °C) followed by a second equivalent of $PhCH_2CH_2SNO$ (dark green trace).

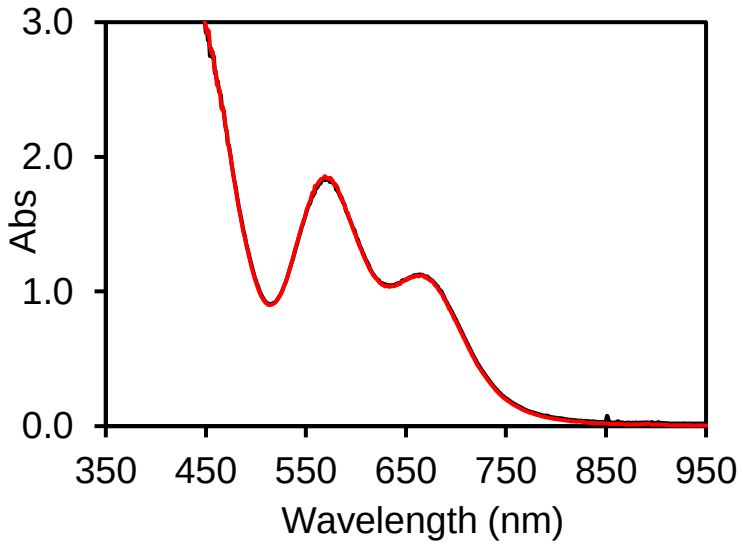

Figure S23. Comparison of UV-Vis spectra of the reaction mixture of **1**-PF_6 with 2.0 eq. $PhCH_2CH_2SNO$ (black trace) and reaction mixture of **1**-$BAr^F{}_4$ with 2.0 eq. $PhCH_2CH_2SNO$ (red trace, acetone, −80 °C).

Reaction of 1-PF_6 with 2.0 eq. $PhCH_2CH_2SNO$ in DCM

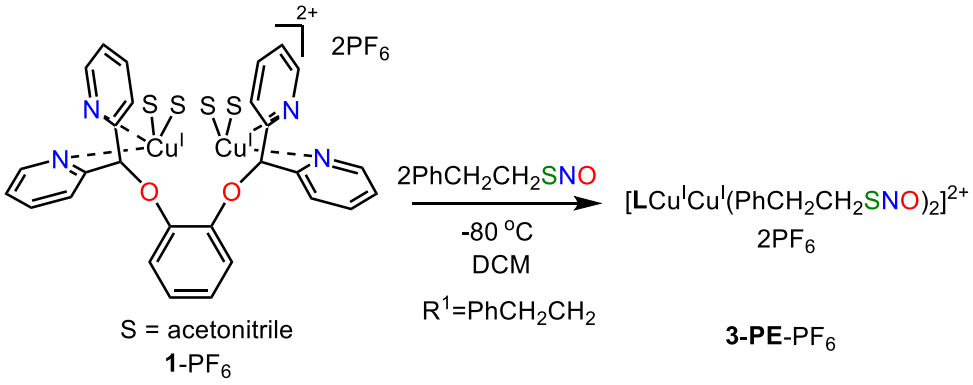

In the glovebox, a dichloromethane solution of **1**-PF_6 (2.3 mg, 2.3 μmol, 2.80 mL) was placed in a quartz cuvette equipped with a rubber septum. The cuvette was sealed and transferred to the UV-Vis spectrometer precooled at −80 °C. After the temperature stabilized, $PhCH_2CH_2SNO$ (0.10 mL, 22.5 mM in DCM, 2.3 μmol, 1.0 equiv.) was injected to the solution, and the reaction progress was monitored by taking a UV-vis spectrum every 60 seconds. A new green species (λ_{max} = 450 nm, ε =5600 $M^{-1}cm^{-1}$, λ_{max} = 545 nm, ε =2100 $M^{-1}cm^{-1}$ and λ_{max} = 675 nm, ε = 2500 $M^{-1}cm^{-1}$) is generated (Figure S24). When a second equivalent of $PhCH_2CH_2SNO$ (0.10 mL, 22.5 mM in DCM, 2.3 μmol, 1.0 equiv.) was injected to the above solution, the reaction progress was monitored for another 6.0 min. The comparison of UV-Vis spectra when 1.0 eq and 2.0 eq. of $PhCH_2CH_2SNO$ are added is shown in Figure S25, which resembles that observed in acetone. These reaction conditions were also employed for the in-situ IR experiments to investigate the N=O stretching frequency. The new green species with PF_6 counter anion started to decay quickly when the cuvette was further warmed to higher than −60 °C in DCM.

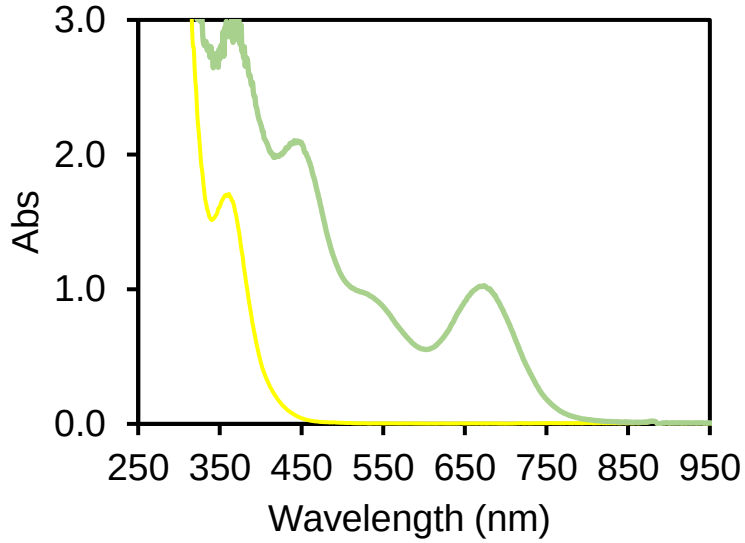

Figure S24. UV-Vis spectra of the reaction mixture of **1**-PF_6 (yellow trace) and 1.0 eq. $PhCH_2CH_2SNO$ (light green trace, DCM, −80 °C)

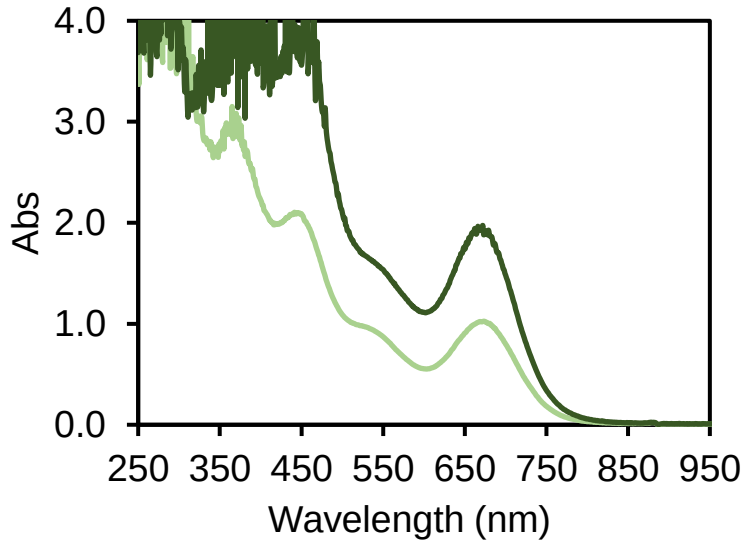

Figure S25. UV-Vis spectra of the reaction mixture of **1**-PF_6 and 1.0 eq. $PhCH_2CH_2SNO$ (light green trace, DCM, −80 °C) followed by a second equivalent of $PhCH_2CH_2SNO$ (dark green trace).

Reaction of 2-BAr$^{F}_{4}$ with two equivalents of PhCH$_2$CH$_2$SH directly

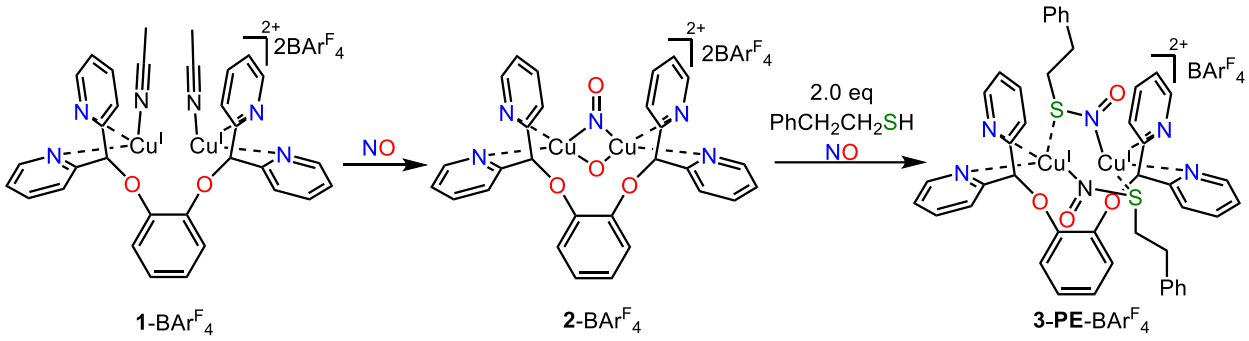

In the glovebox, an acetone solution of **1**-BAr$^{F}_{4}$ (5.4 mg, 2.3 μmol, 2.8 mL) was placed in a Schlenk quartz cuvette. The cuvette was sealed and transferred to the UV-Vis spectrometer precooled at −50 °C. After the temperature stabilized, NO (2.0 mL, 83.3 μmol, 37 eq.) was injected into the solution and the reaction progress was monitored by taking a UV-Vis spectrum every 60 seconds until the dicopper μ-oxo, μ-nitrosyl (**2**-BAr$^{F}_{4}$) band at 520 nm reached an absorbance of *ca.* 1.95 and stabilized. The cuvette was cooled to −80 °C and stabilized before PhCH$_2$CH$_2$SH (0.20 mL, 22.5 mM in acetone, 4.6 μmol, 2.0 equiv.) was injected to the above solution. The reaction progress was monitored by taking a UV-vis spectrum every 60 seconds. After *ca.* 30 min, the Schlenk cuvette was sealed and transferred to a −70 °C cold bath and stored for 24 h. The cuvette was transferred back to the UV-Vis spectrometer precooled at −80 °C and a UV-Vis spectrum was taken every 60 seconds. A new green species (λ_{max} = 575 nm, ε =2500 $M^{-1}cm^{-1}$ and λ_{max} = 675 nm, ε = 1500 $M^{-1}cm^{-1}$) is generated (Figure S26). The comparison of the UV-Vis spectra generated from **1**-BAr$^{F}_{4}$ with two equivalents of PhCH$_2$CH$_2$SNO (red trace) and **2**-BAr$^{F}_{4}$ with two equivalents of 2-phenyl ethanethiol (black trace) in the presence of excess amount of NO is shown in Figure S27, which strongly suggests that the two methods produce the same proposed dicopper(I,I) di-S-nitrosothiols product.

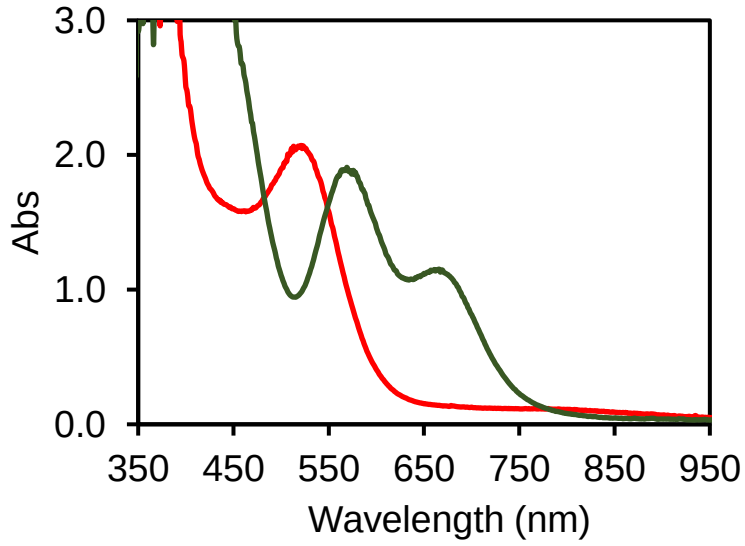

Figure S26. UV-Vis spectra of the reaction mixture of **2**-BAr$^{F}_{4}$ (red trace) and 2.0 eq. PhCH$_2$CH$_2$SH (green trace, −80 °C, after reaction at −70 °C for 24 h)

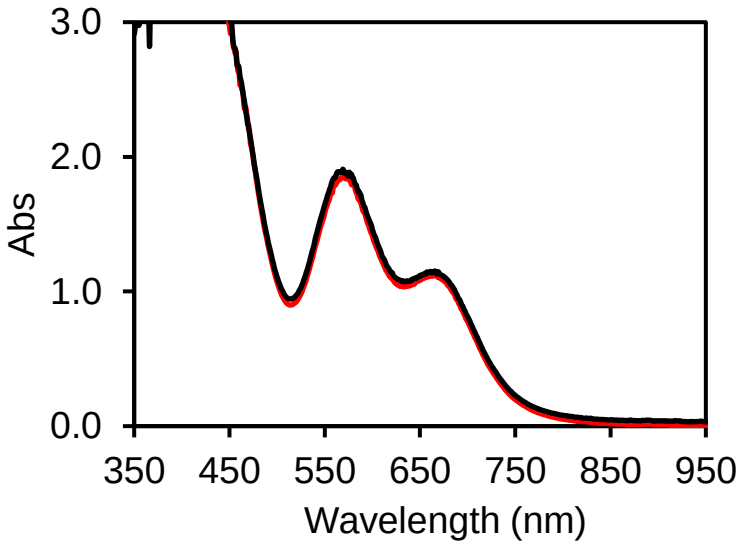

Figure S27. The comparison of UV-Vis spectra of the reaction mixture of **2**-BAr^F_4 with 2.0 eq. $PhCH_2CH_2SH$ in the presence of excess amount of NO (black trace) and that of **1**-BAr^F_4 with 2.0 eq. of $PhCH_2CH_2SNO$ (red trace) in acetone at −80 °C.

Reaction of 2-BAr^F_4 with two equivalents of $PhCH_2CH_2SH$ sequentially

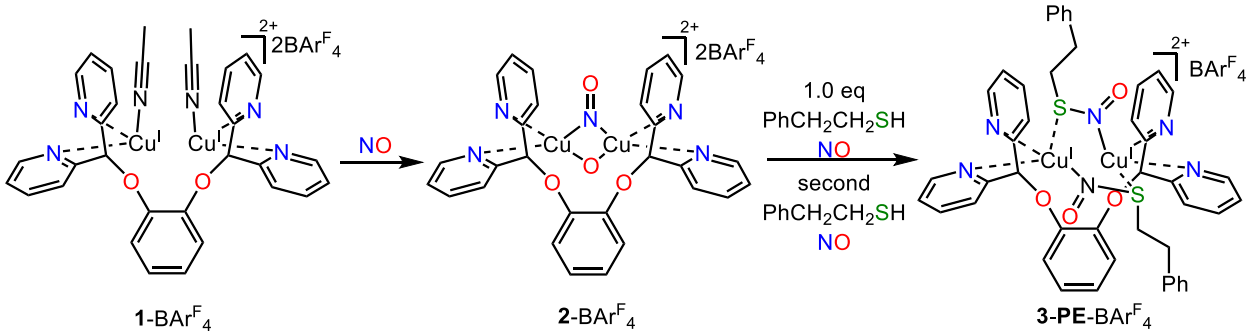

In the glovebox, an acetone solution of **1**-BAr^F_4 (5.4 mg, 2.3 μmol, 2.8 mL) was placed in a Schlenk quartz cuvette. The cuvette was sealed and transferred to the UV-Vis spectrometer precooled at −50 °C. After the temperature stabilized, NO (2.0 mL, 83.3 μmol, 37 eq.) was injected into the solution and the reaction progress was monitored by taking a UV-Vis spectrum every 60 seconds until the dicopper μ-oxo, μ-nitrosyl (**2**-BAr^F_4) band at 520 nm reached an absorbance of *ca.* 1.95 and stabilized. The cuvette was cooled to −80 °C and stabilized before $PhCH_2CH_2SH$ (0.10 mL, 22.5 mM in acetone, 2.3 μmol, 1.0 equiv.) was injected to the above solution. The reaction progress was monitored by taking a UV-vis spectrum every 60 seconds. After *ca.* 30 min, the Schlenk cuvette was sealed and transferred to a −70 °C cold bath and stored for 7 h. The cuvette was transferred back to the UV-Vis spectrometer precooled at −80 °C and a UV-Vis spectrum was taken every 60 seconds. A brown solution is generated (Figure S28). $PhCH_2CH_2SH$ (0.10 mL, 22.5 mM in acetone, 2.3 μmol, 1.0 equiv.) was injected to the above solution under positive nitrogen flow and the Schlenk cuvette was sealed and transferred to a −70 °C cold bath and stored for 30 h. The

cuvette was transferred back to the UV-Vis spectrometer precooled at −80 °C and a UV-Vis spectrum was taken every 60 seconds. A new green species (λ_{max} = 575 nm, ε =2200 $M^{-1}cm^{-1}$ and λ_{max} = 675 nm, ε = 1300 $M^{-1}cm^{-1}$) is generated (Figure S29). The comparison of the UV-Vis spectra generated from **2**-BAr^{F}_{4} with direct two equivalents of $PhCH_2CH_2SH$ (green trace) and sequential addition of two equivalents of 2-phenylethanethiol (blue trace) in the presence of excess amount of NO is shown in Figure S29, which suggests that the two addition methods produce the same proposed dicopper(I,I) di-*S*-nitrosothiols product and the reaction with direct addition of 2-phenylethanethiol is a little cleaner.

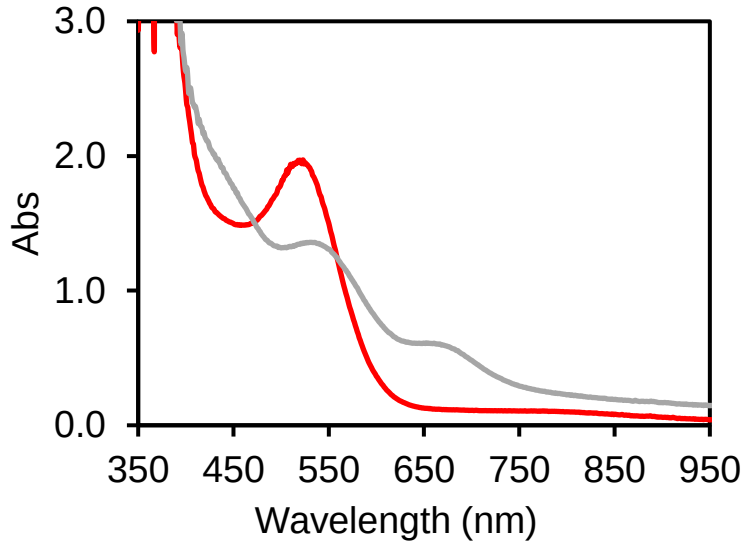

Figure S28. UV-Vis spectra of the reaction mixture of **2**-BAr^{F}_{4} (red trace) and 1.0 eq. $PhCH_2CH_2SH$ (gray trace, −80 °C, after reaction at −70 °C for 7 h)

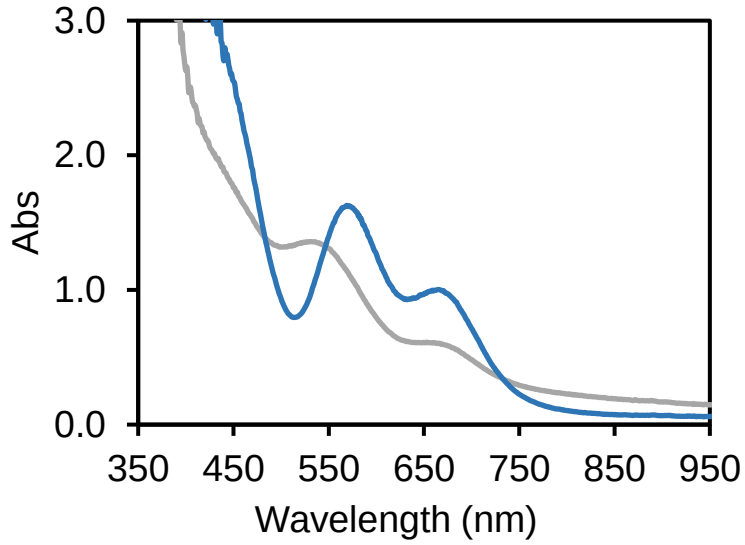

Figure S29. UV-Vis spectra of the reaction mixture of **2**-BAr^{F}_{4} (red trace) with 1.0 eq. $PhCH_2CH_2SH$ (gray trace, −80 °C, after reaction at −70 °C for 7 h) and a second equivalent of $PhCH_2CH_2SH$ (blue trace, −80 °C, after reaction at −70 °C for 30 h)

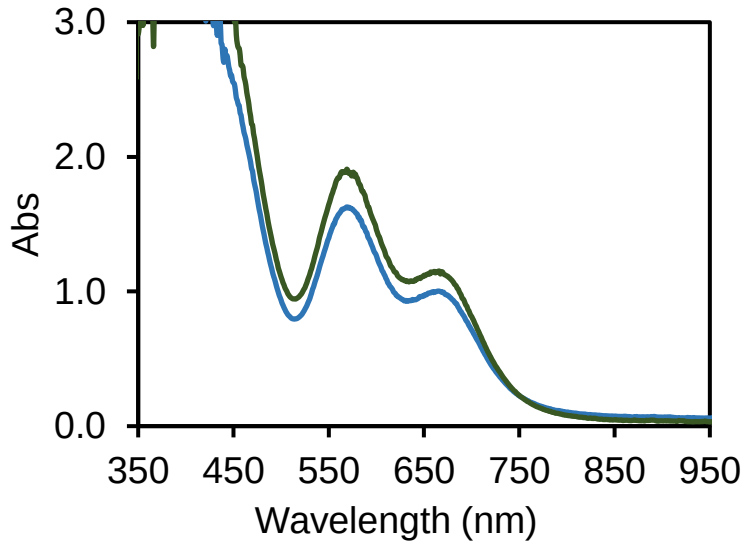

Figure S30. UV-Vis spectra of the reaction mixture of **2**-BAr^F_4 (red trace) with direct 2.0 eq. $PhCH_2CH_2SH$ (green trace, −80 °C, after reaction at −70 °C for 24 h) and sequential 2.0 eq. of $PhCH_2CH_2SH$ (blue trace, −80 °C, after reaction at −70 °C for 30 h)

Reaction of 1-BAr^F_4 with 2.0 eq. $PhCH_2CH_2SNO$ in propionitrile

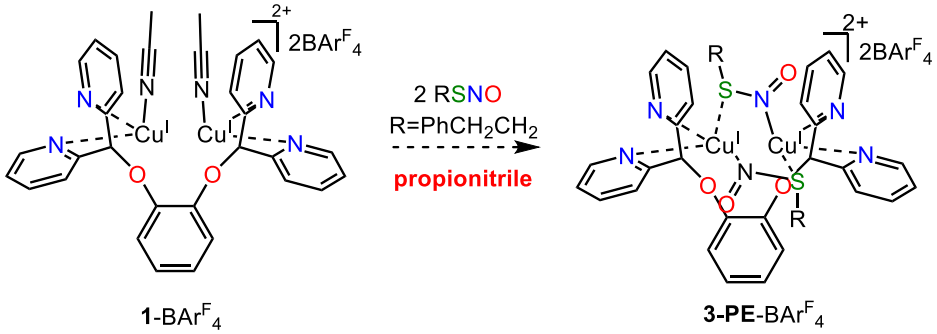

In the glovebox, a propionitrile solution of **1**-BAr^F_4 (5.4 mg, 2.3 μmol, 2.80 mL) was placed in a quartz cuvette equipped with a rubber septum. The cuvette was sealed and transferred to the UV-Vis spectrometer precooled at −80 °C. After the temperature stabilized, $PhCH_2CH_2SNO$ (0.20 mL, 22.5 mM in propionitrile, 4.6 μmol, 2.0 equiv.) was injected to the solution, and the reaction progress was monitored by taking a UV-vis spectrum every 60 seconds. In contrast to reactions in other solvents, such as acetone (Figure S17), THF (Figure S19), or DCM (Figure S25), no new bands around 675 nm and 580 nm were observed (Figure S31). Only free $PhCH_2CH_2SNO$ signals are observed near 550 nm. The free $PhCH_2CH_2SNO$ was stable when the temperature was increased to −60 °C, 0 °C and 20 °C (Figure S32). This experiment suggests that in the presence of excess propionitrile, the binding of S-nitrosothiol to the dicopper(I,I) center is suppressed.

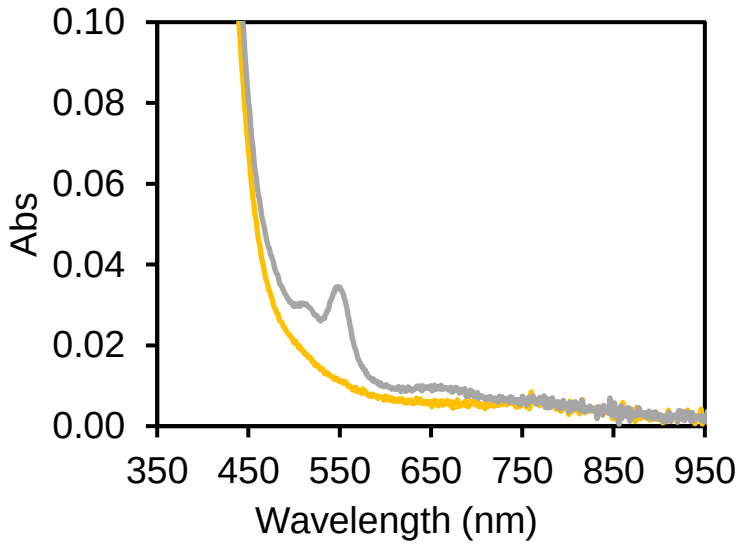

Figure S31. UV-Vis spectra of the reaction mixture of **1**-BAr^F_4 (yellow trace) and 2.0 eq. $PhCH_2CH_2SNO$ (gray trace, propionitrile, −80 °C)

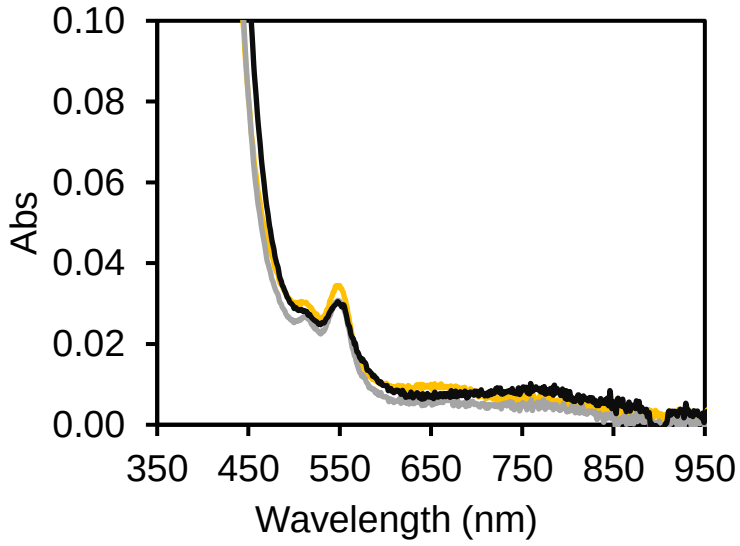

Figure S32. UV-Vis spectra of the reaction mixture of **1**-BAr^F_4 and 2.0 eq. $PhCH_2CH_2SNO$ in propionitrile (yellow trace at −80 °C, gray trace at −60 °C and black trace at 20 °C)

Reaction of excess propionitrile with proposed dicopper(I,I) di-*S*-nitrosothiol

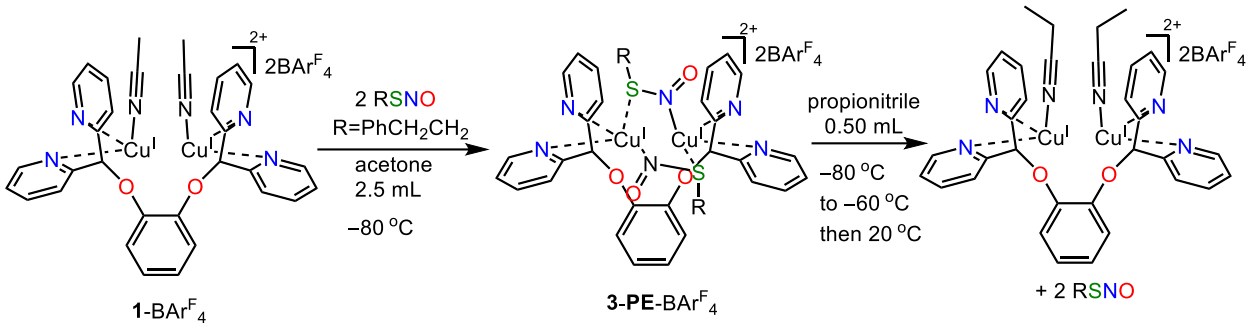

1-BAr$^F_4$ **3-PE**-BAr$^F_4$

In the glovebox, an acetone solution of **1**-BAr$^F_4$ (5.4 mg, 2.3 μmol, 2.30 mL) was placed in a quartz cuvette equipped with a rubber septum. The cuvette was sealed and transferred to the UV-Vis spectrometer precooled at −80 °C. After the temperature stabilized, PhCH$_2$CH$_2$SNO (0.20 mL, 22.5 mM in acetone, 4.6 μmol, 2.0 equiv.) was injected to the solution, and the reaction progress was monitored by taking a UV-vis spectrum every 60 seconds. The proposed dicopper(I,I) di-S-nitrosothiol species (λ_{max} = 575 nm, ε = 2400 $M^{-1}cm^{-1}$ and λ_{max} = 675 nm, ε = 1450 $M^{-1}cm^{-1}$) is generated. After the spectrum stabilized, propionitrile (0.50 mL, 7.2 mmol, 3100 eq.) was injected to the solution and the reaction was monitored by taking a UV-Vis spectrum every 60 seconds. After the spectrum stabilized at −80 °C (Figure S33), the temperature was increased to −70 °C, and the reaction was monitored by UV-vis until stabilized again. These procedures were repeated as the temperature was increased to −60 °C, −50 °C and −40 °C (Figure S34). When the spectrum stabilized at −40 °C, the reaction was warmed up to 20 °C and free S-nitrosothiol PhCH$_2$CH$_2$SNO signals around 550 nm were observed (black trace compared with free PhCH$_2$CH$_2$SNO gray trace in Figure S35). This experiment strongly suggests that an excess amount of propionitrile can displace *S*-nitrosothiol bound to dicopper(I,I). Inspired by this result, we attempt to quantify the amount of PhCH$_2$CH$_2$SNO that is formed from the reaction of dicopper μ-oxo, μ-nitrosyl **2**-BAr$^F_4$ and free thiol PhCH$_2$CH$_2$SH in the presence of excess nitric oxide using ^{1}H NMR.

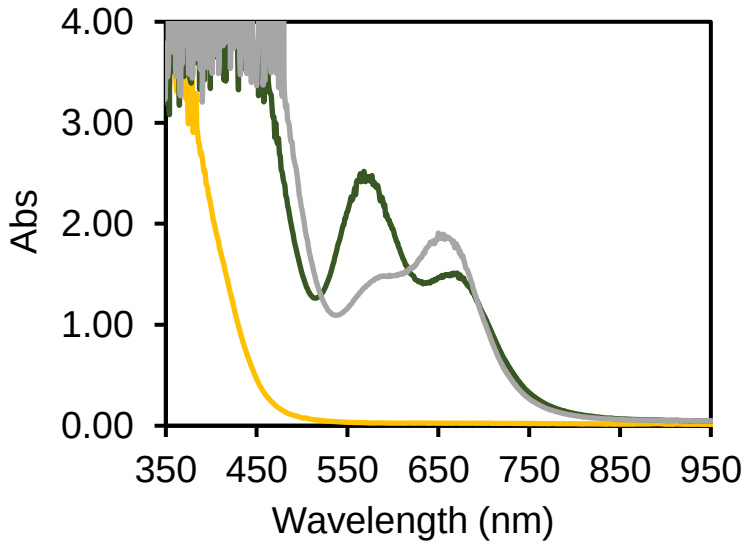

Figure S33. UV-Vis spectra of the reaction mixture of **1**-BAr$^F_4$ (yellow trace) and 2.0 eq. PhCH$_2$CH$_2$SNO (dark green trace) followed by addition of propionitrile (gray trace) at −80 °C.

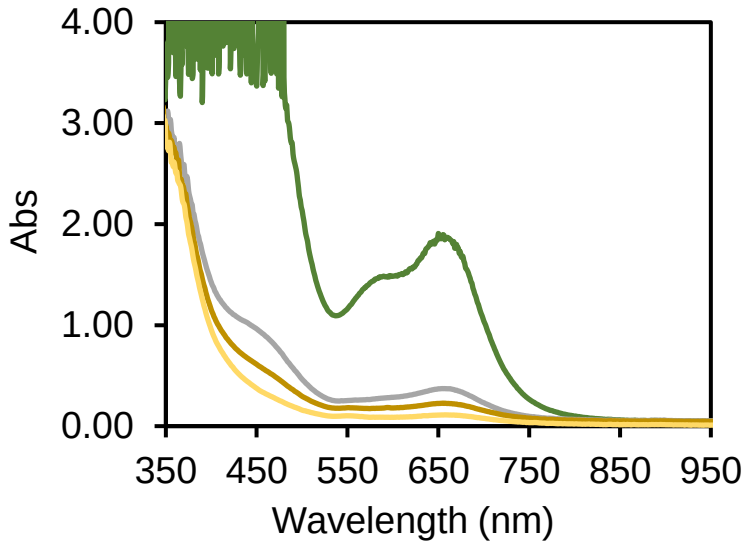

Figure S34. UV-Vis spectra of the reaction mixture of **1**-BAr^F_4 and 2.0 eq. $PhCH_2CH_2SNO$ followed by addition of propionitrile (green trace at −80 °C, gray trace at −70 °C, khaki trace at −60 °C, and yellow trace at −50 °C).

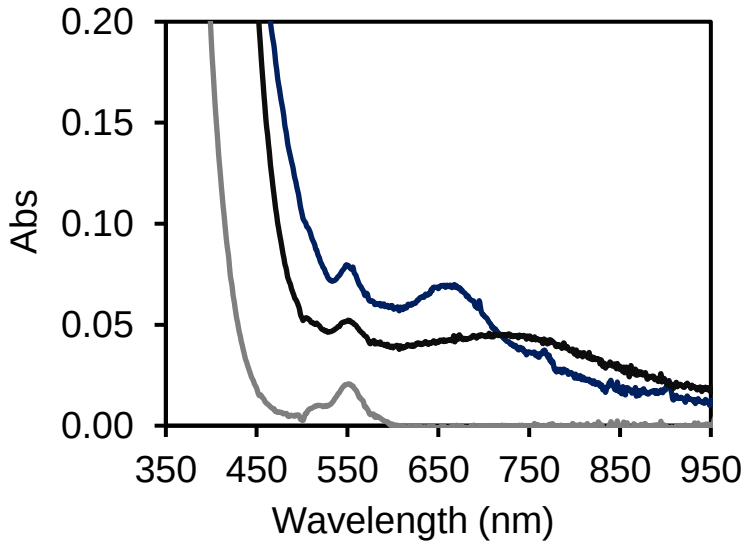

Figure S35. UV-Vis spectra of the reaction mixture of **1**-BAr^F_4 and 2.0 eq. $PhCH_2CH_2SNO$ followed by addition of propionitrile (blue trace at −40 °C, black trace at 20 °C). The gray trace is 1.5 mM free $PhCH_2CH_2SNO$ in the same mixed solvent at 20 °C.

Quantification of $PhCH_2CH_2SNO$ from the reaction of 2-BAr^F_4 with two equivalents of $PhCH_2CH_2SH$

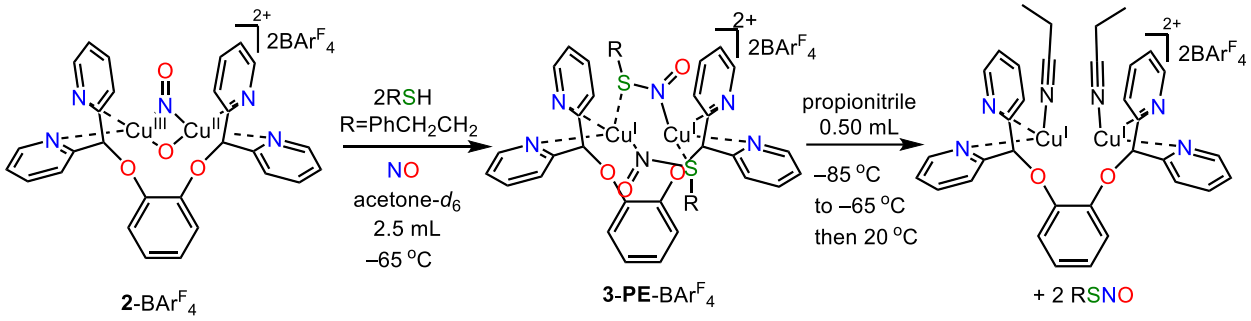

In the glovebox, an acetone-d_6 solution of **1**-BAr^F_4 (5.4 mg, 2.3 μmol, 2.3 mL) and internal standard 1,3,5-trimethoxybenzene (1.2 mg, 7.1 μmol) were placed in a quartz cuvette equipped with a rubber septum. The cuvette was sealed and transferred to the UV-Vis spectrometer precooled at −45 °C. After the temperature stabilized, NO (2.0 mL, 83 μmol, 37 eq.) was injected into the solution and the reaction progress was monitored by taking a UV-Vis spectrum every 60 seconds until the dicopper μ-oxo, μ-nitrosyl **2**-BAr^F_4 band at 525 nm reached an absorbance of *ca.* 2.44 and stabilized. The cuvette was cooled to −80 °C and stabilized before $PhCH_2CH_2SH$ (0.20 mL, 22.5 mM in acetone-d_6, 4.6 μmol, 2.0 equiv.) was injected to the solution, and the reaction progress was monitored by taking a UV-vis spectrum every 60 seconds. The UV-vis bands of the proposed dicopper(I,I) di-S-nitrosothiol species (λ_{max} = 575 nm, ε =2100 $M^{-1}cm^{-1}$ and λ_{max} = 675 nm, ε = 1300 $M^{-1}cm^{-1}$) were observed at −65 °C. After the spectrum stabilized, the solution was cooled to −85 °C and propionitrile (0.50 mL, 7.2 mmol, 3100 eq.) was injected to the solution and the reaction was monitored by taking UV-Vis spectrum every 60 seconds. After the spectra stabilized at −85 °C, the temperature was increased to −65 °C and the reaction was monitored by UV-vis until stabilized. These procedures were repeated as the temperature was increased to −50 °C and −40 °C (Figure S36). Once the spectrum stabilized at −40 °C, the solution was warmed up to 20 °C and free S-nitrosothiol $PhCH_2CH_2SNO$ signals around 550 nm were observed (Figure S37). The resulting solution was analyzed by ^{1}H NMR, however, because of the large amount of propionitrile, the S-nitrosothiol signals can not be quantified very well (Figure S38). With this result, we decide to use CD_3CN instead of propionitrile to reduce its interference during ^{1}H NMR quantification.

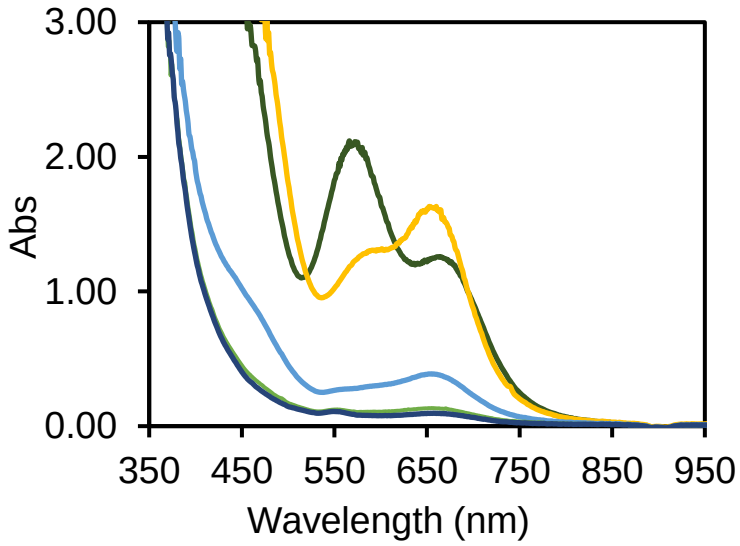

Figure S36. UV-Vis spectra of the reaction mixture of **3-PE**-BAr^F_4 (dark green trace at −65 °C) and excess propionitrile (yellow trace at −85 °C, light blue trace at −65 °C, light green trace at −50 °C and blue trace at −40 °C).

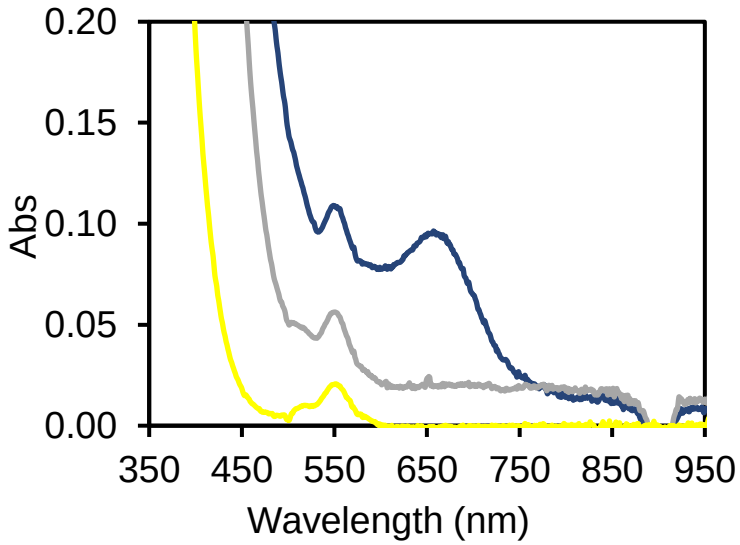

Figure S37. UV-Vis spectra of the reaction mixture of **3-PE**-BAr^F_4 and excess propionitrile (blue trace at −40 °C, gray trace at 20 °C). The 1.5 mM free $PhCH_2CH_2SNO$ spectra in the same mixed solvent is shown as yellow trace for comparison.

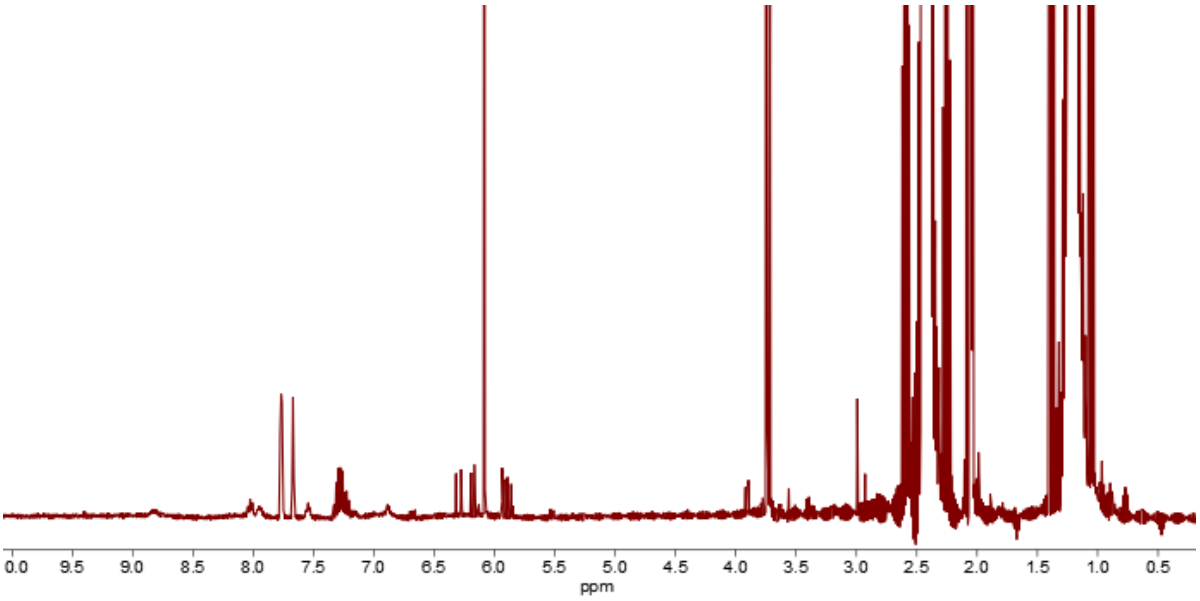

Figure S38. ^{1}H NMR (400 MHz, acetone-d_6) of the reaction mixture of **3-PE**-BAr$^{F}_4$ with excess amount of propionitrile.

Quantification of $PhCH_2CH_2SNO$ from the reaction of 2-BAr$^{F}_4$ with two equivalents of $PhCH_2CH_2SH$ with CD_3CN

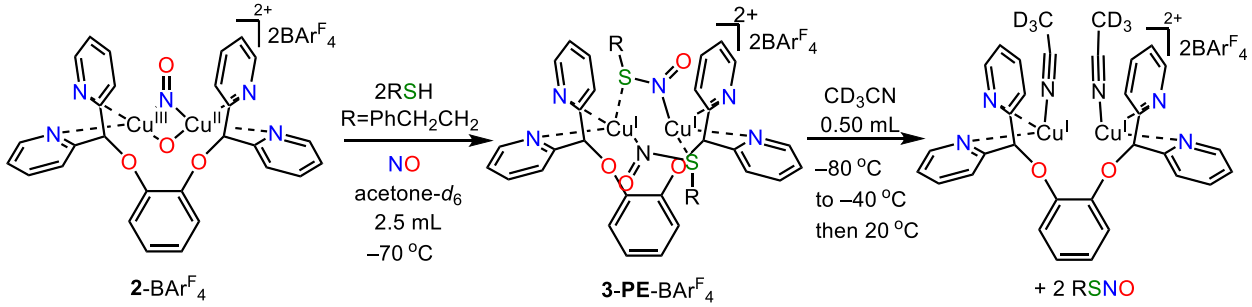

2-BAr$^{F}_4$ **3-PE**-BAr$^{F}_4$

In the glovebox, an acetone-d_6 solution of **1**-BAr$^{F}_4$ (5.4 mg, 2.27 μmol, 2.3 mL) was placed in a Schlenk quartz cuvette. The cuvette was sealed and transferred to the UV-Vis spectrometer precooled at −50 °C. After the temperature stabilized, NO (5.0 mL, 208 μmol, 92 eq.) was injected into the solution and the reaction progress was monitored by taking a UV-Vis spectrum every 60 seconds until the dicopper μ-oxo, μ-nitrosyl **2**-BAr$^{F}_4$ feature band at 525 nm reached an absorbance of *ca.* 2.18 and stabilized. The cuvette was cooled to −80 °C. $PhCH_2CH_2SH$ (0.21 mL, 22.5 mM in acetone-d_6, 4.7 μmol, 2.1 equiv.) was injected to the solution, and the reaction progress was monitored by taking a UV-vis spectrum every 60 seconds. After *ca.* 20 min, the Schlenk cuvette was sealed and transferred to a −70 °C cold bath and stored at this temperature for 24 h. The color of the solution changed from dark red to dark green. The Schlenk cuvette was then transferred back to the UV-Vis spectrometer precooled at −80 °C. After the temperature was stabilized, an acetonitrile-d_3 (0.50 mL, 9.6 mmol, 4300 eq.) solution of internal standard 1,3,5-trimethoxybenzene (1.9 mg, 11.1 μmol) was injected to the solution and the reaction was monitored by taking a UV-Vis spectrum every minute. After the spectrum stabilized at −80 °C, the temperature was increased to −70 °C and the reaction was monitored until the spectrum stabilized. These procedures were

repeated as the temperature was increased to −60 °C, −50 °C, −40 °C, −20 °C, −10 °C, 0 °C and finally 20 °C (Figure S39-40). Free S-nitrosothiol $PhCH_2CH_2SNO$ signals around 550 nm were observed (Figure S37). The resulting solution was analyzed by quantitative ^1H NMR (relaxation time 20s). The existence of free $PhCH_2CH_2SNO$ can be confirmed by comparison with the ^1H NMR spectrum of the pure $PhCH_2CH_2SNO$ containing internal standard 1,3,5-trimethoxybenzene in acetone-d_6 (Figure S41). The amount of $PhCH_2CH_2SNO$ formed in the reaction of dicopper μ-oxo, μ-nitrosyl **2**-$BAr^F{}_4$ with two equivalents of phenylethanethiol is 94% based on the integration of ^1H NMR (Figure S42), considering two equivalents of $PhCH_2CH_2SNO$ would be formed relative to **2**-$BAr^F{}_4$. This *S*-nitrosothiol quantification experiment supports our hypothesis that the new green species (λ_{max} = 575 nm, ε =2400 $M^{-1}cm^{-1}$ and λ_{max} = 675 nm, ε = 1450 $M^{-1}cm^{-1}$) is dicopper(I,I) di-*S*-nitrosothiol complex.

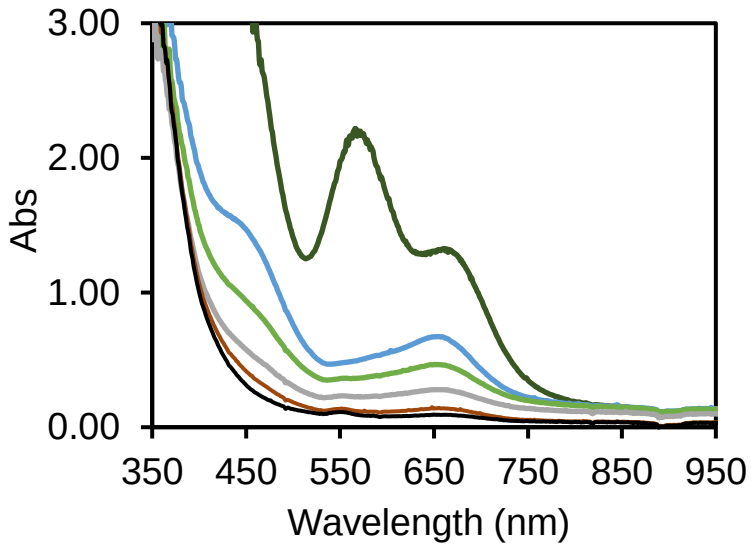

Figure S39. UV-Vis spectra of the reaction mixture of **3-PE**-$BAr^F{}_4$ (dark green trace at −80 °C) and excess acetonitrile-d_3 (blue trace at −80 °C, light green trace at −70 °C, gray trace at −60 °C, brown trace at −50 °C and black trace at −40 °C).

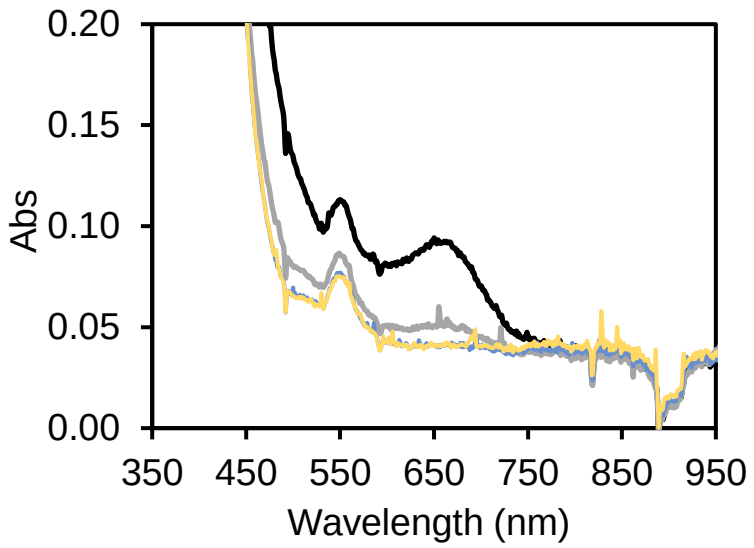

Figure S40. UV-Vis spectra of the reaction mixture of **3-PE**-BAr^F_4 and excess acetonitrile-d_3 (black trace at −40 °C, gray trace at −20 °C, blue trace at 0 °C and yellow trace at 20 °C).

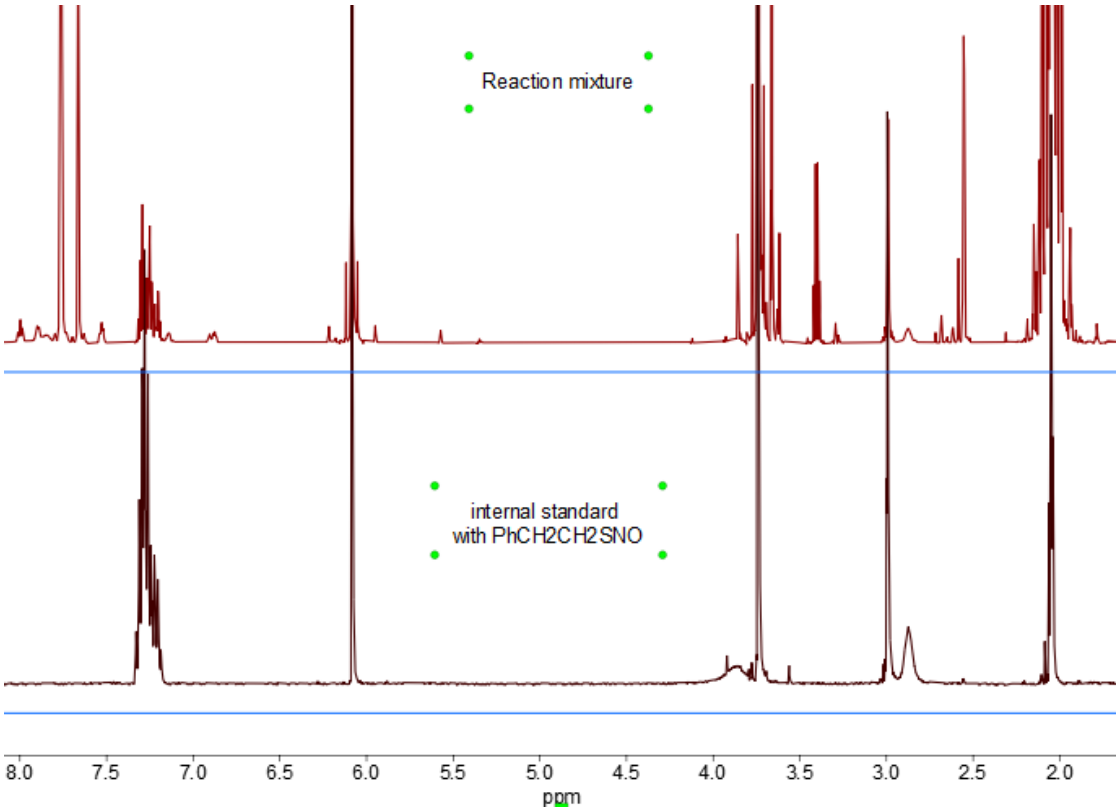

Figure S41. ^{1}H NMR (600 MHz, acetone-d_6) of **1**-BAr^F_4 and NO with two equivalents of 2-phenyl ethanethiol followed by addition of excess acetonitrile-d_3 in acetone-d_6 (top) and free $PhCH_2CH_2SNO$ and internal standard 1,3,5-trimethoxybenzene in acetone-d_6 (bottom).

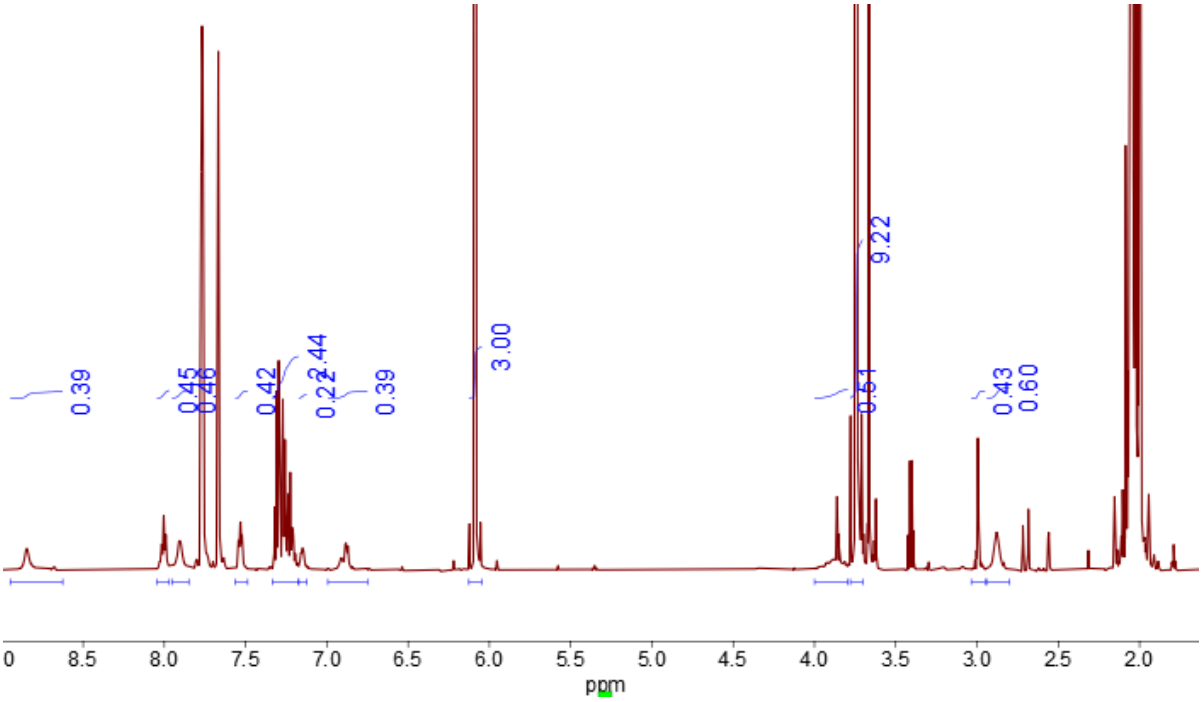

Figure S42. ^{1}H NMR (600 MHz, acetone-d_6) of **3-PE**-BAr$^{F}_{4}$ and excess acetonitrile-d_3 in acetone-d_6.

Note: The amount of internal standard 1,3,5-trimethoxybenzene used in this experiment is 1.9 mg (11.1 μmol). The amount of dicopper (I,I) precursor **1**-BAr$^{F}_{4}$ used in this experiment is 5.4 mg (2.27 μmol). The $PhCH_2CH_2SNO$ has CH_2 signals at 2.995 ppm, 2.878 ppm, 3.891 ppm because of the existence of two isomers and Ph signals are between 7.321 ppm and 7.195 ppm. The total CH_2 signal integral is 0.51+0.43+0.60=1.54, therefore the $PhCH_2CH_2SNO$ generated is 1.54/4×11.1=4.27 μmol. The maximum $PhCH_2CH_2SNO$ that is formed is two equivalents relative to **2**-BAr$^{F}_{4}$, which is 2×2.27=4.54 μmol. As a result, the yield of $PhCH_2CH_2SNO$ formation is 4.27/4.54 = 94%. The recovered dicopper(I,I) precursor **1**-BAr$^{F}_{4}$ has characterized signals in the aromatic area. The recovered amount of **1**-BAr$^{F}_{4}$ is *ca.* 0.42/4×11.1=1.17 μmol, therefore the recovered yield is *ca.*1.17/2.27 = 51%.

Reaction of 1-BAr$^{F}_{4}$ with 2.0 eq. N-acetyl-*L*-cysteine methyl ester *S*-nitrosothiol in acetone

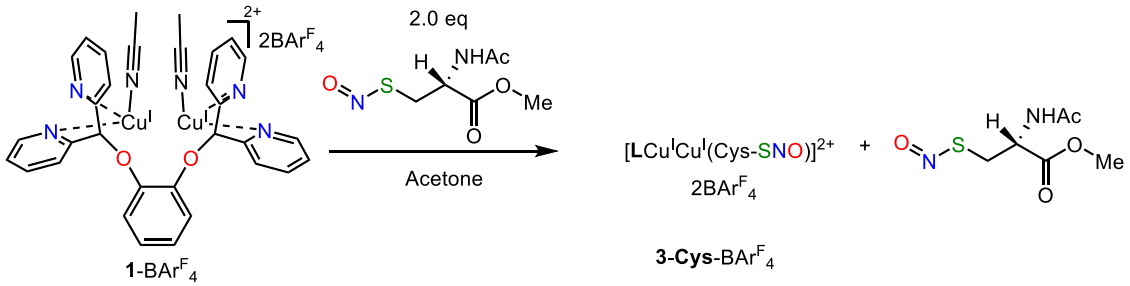

In the glovebox, an acetone solution of **1**-BAr$^{F}_{4}$ (5.4 mg, 2.3 μmol, 2.80 mL) was placed in a quartz cuvette equipped with a rubber septum. The cuvette was sealed and transferred to the UV-Vis spectrometer precooled at −80 °C. After the temperature stabilized, N-acetyl-L-cysteine methyl ester S-nitrosothiol (0.10 mL, 22.5 mM in acetone, 2.3 μmol, 1.0 equiv.) was injected to the solution, and the reaction progress was

monitored by taking a UV-vis spectrum every 60 seconds. A new green species (λ_{max} = 570 nm, ε = 2500 $M^{-1}cm^{-1}$ and λ_{max} = 670 nm, ε = 2200 $M^{-1}cm^{-1}$) is generated (Figure S43). A second equivalent of N-acetyl-L-cysteine methyl ester S-nitrosothiol (0.10 mL, 22.5 mM in acetone, 2.3 μmol, 1.0 equiv.) was injected to the above solution, and the reaction progress was monitored for another 15 min. The stabilized UV-Vis spectra after the addition of one or two equivalents of N-acetyl-L-cysteine methyl ester S-nitrosothiol are shown in Figure S44. The new green species decayed quickly when the cuvette was warmed up to −60 °C in acetone. The titration experiment suggests that only one equivalent of N-acetyl-*L*-cysteine methyl ester S-nitrosothiol binds to dicooper(I,I) precursor **1**-BAr^F_4. It is possible that the SNO moiety binds to one copper(I) center while the ester or amide functional group coordinates to the other copper(I) center in **1**-BAr^F_4.

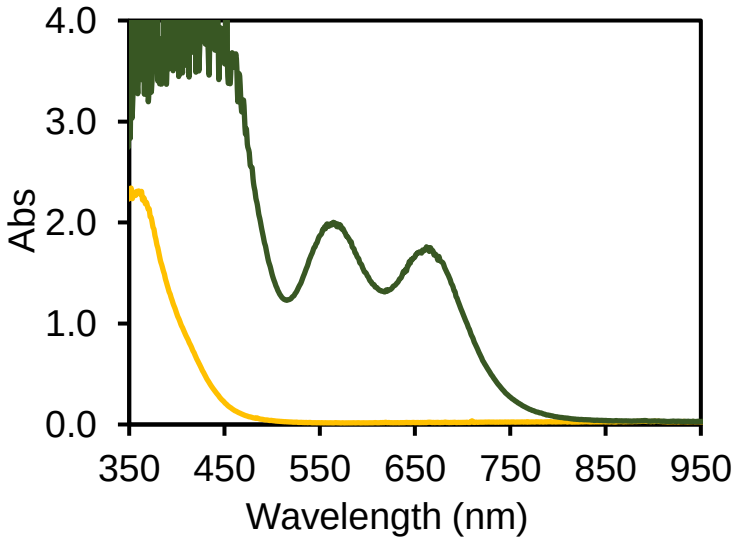

Figure S43. UV-Vis spectra of the reaction mixture of **1**-BAr^F_4 (yellow trace) and one equivalent of S-nitroso N-acetyl-L-cysteine methyl ester (green trace at −80 °C in acetone).

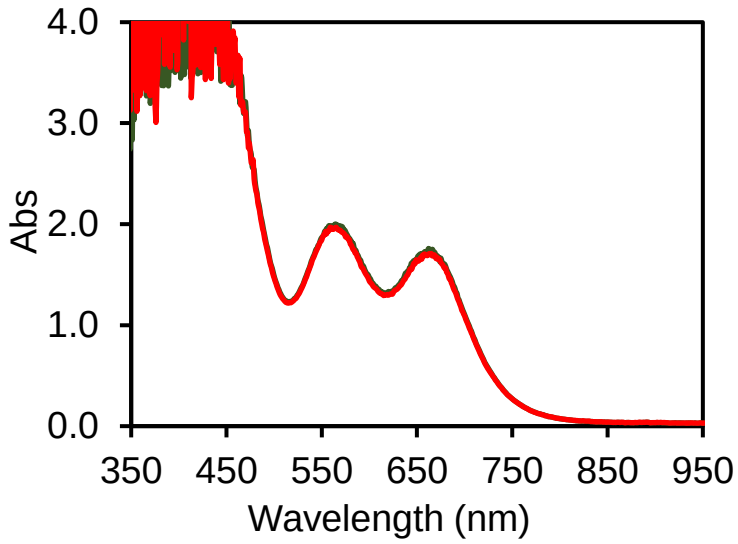

Figure S44. UV-Vis spectra of the reaction mixture of **1**-BAr^F_4 with one equivalent of S-nitroso N-acetyl-L-cysteine methyl ester (green trace at −80 °C in acetone) followed by a second equivalent of S-nitroso N-acetyl-L-cysteine methyl ester (red trace at −80 °C in acetone).

Reaction of 2-BAr^F_4 with 2.0 eq. N-acetyl-*L*-cysteine methyl ester in acetone

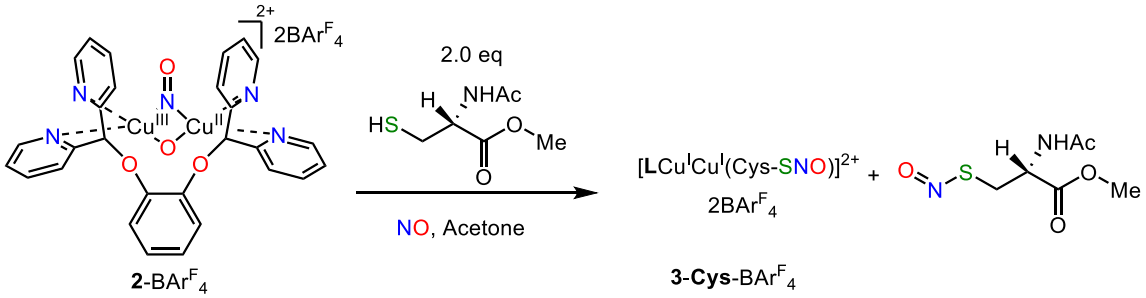

In the glovebox, an acetone solution of **1**-BAr^F_4 (5.4 mg, 2.3 μmol, 2.8 mL) was placed in a Schlenk quartz cuvette. The cuvette was sealed and transferred to the UV-Vis spectrometer precooled at −50 °C. After the temperature stabilized, NO (2.0 mL, 83 μmol, 37 eq.) was injected into the solution and the reaction progress was monitored by taking a UV-Vis spectrum every 60 seconds until the dicopper μ-oxo, μ-nitrosyl **2**-BAr^F_4 band at 525 nm reached absorbance of *ca.* 2.10 and stabilized. The cuvette was cooled to −80 °C before N-acetyl-L-cysteine methyl ester (0.20 mL, 22.5 mM in acetone, 4.5 μmol, 2.0 equiv.) was injected to the solution. The reaction progress was monitored by taking a UV-vis spectrum every 60 seconds. After *ca.* 20 min, the Schlenk cuvette was sealed and transferred to a −70 °C cold bath and stored at this temperature for 24 h. The color of the solution changed from dark red to dark green. The Schlenk cuvette was transferred back to UV-Vis spectrometer precooled at −80 °C. A new green species (λ_{max} = 570 nm, ε = 2500 $M^{-1}cm^{-1}$ and λ_{max} = 670 nm, ε = 2200 $M^{-1}cm^{-1}$) was generated (Figure S45). The comparison of this spectrum with that from the reaction of **1**-BAr^F_4 and one equivalent of S-nitroso N-acetyl-L-cysteine methyl ester is shown in Figure S46, which strongly supports that these two methods generate the same product. To further confirm that two equivalents of S-nitroso N-acetyl-L-cysteine methyl ester were formed

under these conditions, we decided to use CD_3CN to displace the *S*-nitroso N-acetyl-*L*-cysteine methyl ester binding to copper(I) center and quantify the yield by ^1H NMR.

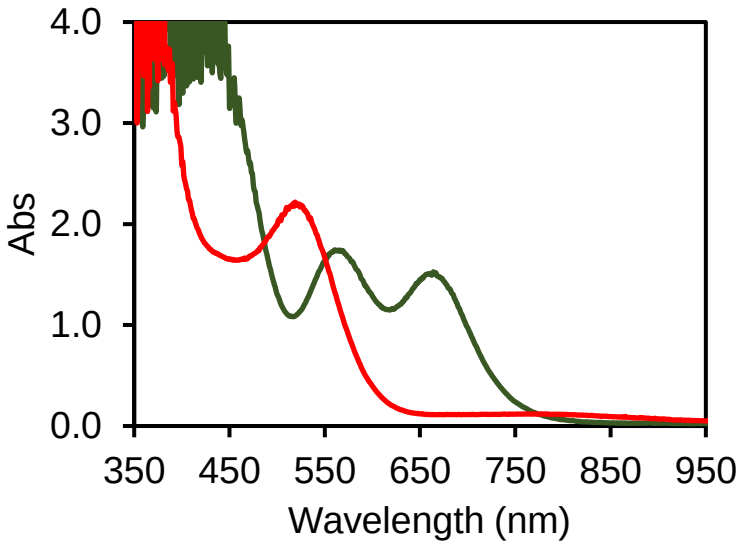

Figure S45. UV-Vis spectra of the reaction mixture of **2**-BAr^F_4 (red trace in acetone at −80 °C) with two equivalents of N-acetyl-L-cysteine methyl ester (green trace at −80 °C in acetone after reaction at −70 °C for 24h).

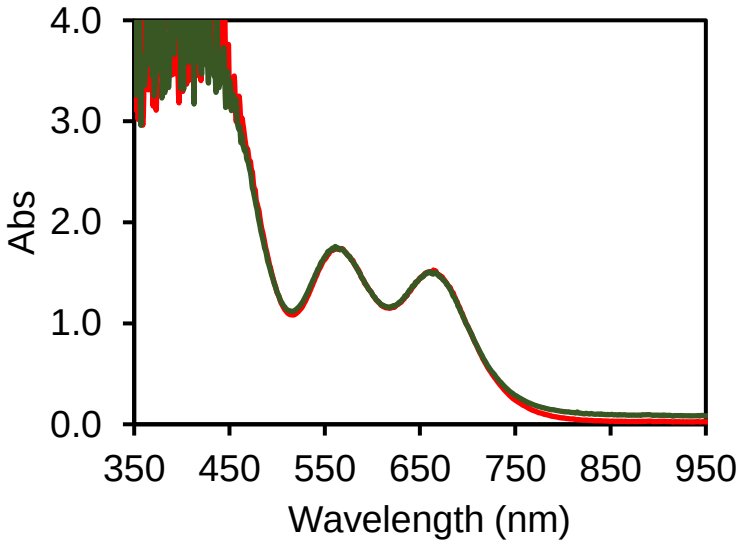

Figure S46. UV-Vis spectra of the reaction mixture of **2**-BAr^F_4 with two equivalents of N-acetyl-L-cysteine methyl ester (green trace at −80 °C in acetone after reaction at −70 °C for 24h) compared with that from reaction mixture of **1**-BAr^F_4 with one equivalent of S-nitroso N-acetyl-L-cysteine methyl ester (black trace at −80 °C in acetone).

Quantification of *S*-nitroso N-acetyl-*L*-cysteine methyl ester from the reaction of 2-BAr$^F_4$ with two equivalents of N-acetyl-*L*-cysteine methyl ester

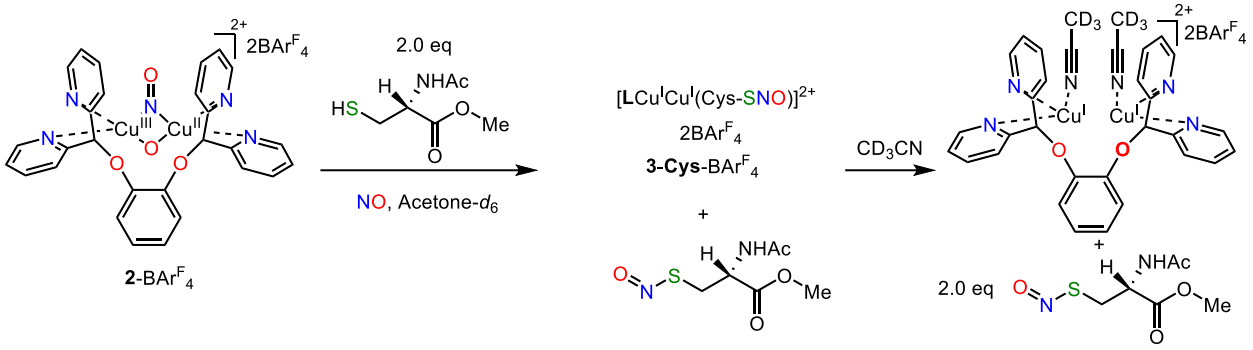

In the glovebox, an acetone-d_6 solution of **1**-BAr$^F_4$ (5.4 mg, 2.27 μmol, 2.8 mL) was placed in a Schlenk quartz cuvette. The cuvette was sealed and transferred to the UV-Vis spectrometer precooled at −50 °C. After the temperature stabilized, NO (3.0 mL, 125 μmol, 56 eq.) was injected into the solution and the reaction progress was monitored by taking a UV-Vis spectrum every 60 seconds until the dicopper μ-oxo, μ-nitrosyl **2**-BAr$^F_4$ band at 525 nm stabilized. The cuvette was cooled to −80 °C before N-acetyl-*L*-cysteine methyl ester (0.10 mL, 45 mM in acetone-d_6, 4.5 μmol, 2.0 equiv.) was injected to the solution, and the reaction progress was monitored by taking a UV-vis spectrum every 60 seconds. After *ca.* 20 min, the Schlenk cuvette was sealed and transferred to a −70 °C cold bath and the reaction continued at this temperature for 20 h. The color of the solution changed from red to dark green. The Schlenk cuvette was then transferred back to UV-Vis spectrometer precooled at −80 °C. The same green species (λ_{max} = 570 nm, ε = 2500 $M^{-1}cm^{-1}$ and λ_{max} = 670 nm, ε = 2200 $M^{-1}cm^{-1}$) was generated. The Schlenk cuvette was further cooled to −90 °C before an acetonitrile-d_3 (0.30 mL, 5.7 mmol, 2500 eq.) solution of internal standard 1,3,5-trimethoxybenzene (2.2 mg, 12.9 μmol) was injected to the solution. After the spectrum stabilized at −90 °C, the temperature was increased to −80 °C and the reaction was monitored with UV-vis until stabilized. These procedures were repeated as the temperature was increased to −70 °C, −60 °C, −50 °C, −40 °C, −20 °C, −10 °C, and finally 0 °C (Figure S47-48). Free S-nitroso N-acetyl-L-cysteine methyl ester signals around 550 nm were observed (Figure S48). The solution was not warmed to room temperature because S-nitroso N-acetyl-L-cysteine methyl ester is unstable at room temperature. The resulting solution was maintained below 0 °C and quickly analyzed by quantitative ^{1}H NMR (relaxation time 20s). We can confirm the existence of free S-nitroso N-acetyl-L-cysteine methyl ester by comparison to the ^{1}H NMR spectrum of pure S-nitroso N-acetyl-L-cysteine methyl in acetone-d_6 (Figure S49). The amount of *S*-nitroso N-acetyl-L-cysteine methyl ester formed in the reaction of dicopper μ-oxo, μ-nitrosyl **2**-BAr$^F_4$ with two equivalents of N-acetyl-L-cysteine methyl ester is 88% based on quantitative ^{1}H NMR (Figure S50) if we consider two equivalents of S-nitrosothiol would be formed relative to **2**-BAr$^F_4$. Based on this NAc-cycteine methyl ester *S*-nitrosothiol quantification experiment (Figure S50) together with the above titration experiments (Figure S43, S44, S46), we conclude that two equivalents of *S*-nitroso N-acetyl-L-cysteine methyl ester were generated in this reaction and one equivalent is bound to dicopper(I,I) complex **1**-BAr$^F_4$ to generate the observed new green species (λ_{max} = 570 nm, ε =2500 $M^{-1}cm^{-1}$ and λ_{max} = 670 nm, ε = 2200 $M^{-1}cm^{-1}$).

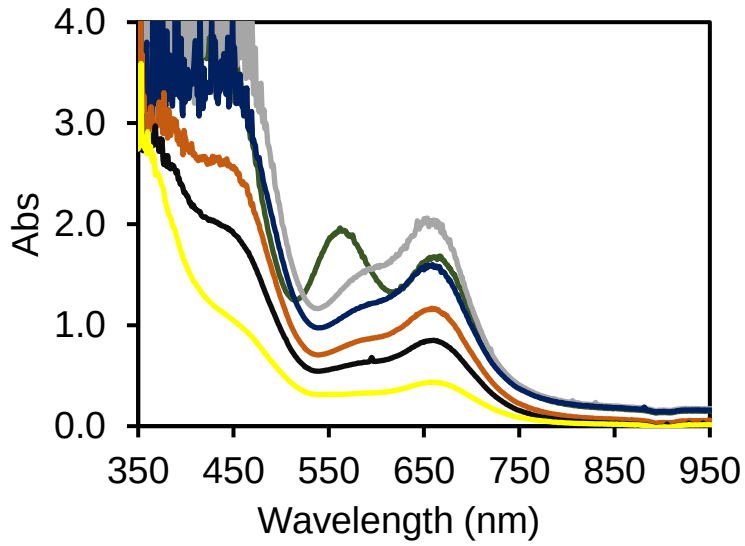

Figure S47. UV-Vis spectra of the reaction mixture of **3-Cys**-BAr^F_4 (dark green trace at −80 °C) with excess acetonitrile-d_3 (gray trace at −90 °C, blue trace at −70 °C, orange trace at −60 °C, black trace at −50 °C, yellow trace at −40 °C).

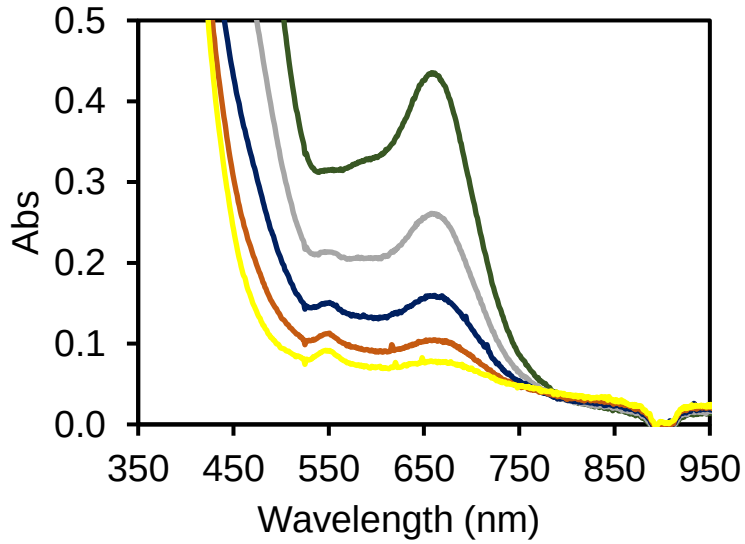

Figure S48. UV-Vis spectra of the reaction mixture of **3-Cys**-BAr^F_4 with excess acetonitrile-d_3 (green trace at −40 °C, gray trace at −30 °C, blue trace at −20 °C, brown trace at −10 °C, yellow trace at 0 °C).

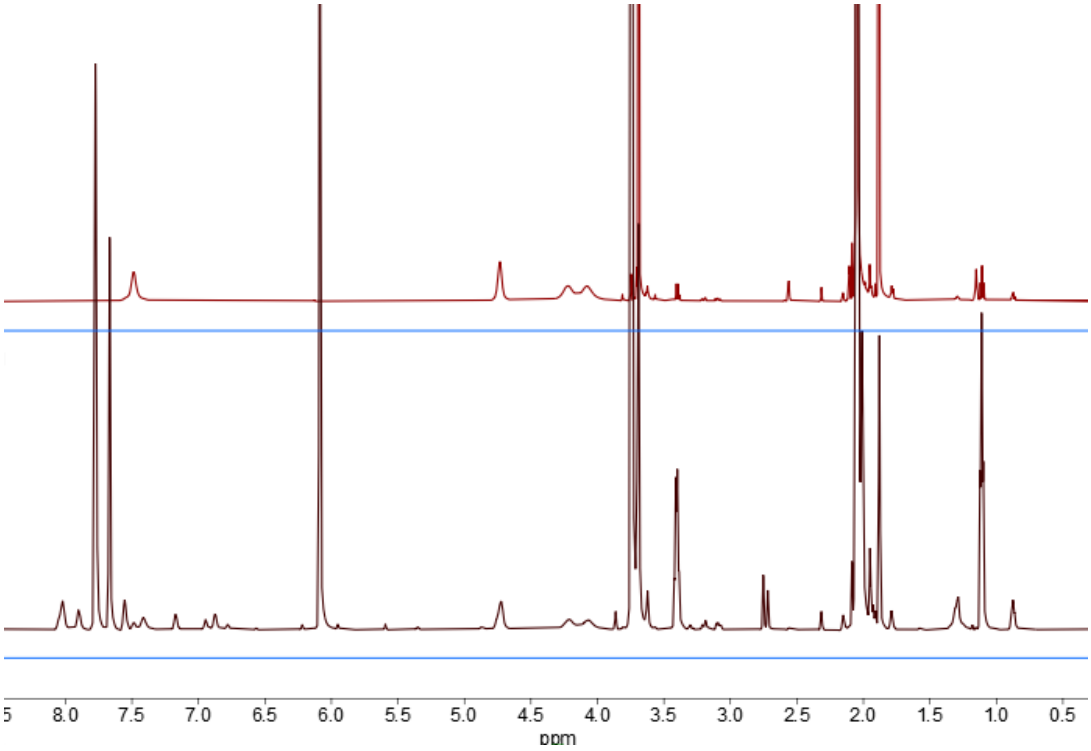

Figure S49. ^{1}H NMR (600 MHz, acetone-d_6) of free S-nitroso N-acetyl-L-cysteine methyl ester in acetone-d_3(up) and reaction mixture of **1**-BAr$^{F}_4$, excess NO with two equivalents of N-acetyl-L-cysteine methyl ester followed by addition of excess acetonitrile-d_3 in acetone-d_6(bottom).

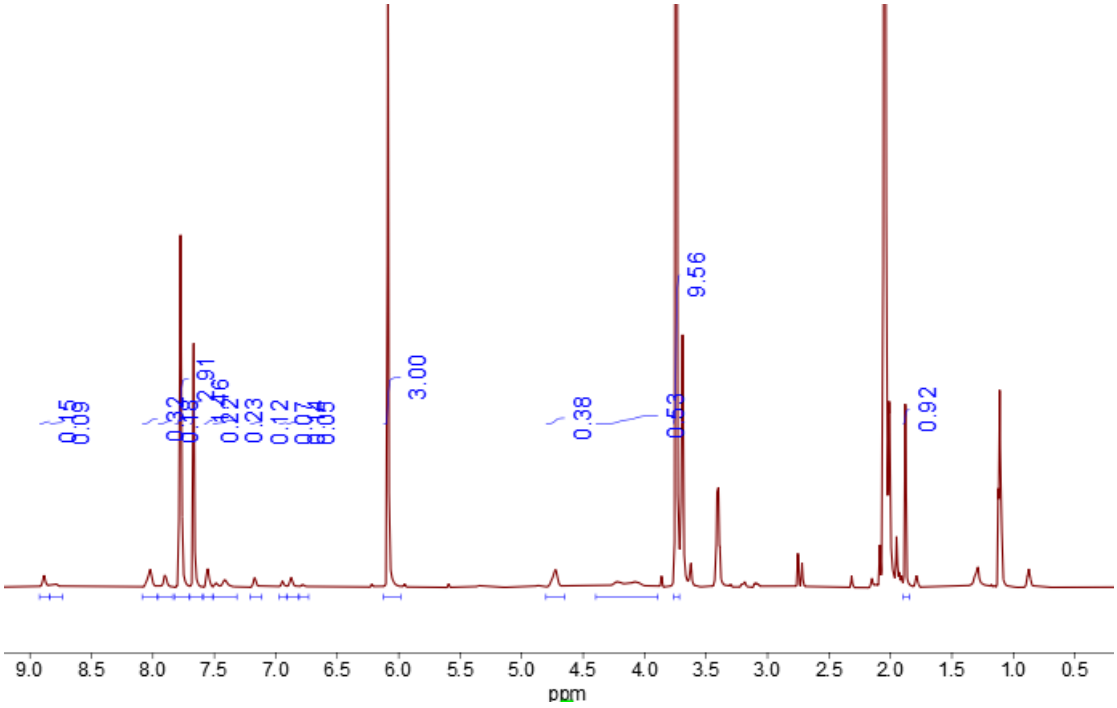

Figure S50. ^{1}H NMR (600 MHz, acetone-d_6) of **3-Cys**-BAr$^{F}_4$ and excess acetonitrile-d_3 in acetone-d_6.

Note: The amount of internal standard 1,3,5-trimethoxybenzene used is 2.2 mg (12.9 μmol). The amount of dicopper (I,I) precursor **1**-BAr^F_4 used is 5.4 mg (2.25 μmol). The S-nitroso N-acetyl-L-cysteine methyl ester has signals at 7.49 ppm, 4.73 ppm, 4.21 ppm, 4.07 ppm, 1.88 ppm. Some of the peaks are overlapped with or very close to internal standard or solvent signals, so we used the characteristic methyl signal at 1.88 ppm to quantify the amount of S-nitrosothiol formed, that is 0.92/3×12.9 = 3.96 μmol. The maximum S-nitroso N-acetyl-L-cysteine methyl ester formed is two equivalents relative to **2**-BAr^F_4, which is 2×2.25=4.50 μmol. As a result, the yield of S-nitroso N-acetyl-L-cysteine methyl ester formation is 3.96/4.50= 88%. At the same time, the recovered dicopper(I,I) precursor **1**-BAr^F_4 has characterized signals in the aromatic area. The recovered amount of **1**-BAr^F_4 is *ca.* 0.12/2×12.9=0.77 μmol so the recovered yield is *ca.*0.77/2.25=34%.

Reaction of 1-OTf with nitric oxide in methanol

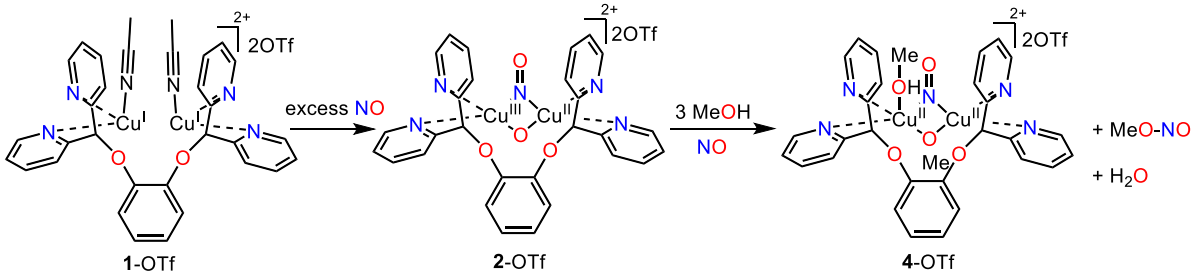

In the glovebox, a methanol solution of **1**-OTf (2.1 mg, 2.3 μmol, 3.0 mL) was placed in a Schlenk quartz cuvette. The cuvette was sealed and connected to a three-way valve which linked both Schlenk line and nitric oxide line. The Schlenk cuvette was cooled in a dry ice/acetone bath and evacuated under vacuum to remove the nitrogen in the headspace and in the solution. The cuvette was sealed. The tubing between Schlenk cuvette and the three-way valve was then filled with pure nitric oxide (*ca.* 30 mL). The Schlenk cuvette and tubing was then transferred to the UV-Vis spectrometer precooled at −80 °C. After the temperature stabilized, the Schlenk cuvette was opened and the NO in the tubing was allowed to diffuse into the solution. The reaction progress was monitored by taking a UV-Vis spectrum every 60 seconds. After *ca.* 15 min, the cuvette was warmed up to −70 °C, then −60 °C, −50 °C, −40 °C and finally −30 °C. A new dark red species (λ_{max} = 540 nm, ε =2000 $M^{-1}cm^{-1}$ and λ_{max} = 475 nm, ε =2200 $M^{-1}cm^{-1}$) is generated which is stable below −30 °C (Figure S51). The single crystal of the product dicopper(II,II) μ-methoxy, μ-nitrosyl **4**-OTf was obtained by using the above conditions to generate the product, which was then recrystallized with toluene and diethyl ether at −40 °C in the glove box.

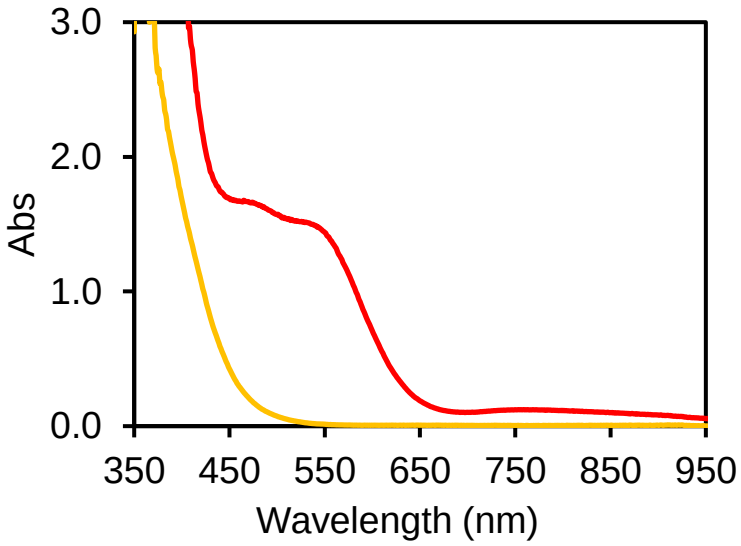

Figure S51. UV-Vis spectra of the reaction mixture of **1**-OTf (yellow trace) and excess nitric oxide in methanol at −30 °C in 0.75 mM concentration (red trace).

Reaction of 1-BAr$^{F}_{4}$ with nitric oxide in methanol

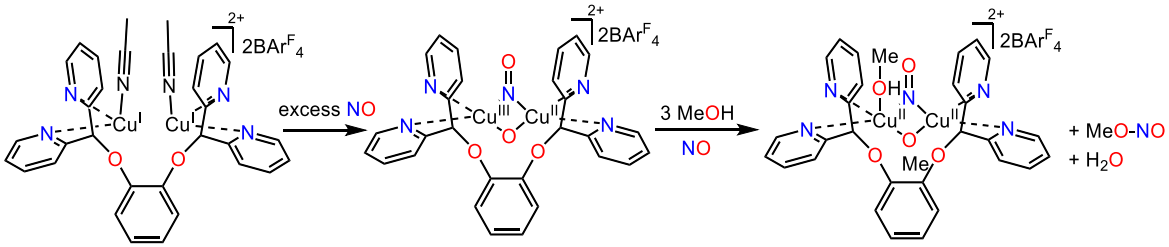

In the glovebox, a methanol solution of **1**-BAr$^{F}_{4}$ (5.4 mg, 2.3 μmol, 3.0 mL) was placed in a quartz cuvette equipped with a rubber septum. The cuvette was sealed and transferred to the UV-Vis spectrometer precooled at −40 °C. After the temperature stabilized, NO (2.0 mL, 83 μmol, 36 eq.) was injected into the solution and the reaction progress was monitored by taking a UV-Vis spectrum every 60 seconds. After *ca.* 20 min, the spectrum stabilized. Additional NO (1.0 mL, 42 μmol, 18 eq) was injected to the solution and the reaction progress was monitored by taking a UV-Vis spectrum every 60 seconds. After *ca.* 30 min, additional NO (2.0 mL, 83 μmol, 36 eq.) was injected into the solution and the reaction was monitored at this temperature by taking UV-Vis spectrum every 60 seconds until the 480 nm and 540 nm bands stabilized. The cuvette was warmed up to −30 °C and the spectra did not change. A new dark red species (λ_{max} = 540 nm, ε =2000 $M^{-1}cm^{-1}$ and λ_{max} = 475 nm, ε =2200 $M^{-1}cm^{-1}$) was generated which is stable below −30 °C (Figure S52). The product spectrum is compared with that from **1**-OTf and excess nitric oxide in methanol at −30 °C (Figure S51) in Figure S53, suggesting both **1**-BAr$^{F}_{4}$ and **1**-OTf can perform the same reductive nitric oxide coupling reaction followed by protonation of μ-oxo moiety with methanol and further reductive *O*-nitrosation, affording methyl nitrite as the byproduct. To support our hypothesis, we

also tried the above reaction at 0.20 mM concentration level to observe the diagnostic "five-finger" features of alkyl nitrite in UV-Vis.

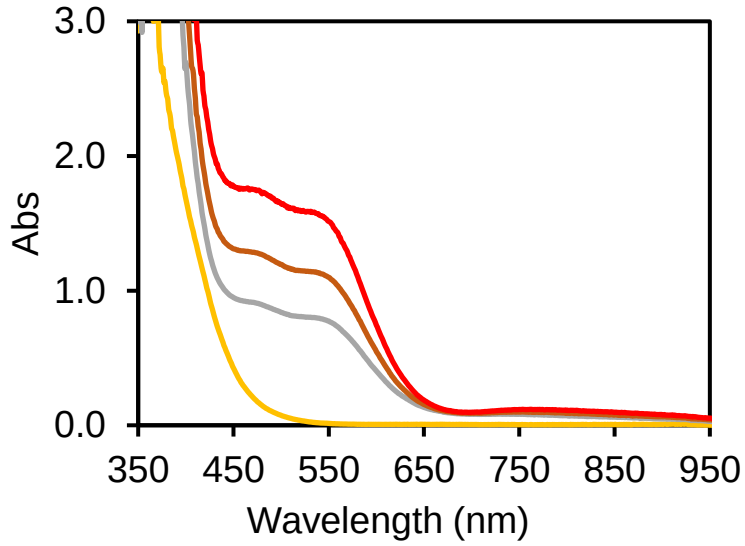

Figure S52. UV-Vis spectra of the reaction mixture of **1**-BAr^{F}_{4} (yellow trace) and nitric oxide in methanol at −30 °C (gray trace with 36 eq. NO, brown trace with 54 eq. NO and finally dark red trace with 90 eq NO).

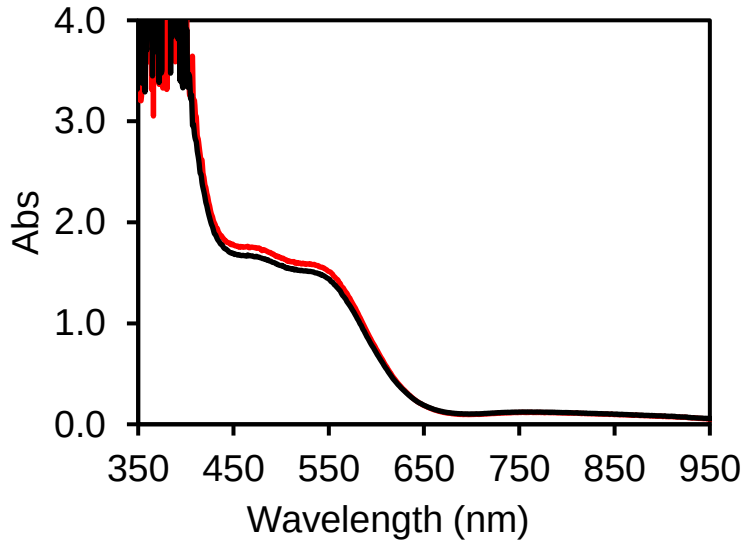

Figure S53. UV-Vis spectra of the reaction mixture of **1** and excess amount of nitric oxide in methanol at −30 °C (black trace with OTf anion and red trace with BAr^{F}_{4} counter anion).

Reaction of 1-BAr$^{F}_{4}$ with nitric oxide in methanol at 0.20 mM concentration

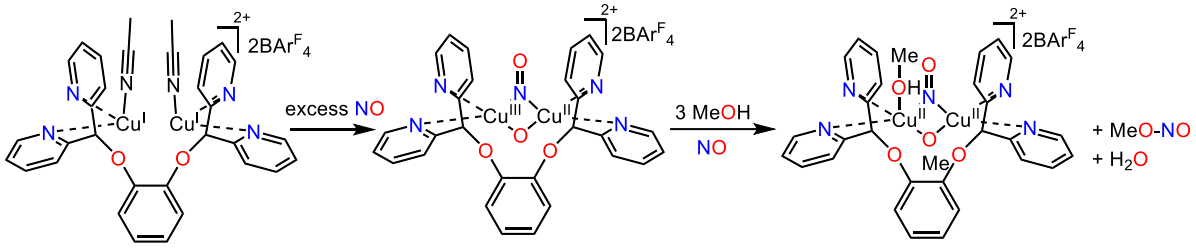

In the glovebox, a methanol solution of **1**-BAr$^{F}_{4}$ (1.4 mg, 0.59 μmol, 3.0 mL, 0.20 mM) was placed in a quartz cuvette equipped with a rubber septum. The cuvette was sealed and transferred to the UV-Vis spectrometer precooled at −40 °C. After the temperature stabilized, NO (2.0 mL, 83 μmol, 140 eq.) was injected into the solution and the reaction progress was monitored by taking UV-Vis spectrum every 60 seconds. After *ca.* 30 min, the spectrum stabilized. Additional NO (2.5 mL, 104 μmol, 176 eq) was injected to the solution and the reaction progress was monitored by taking UV-Vis spectrum every 60 seconds until the 480 nm and 540 nm bands stabilized. The cuvette was warmed up to −30 °C and the spectra did not change. The new dark red species (λ_{max} = 540 nm, ε =2000 $M^{-1}cm^{-1}$ and λ_{max} = 475 nm, ε =2200 $M^{-1}cm^{-1}$) was reproduced at this concentration (Figure S54). In this case, we observed the diagnostic "five-finger" features of alkyl nitrite in UV-Vis spectrum. Based on this experiment and the single crystal structure of dicopper(II,II) μ-methoxy, μ-nitrosyl **4**-OTf, we concluded that when methanol was used as the substrate in this system, stepwise *O*-nitrosation reaction occurs in contrast to the fully S-nitrosation reaction with primary thiols and thiophenols.

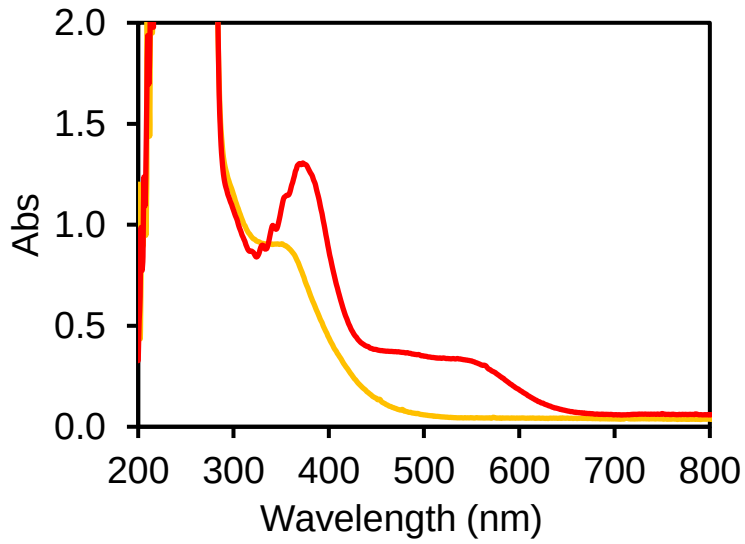

Figure S54. UV-Vis spectra of the reaction mixture of **1**-BAr$^{F}_{4}$ (yellow trace) and excess nitric oxide in methanol at −30 °C in 0.20 mM concentration (red trace).

Reaction of 2-BAr$^{F}_{4}$ with methanol

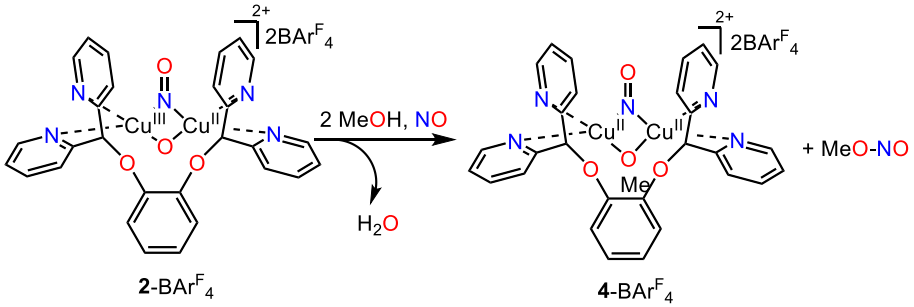

In the glovebox, a solution of **1**-BAr$^{F}_{4}$ (5.4 mg, 2.3 μmol, 3.0 mL) in a 1:1 mixture of DCM and THF was placed in a quartz cuvette equipped with a rubber septum. The cuvette was sealed and transferred to the UV-Vis spectrometer precooled at −40 °C. After the temperature stabilized, NO (2.0 mL, 83 μmol, 37 eq.) was injected into the solution and the reaction progress was monitored by taking UV-Vis spectrum every 60 seconds. After *ca.* 90 min, the spectra with diagnostic **2**-BAr$^{F}_{4}$ band (λ_{max} = 530 nm, ε =2300 $M^{-1}cm^{-1}$) stabilized. Methanol (0.10 mL, 2.47 mmol, 1100 eq) was injected into the solution and the reaction progress was monitored at this temperature by taking UV-Vis spectra every 60 seconds. Similar to the reaction of **1**-BAr$^{F}_{4}$ with NO in pure methanol in Figure S49, a dark red species (λ_{max} = 475 nm, ε =2200 $M^{-1}cm^{-1}$ and λ_{max} = 530 nm, ε =2300 $M^{-1}cm^{-1}$) was generated (Figure S55). This species is stable below −30 °C. To further corroborate that **4**-BAr$^{F}_{4}$ would be directly formed by complex **1**-BAr$^{F}_{4}$ with NO in the same solvents, we performed the following reaction.

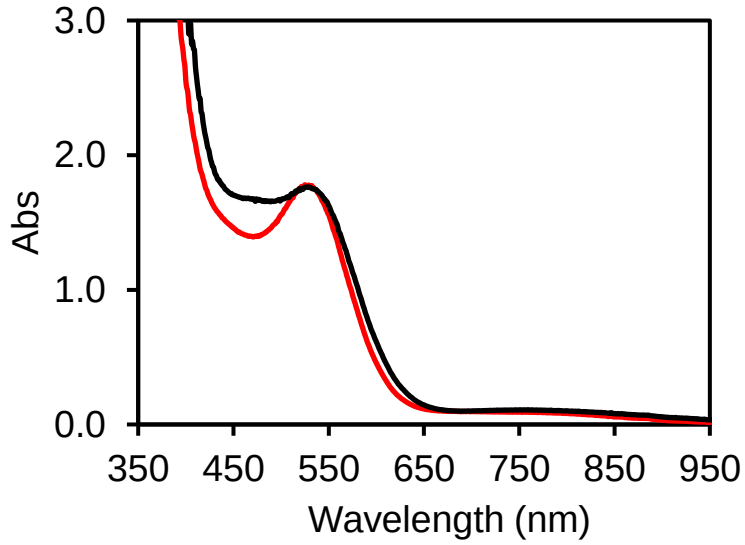

Figure S55. UV-Vis spectra of the reaction mixture of **2**-BAr$^{F}_{4}$ (red trace) and 1100 equivalents of methanol (black trace) at −40 °C.

Reaction of 1-BAr$^{F}_4$ with nitric oxide in mixed solvent

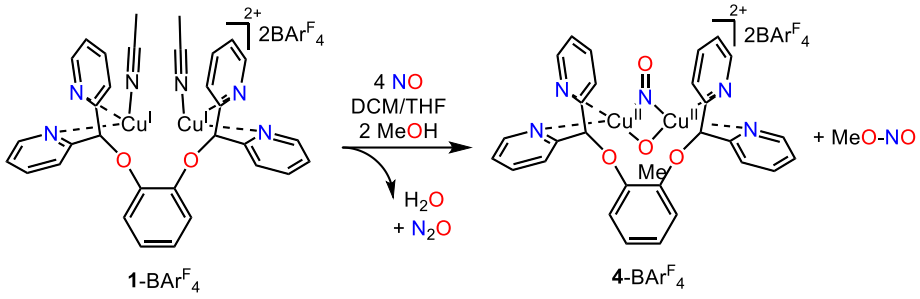

In the glovebox, a solution of **1**-BAr$^{F}_4$ (5.4 mg, 2.3 μmol) in a 1:1 mixture of DCM (1.5 mL) and THF (1.5 mL) together with methanol (0.10 mL, 2.47 mmol, 1100 eq) was placed in a quartz cuvette equipped with a rubber septum. The cuvette was sealed and transferred to the UV-Vis spectrometer precooled at −40 °C. After the temperature stabilized, NO (2.0 mL, 83 μmol, 36 eq.) was injected into the solution and the reaction progress was monitored by taking UV-Vis spectrum every 60 seconds. After *ca.* 60 min, very similar spectra with diagnostic **4**-BAr$^{F}_4$ bands (λ_{max} = 475 nm, ε =2000 $M^{-1}cm^{-1}$ and λ_{max} = 530 nm, ε =2000 $M^{-1}cm^{-1}$) was observed (Figure S56). This spectrum is compared with that from the reaction of **2**-BAr$^{F}_4$ with methanol in the same mixed solvent in Figure S57, which further supports that **4**-BAr$^{F}_4$ is formed by the reaction of methanol with dicopper μ-oxo, μ-nitrosyl intermediate **2**-BAr$^{F}_4$ probably through protonation of **2**-BAr$^{F}_4$ with two equivalents of methanol followed by stepwise reductive *O*-nitrosation. These reaction conditions do not require a large excess amount of nitric oxide. As a result, these conditions were used for in-situ IR experiments to investigate the NO stretch of **4**.

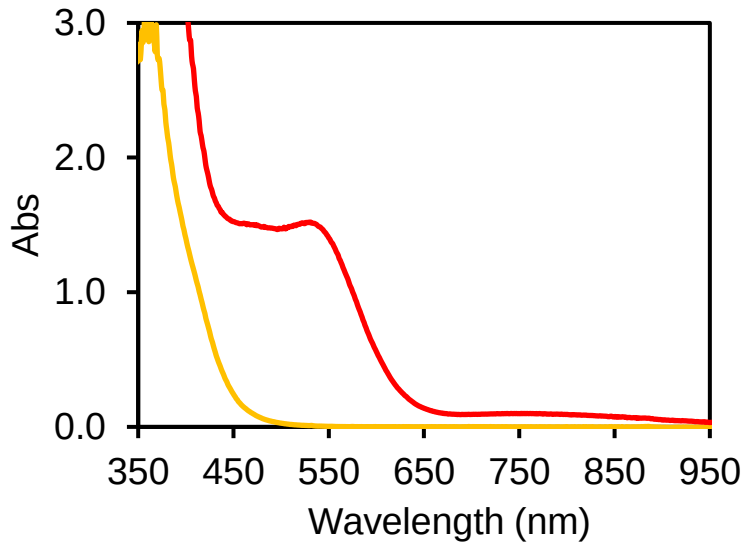

Figure S56. UV-Vis spectra of the reaction mixture of **1**-BAr$^{F}_4$ (yellow trace) and excess NO in the presence of 1100 equivalents of methanol in a 1:1 mixture of DCM and THF (red trace) at −40 °C.

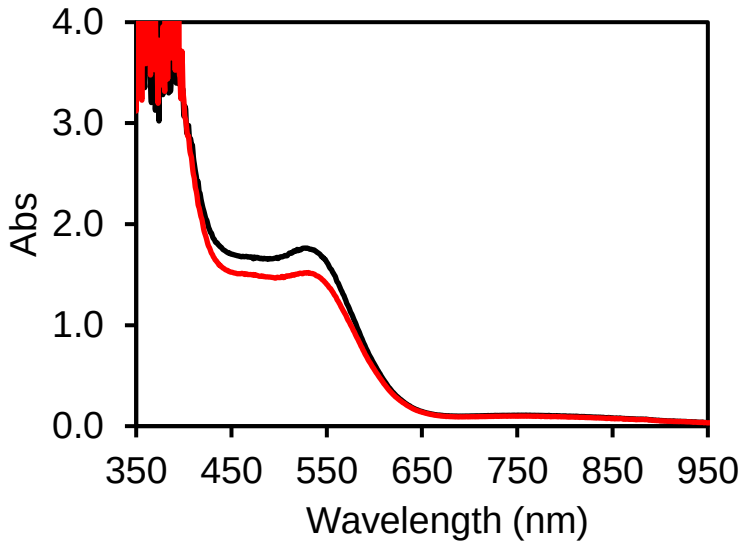

Figure S57. UV-Vis spectra of the reaction mixture of **1**-BAr^F_4 and excess NO in the presence of 1100 equivalents of methanol in a 1:1 mixture of DCM and THF (red trace) at −40 °C compared with that from the reaction of **2**-BAr^F_4 and 1100 equivalents of methanol in the same solvent at −40 °C (black trace).

Reaction of 2-BAr^F_4 with 2-phenylethanethiolate

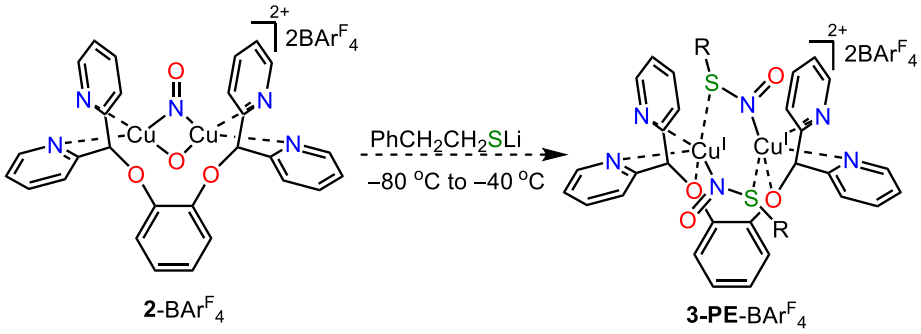

In the glovebox, a solution of **1**-BAr^F_4 (5.4 mg, 2.3 μmol) in a mixture of acetone (1.5 mL) and THF (1.4 mL) was placed in a quartz cuvette equipped with a rubber septum. The cuvette was sealed and transferred to the UV-Vis spectrometer precooled at −40 °C. After the temperature stabilized, NO (2.0 mL, 83 μmol, 36 eq.) was injected into the solution and the reaction progress was monitored by taking a UV-Vis spectrum every 60 seconds. After *ca.* 30 min, dicopper μ-oxo, μ-nitrosyl intermediate **2**-BAr^F_4 band (λ_{max} = 530 nm, ε =2400 $M^{-1}cm^{-1}$) stabilized. The cuvette was cooled to −60 °C and stabilized before 2-phenylethanethiolate (0.10 mL, 22.5 mM in THF, 2.3 μmol) was injected into the above solution. Different from the reaction of **2**-BAr^F_4 with 2-phenylethanethiol, we observed that the 530 nm band decayed gradually, while no new Cu(I)-*S*-nitrosothiol charge transfer bands near 580 nm and 690 nm were observed (Figure S58). This experiment suggests that protonation of the μ-oxo moiety is essential for the following reductive S-nitrosation.

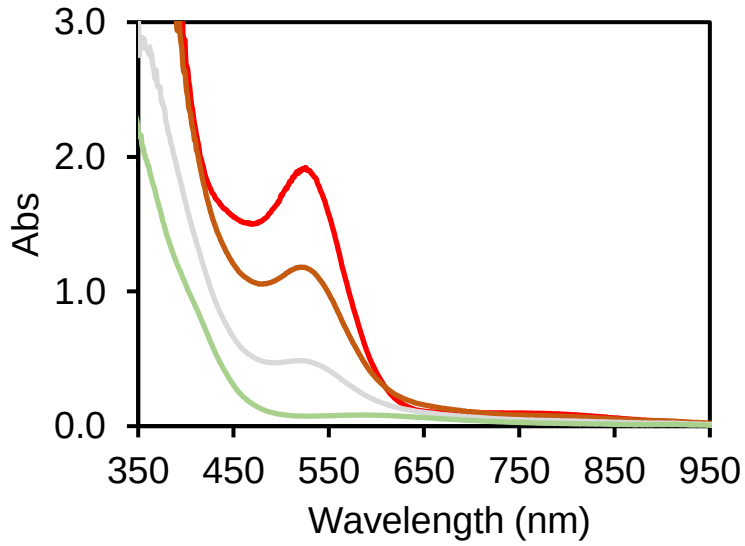

Figure S58. UV-Vis spectra of the reaction mixture of **2**-BAr^F_4 (red trace) and one equivalent of 2-phenylethanethiolate (brown trace at −60 °C, gray trace at −50 °C and light green trace at −40 °C).

^{15}N NMR characterization of proposed dicopper(I,I) di-*S*-nitrosothiol

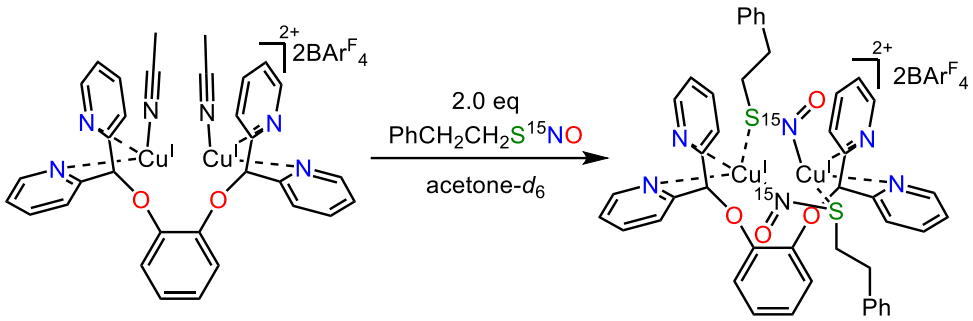

In the glovebox, **1**-BAr^F_4 (183 mg, 76.8 μmol) was dissolved in acetone-d_6 (320 μL) to make a 240 mM solution. $PhCH_2CH_2S^{15}NO$ (48.4 mg, 288 μmol) was dissolved in acetone-d_6 (200 μL) to make a 1440 mM solution in the dark. The above acetone-d_6 solution of **1**-BAr^F_4 (240 mM, 0.300 mL, 72 μmol) was transferred into an NMR tube with a screw cap and septum seal. The NMR tube was sealed and transferred out of the glove box and connected to a Schlenk adapter through a rubber septum. The Schlenk adapter was evacuated under vacuum and refilled with nitrogen. The vacuum/refill cycle was repeated five times. The bottom of the NMR tube (*ca.* 5.0 cm long) was cooled in a dry ice/acetone bath for at least 20 min before the above $PhCH_2CH_2S^{15}NO$ solution in acetone-d_6 (1440 mM, 0.120 mL, 173 μmol, 2.4 eq) was injected into the NMR tube dropwise through the septum under positive nitrogen flow. The NMR tube was then sealed quickly with parafilm under positive nitrogen flow and transferred to a −75 °C cold bath. After *ca.* 15 min, the NMR tube was shaken quickly for *ca.* 5 seconds and put back to −75 °C cold bath. These procedures were repeated 5 times to help mix the two substrates as the mixture is very viscous at −75 °C.

The cold NMR tube was transferred to the NMR instrument with the probe pre-cooled at −80 °C. ^{15}N NMR spectrum was collected at −80 °C (Figure S59).

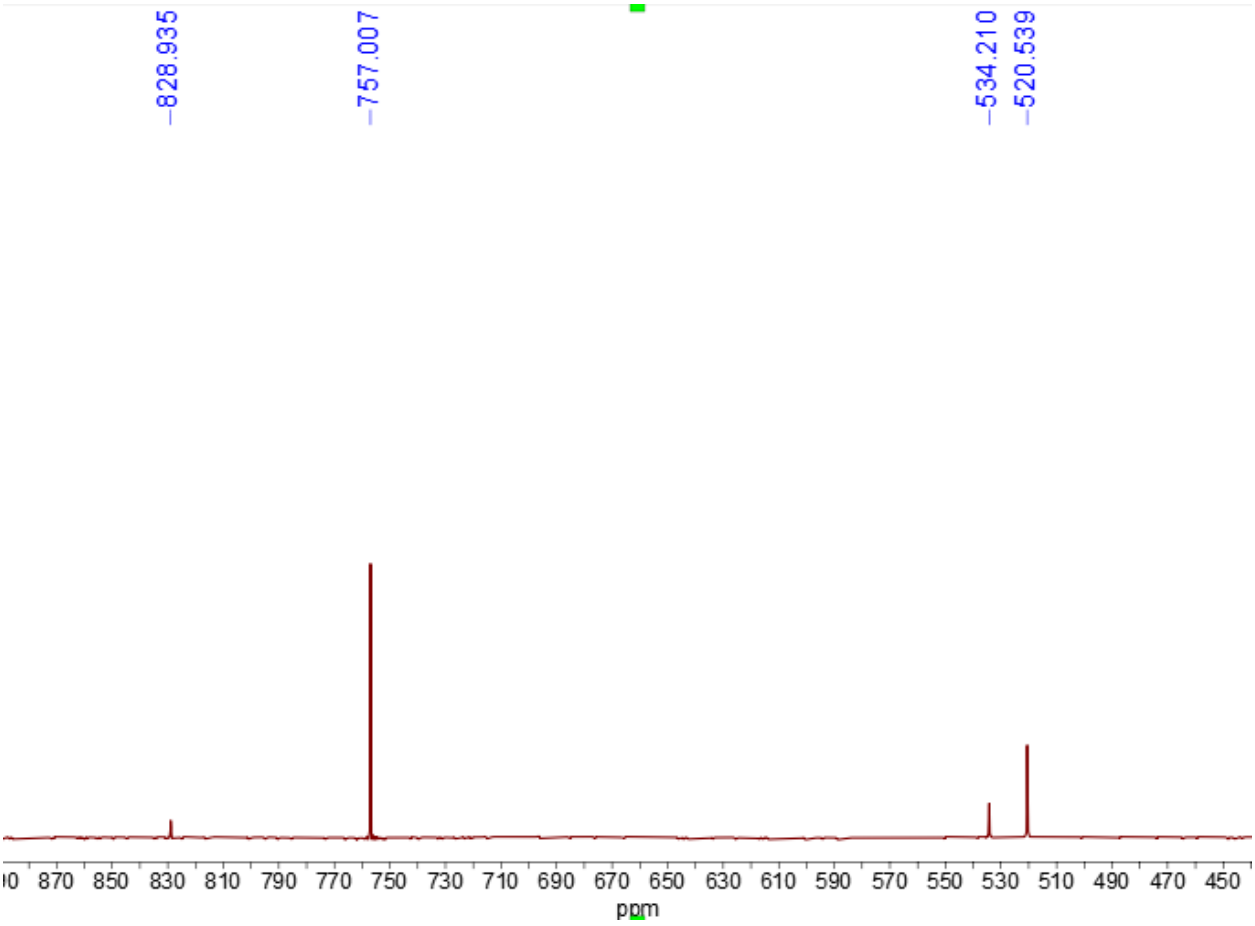

Figure S59: ^{15}N NMR (61 MHz, acetone-d_6) spectrum of reaction mixture of **1**-BAr$^{F}_{4}$ with 2.4 eq of $PhCH_2CH_2S^{15}NO$ at −80 °C. The ^{15}N chemical shift is referenced to NH_3 (0 ppm).

Solvent effect on *S*-nitroso-2-phenylethanethiol binding to dicopper(I,I) complex

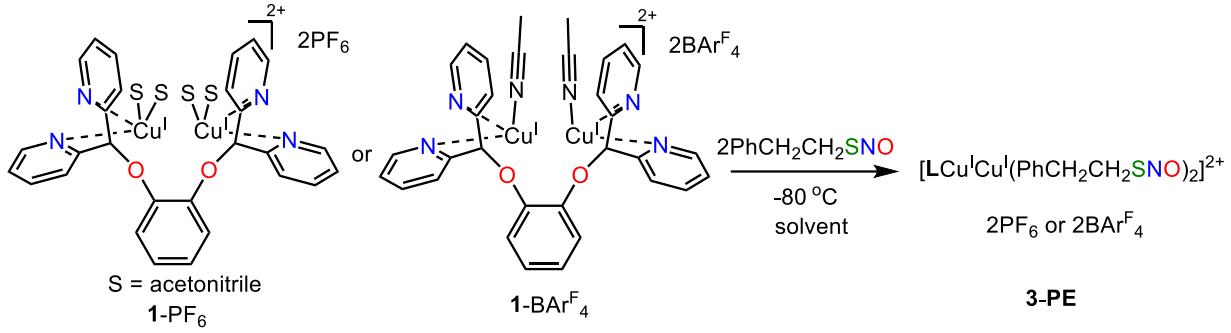

In the glovebox, a diethyl ether solution of **1**-BAr^F_4 (5.4 mg, 2.3 μmol, 2.80 mL) was placed in a quartz cuvette equipped with a rubber septum. The cuvette was sealed and transferred to the UV-Vis spectrometer precooled at −80 °C. After the temperature stabilized, $PhCH_2CH_2SNO$ (0.20 mL, 22.5 mM in diethyl ether, 4.5 μmol, 2.0 equiv.) was injected to the solution, and the reaction progress was monitored by taking a UV-vis spectrum every 60 seconds. A new green species (λ_{max} = 595 nm, ε = 1900 $M^{-1}cm^{-1}$ and λ_{max} = 645 nm, ε = 2200 $M^{-1}cm^{-1}$) is generated (Figure S60, green trace). The product spectrum in diethyl ether solvent is compared to that derived from **1**-BAr^F_4 and two equivalents of $PhCH_2CH_2SNO$ in acetone (Figure S60, gray trace), THF (Figure S60, black trace) and **1**-PF_6 with two equivalents of $PhCH_2CH_2SNO$ in DCM (Figure S60, red trace) at the same concentration.

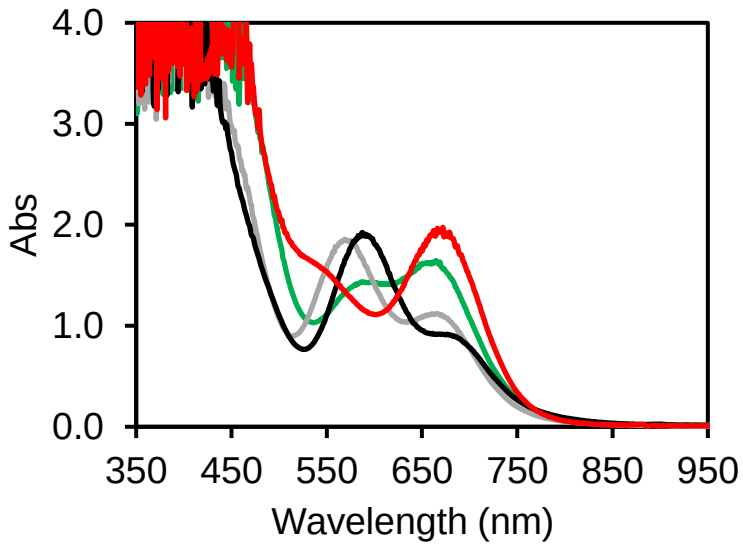

Figure S60. Experimental spectra of **3-PE** from reaction mixture of dicopper(I,I) precursor **1** and two equivalents of $PhCH_2CH_2SNO$ in different solvents at −80 °C (red trace, DCM; green trace, diethyl ether; black trace, tetrahydrofuran; gray trace, acetone.)

3. X-ray Crystallographic Data

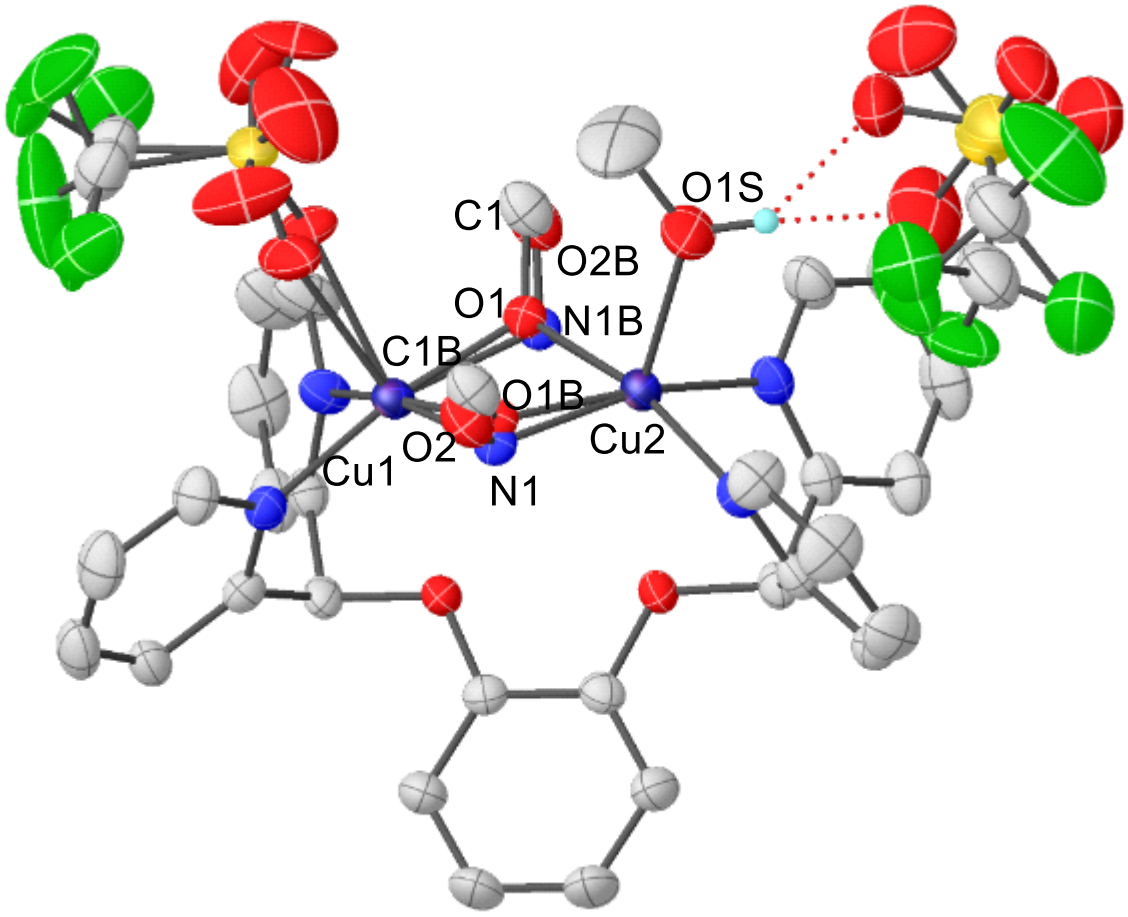

Figure S61: X-ray structure of **4**–OTf with thermal ellipsoids of 50% probability. Hydrogen atoms are omitted for clarity except for one with hydrogen bonding. Selected bond lengths (Å) and angles (°) for **4**–OTf: Cu1–N1 = 1.976(16), Cu2–N1 = 2.00(3), Cu1–O1 = 1.871(15), Cu2–O1 = 1.950(13), N1–O2 = 1.32(5), N1B-O2B = 1.27(4), Cu1-N1-Cu2 = 97.1(12), Cu2-O1S = 2.227(3).

Table S1: Crystal Data and Structure Refinement for Complexes**.**

	4
CCDC	
Empirical formula, FW (g/mol)	$C_{35.50}H_{33}Cu_2F_6N_5O_{11}S_2$, 1010.87
Color	Red
Temperature (K)	150
Wavelength (Å)	0.71073
Crystal system, Space group	Triclinic, P-1
Unit cell dimensions a (Å)	10.1398(11)
b (Å)	13.6935(16)
c (Å)	14.7211(17)
α(°)	95.640(4)
β(°)	92.763(4)
γ(°)	93.199(4)
Volume ($Å^3$)	2028.0(4)
Z	2
Density (calc., g/cm^{-3})	1.655
Absorption coefficient (mm^{-1})	1.244
F(000)	1026
Theta range for data collection (°)	2.785 to 26.394
Index ranges	-12<=h<=12, -17<=k<=17, -18<=l<=18
Reflections collected	77507
Independent reflections, R_{int}	8302 [R(int) = 0.0644, R(sigma) = 0.0356]
Completeness to θ_{max} (%)	99.8
Absorption correction	Semi-empirical from equivalents
Refinement method	Full-matrix least-squares on F^2

Data / restraints / parameters	8302 / 232 / 670
Goodness-of-fit	1.067
Final R indices [I>2sigma(I)]	R1 = 0.0479, wR2 = 0.1100
Largest diff. peak and hole ($e \cdot Å^{-3}$)	1.139 and -0.943

4. In-situ IR to investigate N=O stretching frequency

IR of 1-BAr$^{F}_{4}$ reacting with two equivalents of PhCH$_2$CH$_2$SNO and PhCH$_2$CH$_2$S^{15}NO in THF-d_8

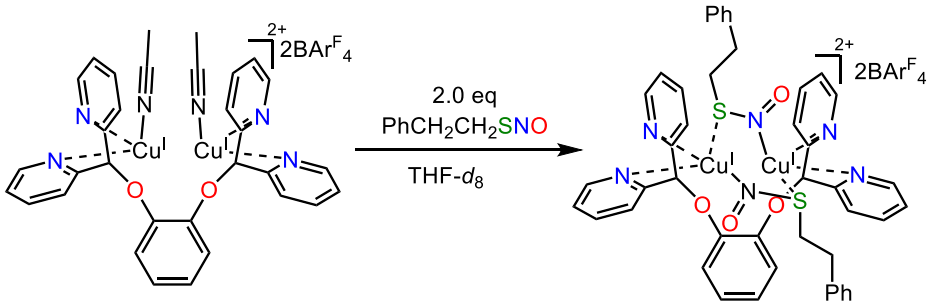

1-BAr$^{F}_{4}$ (57.6 mg, MW=2382.15 g/mol, 24.2 μmol) was dissolved in THF-d_8 (1.1 mL) to afford a 22 mM solution. PhCH$_2$CH$_2$SNO (14.7 mg, 87.9 μmol) was dissolved in THF-d_8 (0.20 mL) to afford a 440 mM solution. PhCH$_2$CH$_2$S^{15}NO (14.8 mg, 87.9 μmol) was dissolved in THF-d_8 (0.20 mL) to afford a 440 mM solution. The **1**-BAr$^{F}_{4}$ (1.0 mL, 22 mM solution in THF-d_8, 22 μmol) solution was injected into a three-neck cell that had been connected to the react IR probe and purged with nitrogen for *ca.* 2.5 h. The cell was cooled in a dry ice/acetone bath (−78 °C) for *ca.* 20 min. After the temperature inside the cell stabilized, PhCH$_2$CH$_2$SNO or PhCH$_2$CH$_2$S^{15}NO (0.10 mL, 440 mM solution in THF-d_8, 44 μmol, 2.0 equiv.) was injected into the cold solution dropwise, and the reaction progress was monitored for *ca.* 1.5 h at this temperature. The IR spectra of *S*-nitrosothiol bound dicopper(I,I) complex synthesized from PhCH$_2$CH$_2$SNO (black trace) or PhCH$_2$CH$_2$S^{15}NO (red trace) are shown in Figure S62. Subtraction of the IR spectra of S-nitrosothiol-bound dicopper complex synthesized with PhCH$_2$CH$_2$S^{15}NO from that with PhCH$_2$CH$_2$SNO generates the ^{14}N/^{15}N differential spectrum in Figure S63. Based on this experiment, two N=O stretches at 1512 cm^{-1} and *ca.* 1505 cm^{-1} are shifted to 1491 cm^{-1} and 1479 cm^{-1} respectively when PhCH$_2$CH$_2$S^{15}NO is used instead of PhCH$_2$CH$_2$S^{14}NO to bind to **1**-BAr$^{F}_{4}$. These N=O peaks can be assigned as symmetric and unsymmetric stretches of two N=O motifs.

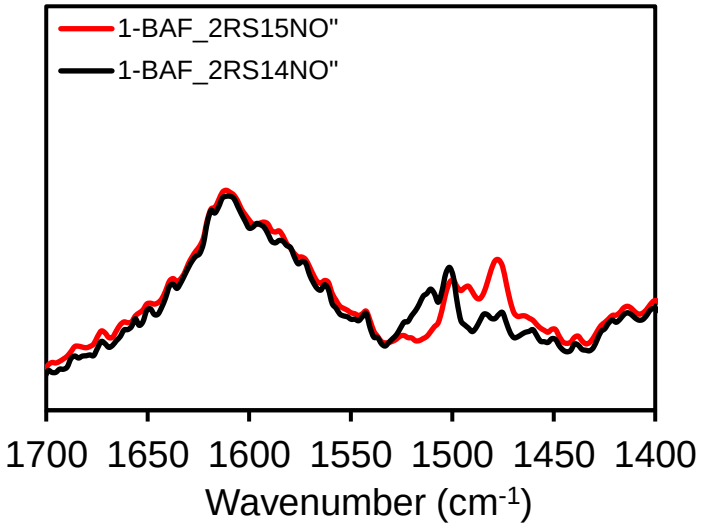

Figure S62. IR spectra of *S*-nitrosothiol-bound dicopper(I,I) complex from **1**-BAr$^{F}_{4}$ with PhCH$_2$CH$_2$SNO (black trace), or PhCH$_2$CH$_2$S^{15}NO (red trace) in THF-d_8 solvent in a dry ice/acetone bath. νNO_{14N} = *ca.*

1512 and 1505 cm^{-1}; νNO_{15N} = *ca.* 1491 and 1479 cm^{-1} $\Delta\nu NO_{14N-15N}$ = 21 and 26 cm^{-1}; $\Delta\nu NO_{14N-15N}$ calculated from Hooke's Law is 27 and 27 cm^{-1}.

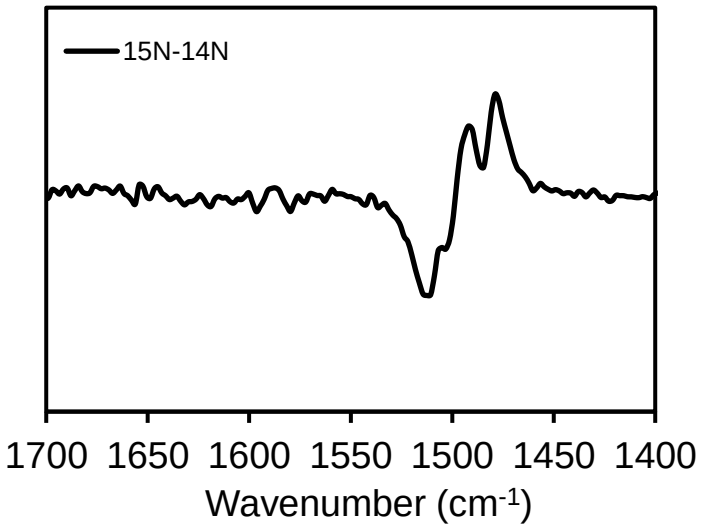

Figure S63. IR spectrum of S-nitrosothiol bound dicopper(I,I) complex synthesized with $PhCH_2CH_2S^{15}NO$ subtracted from that with $PhCH_2CH_2SNO$. νNO_{14N} = 1512 and 1505 cm^{-1}; νNO_{15N} = 1491 and 1479 cm^{-1} $\Delta\nu NO_{14N-15N}$ = 21 and 26 cm^{-1}; $\Delta\nu NO_{14N-15N}$ calculated from Hooke's Law is 27 and 27 cm^{-1}.

IR of free $PhCH_2CH_2SNO$ and $PhCH_2CH_2S^{15}NO$

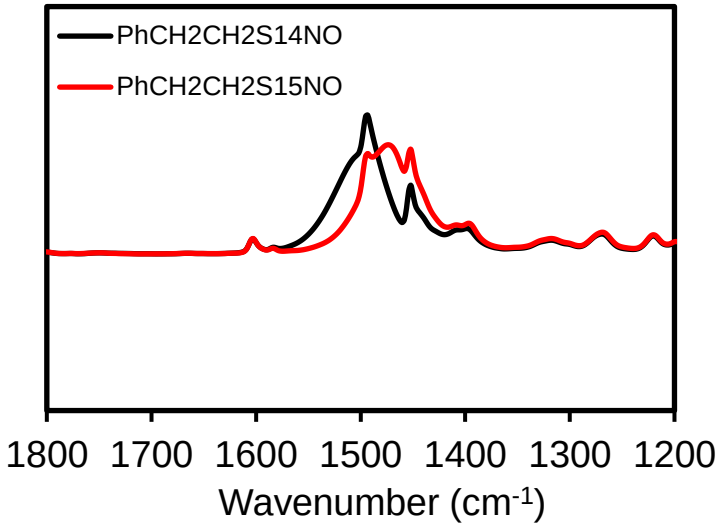

Figure S64. Infrared spectra of free $PhCH_2CH_2SNO$ (black trace) and $PhCH_2CH_2S^{15}NO$ (red trace). νNO_{14N} = 1495; νNO_{15N} = 1468 cm^{-1} $\Delta\nu NO_{14N\text{-}15N}$ = 27 cm^{-1}; $\Delta\nu NO_{14N-15N}$ calculated from Hooke's Law is 27 cm^{-1}.

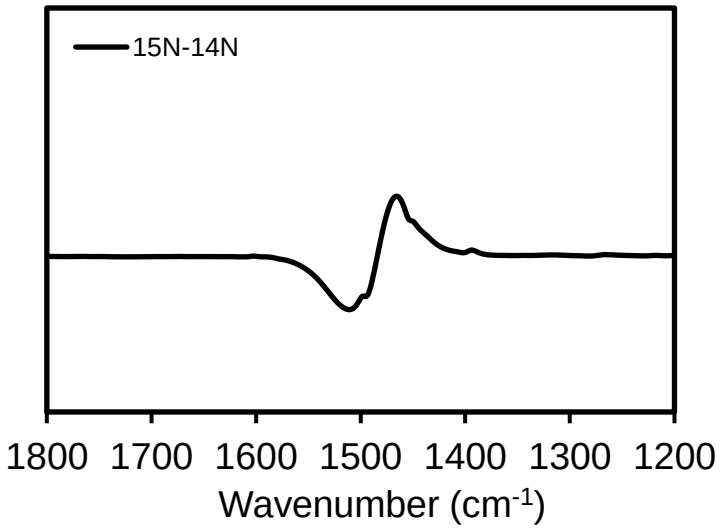

Figure S65. IR spectra of free $PhCH_2CH_2S^{15}NO$ subtracted from that of $PhCH_2CH_2SNO$. νNO_{14N} = 1495 cm^{-1}; νNO_{15N} = 1468 cm^{-1} $\Delta\nu NO_{14N\text{-}15N}$ = 27 cm^{-1}; $\Delta\nu NO_{14N-15N}$ calculated from Hooke's Law is 27 cm^{-1}.

IR of 1-OTf reacting with NO and ^{15}NO in the presence of methanol

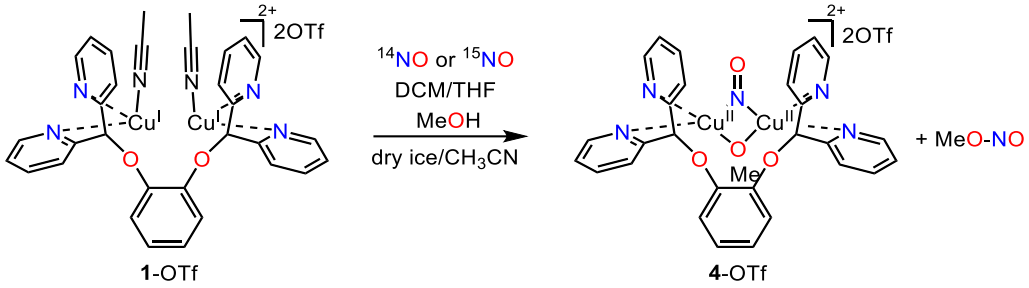

Complex **1**-OTf (15.7 mg, 16.5 μmol) was dissolved in a mixture of dichloromethane (0.50 mL), THF (0.40 mL), and methanol (0.20 mL) to afford a 15 mM solution. The solution was injected into a three-neck cell that had been connected to the react IR probe and purged with nitrogen for *ca.* 1.5 h. The cell was cooled in a dry ice/acetonitrile bath (−40 °C) for *ca.* 20 min. After the temperature inside the cell stabilized, NO• or ^{15}NO• (4.0 mL, 167 μmol, 10 equiv.) was injected into the cold solution and the reaction progress was monitored for *ca.* 2.0 h at this temperature. The IR spectra of **4b** synthesized from NO• or ^{15}NO• (Figure S66) are shown. The IR spectrum from reaction of **1**-OTf and ^{15}NO• subtracted from that of NO• is shown in Figure S67. Based on the N=O stretch at 1567 cm^{-1}, the μ-nitrosyl motif can be assigned as NO$^-$.

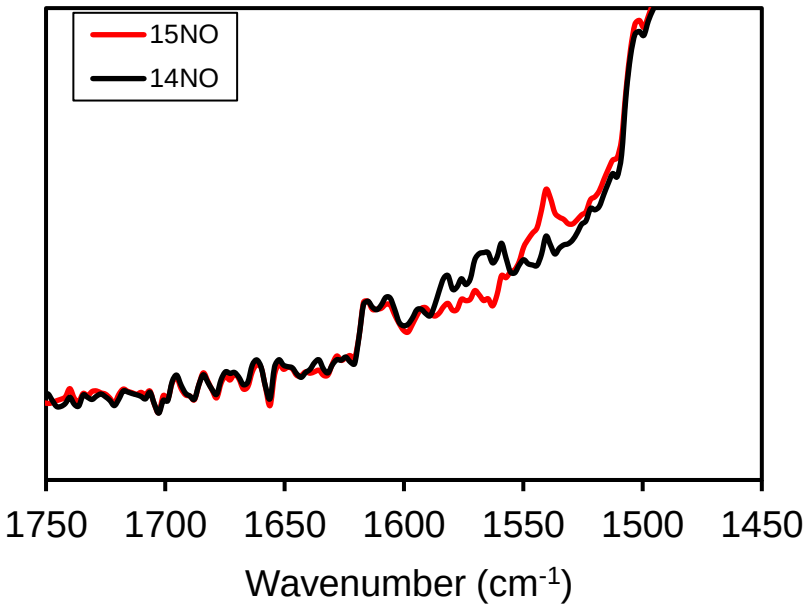

Figure S66. IR spectra of **4b** synthesized from **1**-OTf with ^{14}NO• (black trace) and ^{15}NO• (red trace) in a mixture of DCM, THF and methanol in a dry ice/acetonitrile bath.

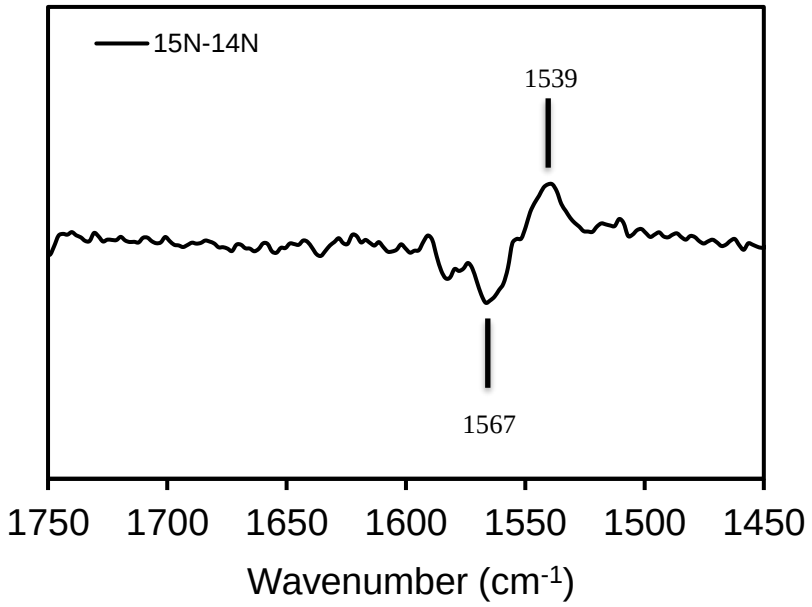

Figure S67. IR spectrum of **4b** synthesized from **1**-OTf with $^{15}NO\bullet$ (baseline adjusted) subtracted from that of $^{14}NO\bullet$ in a mixture of DCM, THF and methanol in a dry ice/acetonitrile bath. νNO_{14N} = 1567 cm^{-1}; νNO_{15N} = 1539 cm^{-1} $\Delta\nu NO_{14N-15N}$ = 28 cm^{-1}; $\Delta\nu NO_{14N-15N}$ calculated with Hooke's Law is 28 cm^{-1}.

5. X-band EPR details

All samples were measured in 4 mm septum-capped EPR quartz tubes (Wilmad Lab glass, 727-SQ-250MM).

4-OTf single crystal (26.0 mg, 26.9 µmol) was dissolved in cold acetone (1.0 mL) to make 26.9 mM solution of **4**-OTf and it was stored in the freezer of the glove box (−40 °C). 18.6 µL (0.500 µmol) of this 26.9 mM cold **4**-OTf solution was transferred into a precooled vial and diluted with 981 µL of cold acetone to make 0.50 mM **4**-OTf in acetone. 0.20 mL of this 0.50 mM solution was transferred into a precooled EPR tube inside the freezer of the glove box and the cold EPR tube with 0.50 mM solution of **4**-OTf was transferred quickly out of glove box and frozen in liquid nitrogen. To make a higher concentration sample for comparison, 112 µL (3.0 µmol) of the 26.9 mM cold **4**-OTf solution was transferred into a precooled vial and diluted with 888 µL of cold acetone to make 3.0 mM **4**-OTf in acetone. 0.20 mL of this 3.0 mM solution was transferred into a precooled EPR tube inside the freezer of the glove box and the cold EPR tube with 3.0 mM solution of **4**-OTf was transferred quickly out of glove box and frozen in liquid nitrogen.

Spectra were collected at 20 K with a modulation frequency of 100 kHz and a modulation amplitude of 5 G using 35 dB attenuation. A time constant of 40.96 ms and a conversion time of 70.59 ms were used. All spectra were baseline-corrected using Igor Pro (Wavemetrics, Lake Oswego, OR) software.

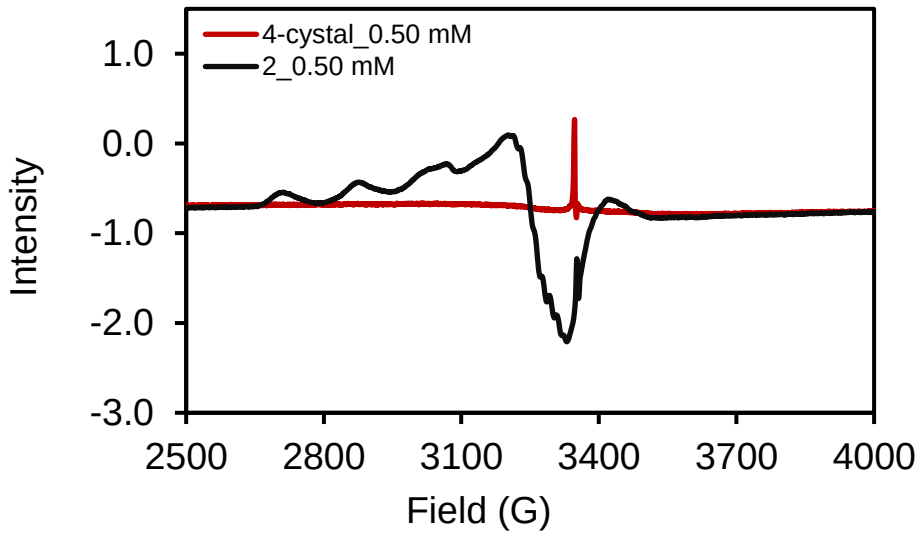

Figure S68. X-band EPR spectra (20 K) of **4**-OTf at 0.50 mM concentration (red trace, EPR silent) compared with **2**-BAr^{F}_{4} at 0.50 mM concentration (black trace) which has been characterized previously[8].

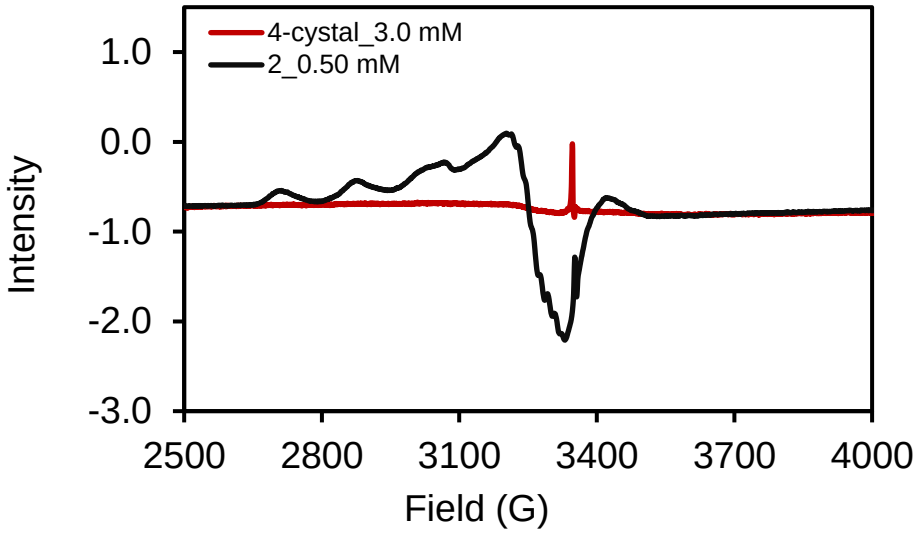

Figure S69. X-band EPR spectra (20 K)of **4**-OTf at 3.0 mM concentration (red trace, EPR silent) compared with **2**-BAr^F_4 at 0.50 mM concentration (black trace) which has been characterized previously.[8]

4-OTf is EPR silent regardless of its concentration. Combining X-ray single-crystal structure, EPR, and in-situ IR investigation of NO stretch, **4**-OTf is assigned as dicopper(II,II) μ-methoxo, μ-NO^- complex.

6. Computational details

All computations were performed in parallel on 16 processors using Gaussian or ORCA[9] programs and the structures were visualized in the ChemCraft program. DFT geometry optimizations of [**L**Cu^{II}_2(μ-NO)(μ-OMe)]$^{2+}$ and [**L**Cu^{II}_2(μ-NO)(μ-SMe)]$^{2+}$ were performed using B3LYP[10]-D3[11] method with def2-TZVP basis set[12]. Energy minima were confirmed by a vibrational frequency calculation, and no imaginary frequencies were observed. All DFT calculations were performed using very tight convergence thresholds for the energy (10^{-9} E_h).

Optimized coordinates of complex **4** ([**L**Cu^{II}_2(μ-NO)(μ-OMe)]$^{2+}$)

29	5.343695309	6.352154954	2.711849168
29	4.581257898	3.617051960	1.575585422
8	7.109214289	3.267808374	1.250803129
8	7.776400859	5.650135980	2.245113453
8	4.215371455	5.522569602	1.349775261
7	4.568312021	4.561897350	3.424560745
7	4.813671747	2.817424977	-0.314182973
7	6.255970798	7.982917043	1.833097285
7	5.012562820	1.852927668	2.439985558
7	6.345201459	6.643244352	4.431541954
8	3.591888428	4.574120313	4.049488633
6	8.018717841	4.021358576	0.522744363
6	2.853083274	5.928761930	1.287106895
1	2.313738006	5.694756576	2.215445644
1	2.353763200	5.418341104	0.460474008
1	2.797102459	7.006523475	1.118349498
6	6.104720404	1.243967715	1.943739527
6	8.173115517	6.892786615	2.850175709
1	9.259852384	6.980906904	2.866910009
6	5.865184300	1.988944420	-0.422850308
6	6.792797462	1.943341819	0.788924082
1	7.702983812	1.396873645	0.539974550
6	7.565675122	8.083853846	2.113012968
6	7.665347774	6.851405801	4.277338804
6	8.371075275	5.279080745	1.047766339
6	6.073559272	1.216245749	-1.554020740
1	6.926421703	0.551949926	-1.612400093
6	4.327315203	1.276799888	3.435653057
1	3.461371918	1.814708731	3.800155638
6	8.302276888	9.206409345	1.770519896
1	9.355582665	9.263931388	2.014031120
6	8.603110979	3.593677973	-0.662870965
1	8.349864475	2.634818831	-1.085072409
6	9.295261909	6.062623084	0.368021980
1	9.582113867	7.028930427	0.749804225
6	6.543837876	0.027531240	2.441106636
1	7.430755456	-0.438499183	2.032852997
6	5.647863587	8.978049147	1.176292496

1	4.595884738	8.841220791	0.963718942
6	7.667540843	10.249072679	1.102392798
1	8.220413485	11.136517425	0.822493366
6	3.957875769	2.927463809	-1.337381713
1	3.135745243	3.618059360	-1.204137718
6	8.497887311	7.054781265	5.366125386
1	9.558261467	7.210217662	5.218113525
6	5.175403153	1.317251562	-2.612118365
1	5.316010660	0.725612908	-3.507531891
6	5.827323679	-0.579777839	3.468277978
1	6.149299565	-1.531906661	3.869934178
6	4.699751241	0.054228991	3.973987724
1	4.114641444	-0.385366165	4.769976909
6	9.528798360	4.387843550	-1.334850907
1	9.970469271	4.029791364	-2.254901322
6	6.319676277	10.128650617	0.789262453
1	5.792147733	10.911262651	0.261576735
6	9.875022629	5.622648661	-0.819189178
1	10.593566327	6.251639588	-1.326963208
6	4.105184766	2.196431676	-2.507378868
1	3.391034858	2.312320054	-3.310982311
6	5.815127572	6.632544705	5.661100585
1	4.749356433	6.453609239	5.725759377
6	7.948398440	7.055870841	6.644914118
1	8.578711992	7.216548210	7.510032241
6	6.584337663	6.842103182	6.795812291
1	6.118547964	6.837585543	7.771627733

Optimized coordinates of complex **7** [**L**Cu^{II}_2(μ-NO)(μ-SMe)]$^{2+}$

29	7.294576189	7.821402198	3.965351001
29	6.397457501	4.989309306	2.749806602
8	8.917800465	4.506521761	2.743537757
8	9.661497704	6.853047467	3.754590154
16	5.904705480	7.179666619	2.248235710
7	6.434552455	6.015172606	4.567609930
7	6.795045196	4.032809945	0.969672519
7	8.479434901	9.348458299	3.253715542
7	6.661784394	3.258723623	3.795130968
7	8.145623330	7.955934506	5.813161520
8	5.488658706	6.022360421	5.248553912
6	9.942095210	5.174479009	2.089143031
6	4.189803441	7.468628883	2.843911849
1	4.051121102	7.077883609	3.854358126
1	3.499375285	6.971919834	2.165913114
1	3.997909472	8.539263363	2.840348015
6	7.767480306	2.572195715	3.456448665
6	10.140912342	8.028362150	4.431222982
1	11.223927611	7.983842256	4.552175491
6	7.806005362	3.151649253	1.034755664

6	8.601392317	3.163384462	2.337373401
1	9.512448582	2.574871510	2.222703675
6	9.752255730	9.297824714	3.678202995
6	9.488882573	8.019868537	5.799456358
6	10.335755140	6.415729885	2.624183072
6	8.083510621	2.279660959	-0.005718271
1	8.901946632	1.575536733	0.074917082
6	5.855614976	2.783999771	4.751687490
1	4.987908727	3.384927634	4.992884300
6	10.636662893	10.342492466	3.462656782
1	11.656590497	10.277579933	3.819980205
6	10.594674001	4.681557519	0.966180129
1	10.308146270	3.735059587	0.536952498
6	11.368429407	7.119634318	2.017550969
1	11.685224860	8.073256595	2.407952802
6	8.096446624	1.376324333	4.074132661
1	8.996388684	0.846761774	3.790940651
6	8.055320079	10.420659513	2.573812193
1	7.026228131	10.398718184	2.240136536
6	10.192817592	11.466449226	2.772237637
1	10.863564466	12.296071515	2.589417227
6	6.051182430	4.099230077	-0.141168584
1	5.262793691	4.840366294	-0.144909012
6	10.222792784	8.110309533	6.971220896
1	11.303338965	8.150931825	6.935105131
6	7.299656979	2.333881471	-1.154479492
1	7.495752128	1.664660733	-1.982300277
6	7.252047854	0.872564668	5.059432530
1	7.485596846	-0.061860776	5.553271831
6	6.112345266	1.587290347	5.404623719
1	5.430815982	1.229655820	6.164101023
6	11.630251228	5.395224896	0.368018691
1	12.124128651	4.988336958	-0.503945290
6	8.883300860	11.502171231	2.309905259
1	8.503988884	12.351743661	1.758946159
6	12.017096308	6.614024348	0.893659647
1	12.820018588	7.180333806	0.441546808
6	6.273024275	3.266818950	-1.228722616
1	5.649622572	3.348826078	-2.108411592
6	7.494408335	7.977936797	6.981804336
1	6.414963002	7.909686267	6.933459496
6	9.547430585	8.147970443	8.187811087
1	10.098702254	8.222723767	9.116295698
6	8.160208090	8.081065399	8.194414425
1	7.598627148	8.108265586	9.118036056

References

[1] M. Brookhart, B. Grant, A. F. Volpe, *Organometallics* **1992**, *11*, 3920–3922.

[2] G. Roelfes, V. Vrajmasu, K. Chen, R. Y. N. Ho, J.-U. Rohde, C. Zondervan, R. M. la Crois, E. P. Schudde, M. Lutz, A. L. Spek, et al., *Inorg. Chem.* **2003**, *42*, 2639–2653.

[3] O. Rivada-Wheelaghan, S. L. Aristizábal, J. López-Serrano, R. R. Fayzullin, J. R. Khusnutdinova, *Angew. Chemie* **2017**, *129*, 16485–16489.

[4] C. E. Aroyan, S. J. Miller, *J. Am. Chem. Soc.* **2007**, *129*, 256–257.

[5] N. Arulsamy, D. S. Bohle, J. A. Butt, G. J. Irvine, P. A. Jordan, E. Sagan, *J. Am. Chem. Soc.* **1999**, *121*, 7115–7123.

[6] M. M. Melzer, S. Mossin, A. J. P. Cardenas, K. D. Williams, S. Zhang, K. Meyer, T. H. Warren, *Inorg. Chem.* **2012**, *51*, 8658–8660.

[7] C. M. Park, T. D. Biggs, M. Xian, *J. Antibiot. (Tokyo).* **2016**, *69*, 313–318.

[8] W. Tao, J. K. Bower, C. E. Moore, S. Zhang, *J. Am. Chem. Soc.* **2019**, *141*, 10159–10164.

[9] F. Neese, F. Wennmohs, U. Becker, C. Riplinger, *J. Chem. Phys.* **2020**, *152*, 224108.

[10] P. J. Stephens, F. J. Devlin, C. F. Chabalowski, M. J. Frisch, *J. Phys. Chem.* **1994**, *98*, 11623–11627.

[11] S. Grimme, J. Antony, S. Ehrlich, H. Krieg, *J. Chem. Phys.* **2010**, *132*, DOI 10.1063/1.3382344.

[12] A. Schäfer, H. Horn, R. Ahlrichs, *J. Chem. Phys.* **1992**, *97*, 2571–2577.